Enhancing Radiosensitivity of Murine Hepatocytes in Hypoxia through HIF-1α Depletion

Inaugural-Dissertation zur

Erlangung des Doktorgrades

Dr. rer. nat.

der Fakultät für

Biologie

an der

Universität Duisburg-Essen

vorgelegt von

Akram Hamidi

aus Isfahan

Jun, 2023

Die der vorliegenden Arbeit zugrunde liegenden Experimente wurden am Institut für Physiologie in der Arbeitsgruppe von Prof. Dr. Metzen, Universitätsklinikum Essen, Universität Duisburg-Essen durchgeführt.

1. Gutachter: Prof. Dr. med. Eric Metzen

2. Gutachter: Prof. Dr. Doris Hellerschmied-Jelinek

Vorsitzender des Prüfungsausschusses: Prof. Dr. Ralf Küppers

Tag der mündlichen Prüfung: 18.09.2023

DOI: 10.17185/duepublico/79146
URN: urn:nbn:de:hbz:465-20231031-085102-2

“Science is not limited to laboratories; it is a mindset that embraces curiosity, critical thinking, and a relentless pursuit of truth."

Dr. Rosalind Franklin

Table of Contents

1 Introduction

1.1 The need for hepatocyte cell models

The liver is a vital organ that performs a variety of functions crucial for maintaining homeostasis in the body. The liver is primarily composed of hepatocytes, i.e. highly polarized epithelial cells that perform nearly all of the liver's biotransformation functions[1]. These cells are responsible for the exchange of metabolites with the blood and secreting bile, detoxification products, cholesterol, and phospholipids which eventually drain into the bile duct[2]. Hepatocytes have an average lifespan of 5 months and can regenerate, which has functional implications, such as improving metabolic functions by influencing gene expression profiles. These cells play an important role in regulating a wide range of important biochemical functions in the body, including metabolism, synthesis, detoxification, and excretion. The liver's main tasks are protein and lipid metabolism. Additionally, the liver plays multiple roles in carbohydrate metabolism, including gluconeogenesis, glycogen synthesis, and glycogenolysis. The liver synthesizes amino acids, hormones, and plasma proteins. Moreover, the liver secretes bile into the gastrointestinal (GI) tract to emulsify lipids and promote lipid digestion. The nonparenchymal cells in the liver, such as Kupffer cells, endothelial cells, hepatic stellate cells, and pit cells, work together to ensure the proper functioning of this important organ[3].

In vitro liver models have broad applications, from drug development to clinical trials, and offer advantages over animal models, such as mimicking liver disease in a simplified and more reproducible manner. Preclinical development requires efficient prediction of efficacy and safety due to the high costs involved in drug failures during clinical trials and the stringent drug development regulations. Liver models can help evaluate safety at preclinical stages, increasing predictability and reducing costs during drug development[4]. Liver disease affects over 600 million people worldwide, resulting in over one million deaths per year[5]. Orthotopic transplants are currently the only available treatment, but cell-based therapies, engineered tissue transplantation, or bio-artificial livers are among the methods being explored to extend survival and overcome the shortage of liver donors. The liver plays such an important role in all these processes that transplantation is the only option in cases of irreversible acute or chronic liver failure. Transplanting liver cells may be a promising therapy for fixing metabolism-related errors[6,7]. However, the availability of primary human hepatocytes for biomedical research is extremely limited, even though protocols have been developed to cultivate human hepatocytes

for short periods or to cultivate hepatocyte-like cells differentiated from non-parenchymal epithelia for extended periods[8,9]. Hepatocytes isolated from rodents have also been cultured, but there appears to be a significant reduction in complexity compared to *in vivo* culture, and the highly proliferative state required for cell culture can cause rapid dedifferentiation. It would be highly desirable to have a reliable, long-term culture method that can generate differentiated hepatocytes from the vast array of genetically modified mice that are commercially available. Moreover, hepatocyte culture technology could be useful for reducing and refining animal experiments.

1.2 Upcyte® technology

Hepatocytes have limited proliferation capacity *in vitro* but demonstrate significant growth *in vivo*, especially after partial hepatectomy. To bridge the gap between primary cells and cell lines, a technology called "Upcyte®" has been developed. This technology uses lentiviral vectors to transduce primary human cells with proliferation-inducing genes[10], resulting in proliferating cells referred to as "Upcyte®" cells. Upcyte® cells can undergo only a limited number of cell divisions, typically 20-40 population doubling cycles, without losing their adult cell phenotypic characteristics. After additional population doublings, Upcyte® cells become senescent [11].

Unlike permanent cell lines, Upcyte® cells are not immortalized and exhibit a proliferative capacity. Therefore, cells are seeded at a low density after the Upcyte® process, allowing them to proliferate. Since non-transduced cells have a limited lifespan, selection is unnecessary. One vial of primary human hepatocytes can generate more than 12 billion Upcyte® hepatocytes using Upcyte® technology. With the refinement of the Upcyte® process, Upcyte® hepatocytes produced higher levels of cytochrome P450 (CYP) than those generated in the first generation. Moreover, Upcyte® hepatocytes exhibit adult cell markers, produce albumin, and demonstrate the metabolic activities associated with phase 1 and phase 2 drug metabolism. This means that these cells possess the enzymatic capabilities to perform phase 1 reactions, which involve the introduction or exposure of functional groups on drug molecules, as well as phase 2 reactions, which involve the conjugation or coupling of drugs or their metabolites with endogenous molecules. Upcyte® technology is not limited to hepatocytes but can also be applied to various cell types, such as liver sinusoidal endothelial cells (LSECs)[12] and microvascular endothelial cells (mvEC), allowing a variety of primary cells from multiple donors to have a longer lifespan. Cells can be generated easily and in large numbers from a single donor, making

Upcyte® technology suitable for the production of adequate quantities of various cell types for human-based cell screening research, and it is particularly useful for the normalization of *in vitro* test structures and tissue engineering (Figure 1).

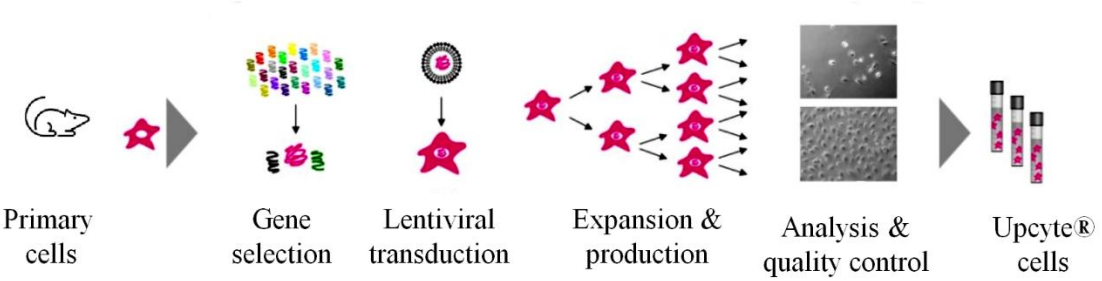

Figure 1: Generation of Upcyte® mouse hepatocytes. Upcyte® technology involves inducing primary human cells to proliferate by utilizing a combination of cellular and viral genes. The Upcyte® technology bypasses the cell cycle control mechanism, which leads to controlled cell growth without immortalizing them. The cells that proliferate are specifically chosen and designated as "Upcyte®" cells[13].

1.3 Hypoxia and the HIF-1α pathway

The term hypoxia is basically defined as a state in which tissue oxygen (O_2) levels are below physiological levels. In general, hypoxia refers to an inadequate supply of oxygen that may cause a lack of cellular energy but that, for example, also contributes to making cells radioresistant and often occurs within solid tumors, mainly as a result of abnormal blood vessel formation, impaired blood perfusion and disturbed microcirculation[14]. At the systemic and cellular levels, hypoxia causes a range of adaptive responses in organisms[15]. Adaptation to hypoxia involves the expression of specific proteins that enable cell survival. However, cells require an appropriate amount of oxygen for long-term survival. One of the essential responses to low pO_2 (oxygen tension) is the hypoxia-induced renal synthesis of erythropoietin (Epo). This hormone accelerates the production of erythrocytes, enhancing the blood's oxygen-carrying capacity[16]. Moreover, proteins such as vascular endothelial growth factor (VEGF), a hypoxia-inducible angiogenic factor, frequently promote neovascularization in response to hypoxia[17]. Previous reports have described how tumor cells adapt in order to survive. Otto Warburg, the Nobel prize winner who discovered cytochrome c oxidase, initially discovered the abnormal energy metabolism of cancer cells in 1924. In the presence of oxygen, normal cells convert glucose to pyruvate in the cytosol by glycolysis. However, only two ATPs are

produced per molecule of glucose in this pathway. Then, they oxidize the pyruvate in the mitochondrial tricarboxylic acid (TCA) cycle. This reaction produces the reduced form of nicotinamide adenine dinucleotide (NADH), which is required for oxidative phosphorylation of glucose with up to 36 adenosine 5´-triphosphates (ATP) per molecule[18]. In contrast to normal cells, many types of cancer cells rely on glycolysis to produce high levels of lactate regardless of oxygen supply. This behavior of cancer cells has been termed the Warburg effect[19]. Hypoxia-inducible lactate dehydrogenase-A (LDH-A), which is involved in the interconversion of pyruvate and lactate, is overexpressed in several malignancies[20]. Increased glucose consumption compensates for the lower energy, which is thought to represent a response to intermittent hypoxia in tumors[21]. It was also discovered that a rise in glucose absorption is linked to tumor aggressiveness and a bad prognosis. As a result, increased lactate production causes acidosis, which is a symptom of tissue hypoxia. Furthermore, higher glucose absorption under hypoxia is linked to increased expression of the glycolysis-related glucose transporters GLUT-1 and GLUT-3[22]. Hypoxia also affects cancer epigenetics, causing histone alterations that are linked to transcriptional suppression[23]. In 2016, the Albert Lasker Basic Medical Research Award was awarded for the discovery of molecular processes associated with hypoxia. The honorees were Peter Ratcliffe, Gregg Semenza and William Kaelin. They were also awarded the Nobel Prize in 2019 for their pioneering research into how cells detect and adapt to oxygen availability[24].

The hypoxia-inducible factors (HIFs) are crucial regulators of hypoxic signaling, responsible for inducing genes that allow cells to survive in low oxygen conditions[25]. HIF is composed of two subunits: the α-subunit, which is oxygen-regulated and weighs 120 kDa, and the β-subunit, which weighs between 91 to 94 kDa and is also known as aryl hydrocarbon receptor nuclear translocator (ARNT) or HIF-1β[26]. Both subunits are considered basic-helix-loop-helix (bHLH)-PER-ARNT-SIM (PAS) proteins, and the bHLH and PAS domains facilitate the interaction with target genes through DNA binding and protein interaction (Figure 2). The transcriptional activity of HIF is regulated by both the N-TAD and the C-TAD[27]. These domains share a homology region with the protein product of the *D. melanogaster* period clock protein (PER), as well as with a product of the D. melanogaster single-minded locus (SIM)[28,29]. HIF consists of significant isoforms, including the oxygen-sensitive HIF1α, HIF2α, or HIF3α, and the oxygen-insensitive HIF1β and HIF1β2[30,31]. HIF-1α is expressed in various tissues, while HIF-2α, initially called endothelial PAS protein 1 (EPAS1), is characteristic of specific cell types, such as kidneys, endothelium, small intestines, heart, and lungs[32,33]. HIF-3α,

expressed in the heart, brain, adult thymus, kidneys, and lungs, is the most structurally distant among HIF-αs, but its function in tissues is not yet well understood. Variants of HIF-3α mRNA may determine whether the HIF complexes are activated or inhibited. One of the alternative transcripts of the HIF-3α gene, known as inhibitory PER-ARNT-SIM protein (IPAS), functions as a negative regulator for HIF-α[14,34]. HIF-1β, which is constitutively expressed, controls the transcriptional activity of HIF-α by binding to it and forming a transcriptionally active dimer[35,36]. Regardless of the oxygen levels, HIF-α is constitutively transcribed and translated but instantly degraded as long as oxygen is present[37]. HIF-α subunits have a short half-life of 5-8 min under normoxic conditions, and they are rapidly ubiquitinated and degraded by proteasomes via a pathway involving the von HippelLindau protein (pVHL), a member of the E3 ubiquitin-ligase family[38,39]. The oxygen-dependent PHDs are suppressed under hypoxic conditions, and the oxygen-dependent degradation domain (ODDD) cannot be hydroxylated, resulting in HIF-α subunit stabilization. HIF-α then enters the nucleus, binds to HIF-1β, and stimulates the transcription of target genes regulated by HIF-binding sequences, also termed hypoxia response elements (HREs). The active HIF complex in the nucleus activates several hypoxia-inducible genes crucial to adaptation to low oxygen levels[40,41] (Figure 3).

For example, increasing the expression of the GLUT-1 increases glucose uptake, thereby increasing the intracellular levels of glycolytic substrate[42,43]. The expression of vascular endothelial growth factor (VEGF) promotes angiogenesis, stimulating the formation of blood vessels, and thus increasing oxygen levels[44]. Monocarboxylate transporter 4 (MCT-4) and carbonic anhydrase IX (CAIX) are also essential in controlling intracellular pH. Lactate levels are decreased by high MCT-4 activity because it expels the lactate produced during glycolysis[45].

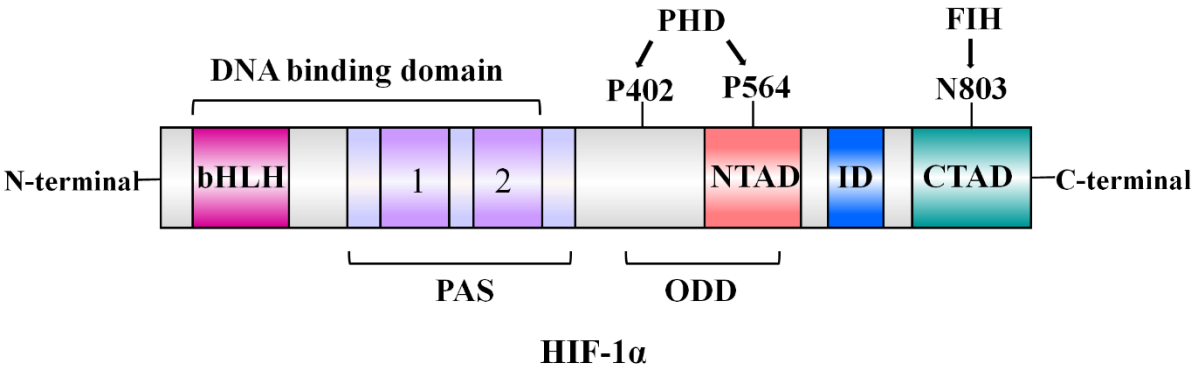

Figure 2: Structure of HIF1α. Diagram representing the structural domains of HIF1α. Posttranslational modifications include hydroxylation and phosphorylation. bHLH: basic-helix-loop-helix, PAS: PER-ARNT-SIM, ODD: oxygen-dependent degradation domain, NTAD: N-terminal transactivation domain, ID: inhibitory domain, CTAD: C-terminal transactivation domain[46].

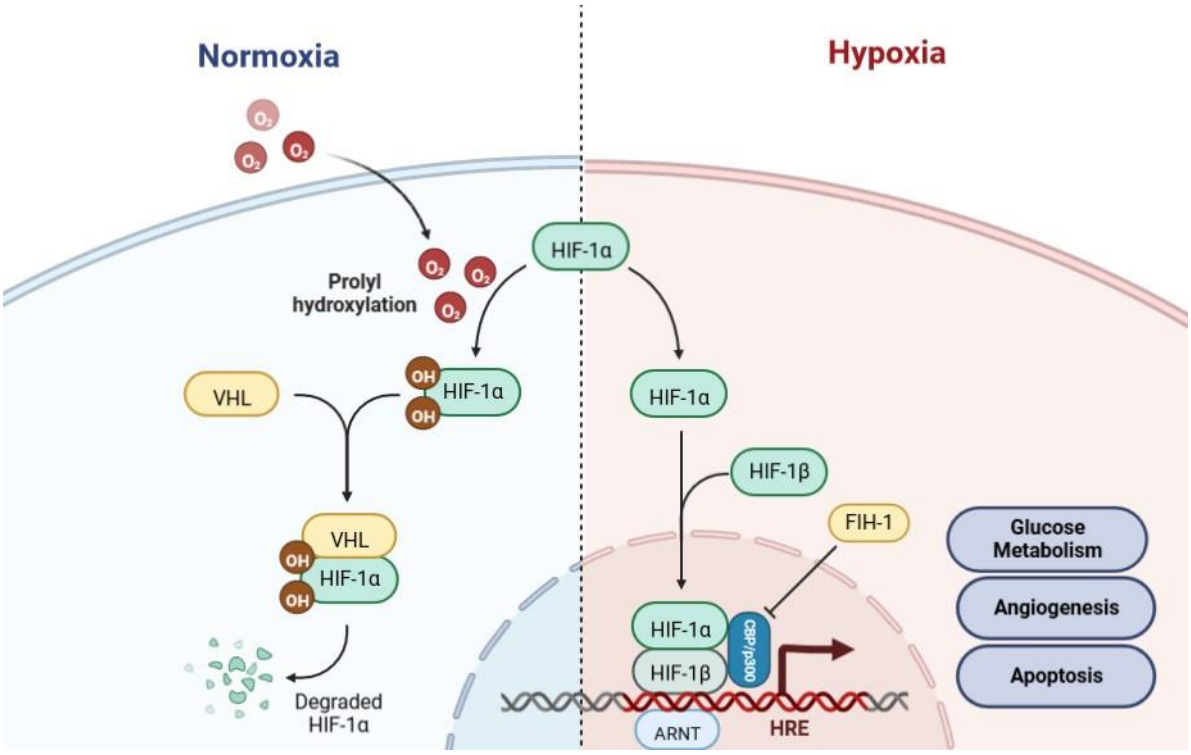

Figure 3: Schematic highlighting the HIF pathway. Under normoxic conditions HIF-1α is hydroxylated and rapidly degraded. Under hypoxic conditions the HIF-1 complex is stabilised and initiates the transcription of its target genes[47].

In addition to oxygen-dependent degradation, Factor inhibiting HIF-1 (FIH-1) hydroxylates the asparaginyl residue N803 and therefore prevents recruitment of cAMP response element-binding (CREB)-binding protein (CBP) and 300 kDa coactivator protein (p300) under normoxia. Thus, in the absence of oxygen, HIF-1α is stabilized and more efficiently interacts with cofactors such as HIF-1ß and CBP/p300 to maintain binding to the hypoxia-responsible element (HRE). In addition, some protein kinases have been reported to be involved in either directly or indirectly regulating HIF-1, indicating that HIF-1 phosphorylation modifies hypoxia-dependent regulation of HIF-1 stability, nuclear localization, DNA binding, and transcriptional activity[48–50].

HIF-1 is required for glucose and energy metabolism and homeostasis in hypoxia. It stimulates the transcription of target genes involved in glycolysis, such as GLUT1, GLUT3, hexokinase 2 (HK2), and LDHA[51–55]. HIF-1 also plays a role in suppressing oxidative metabolism through the activation of pyruvate dehydrogenase (PDH) kinase isozyme 1 (PDK1), which leads to the inhibition of PDH activity by phosphorylation. As a result, the conversion of pyruvate into acetyl-CoA and its entry into the TCA cycle are hindered. Additionally, HIF-1 has been found to induce a transition in the subunits of cytochrome c oxidase (COX) from COX4-1 to COX4-2. This alteration enhances the efficiency of electron transfer to oxygen while preventing an accumulation of reactive oxygen species (ROS) levels[56]. HIF-1 also regulates two important adaptation processes under hypoxic conditions, which are vascular remodeling and angiogenesis, through the activation of genes such as VEGF, stromal derived factor 1 (SDF1), and platelet-derived growth factor B (PDGFB)[57]. In addition to angiogenesis and glycolysis, hypoxia can cause apoptosis and growth arrest. HIF-1 has been linked to the activation of several pro-apoptotic genes. One of them is the crucial tumor suppressor p53, which interacts with HIF-1 to promote p53-dependent apoptosis.

The mentioned factors point to HIF-1's critical role in physiological processes. On the other hand, activation of HIF has a severe disadvantage: it promotes the survival of normal cells, but also of cells that have undergone mutations, such as tumor cells.

1.4 The effect of HIF-1α on metabolic profiling

In normal mammalian cells, glycolysis, the TCA cycle, and oxidative phosphorylation (OXPHOS) are the three phases of the metabolic process[58]. Under oxygen-deprived conditions, PDK1 phosphorylates pyruvate dehydrogenase, leading to the conversion of pyruvate into

lactic acid. This process is regulated by HIF-1α, which upregulates LDHA, causing the conversion of pyruvate into lactic acid and its excretion into the extracellular space through MCT4 upregulation. The HIF-1α-dependent upregulation of Bcl2/adenovirus E1B 19-kDa interacting protein 3 (BNIP3) and BNIP3L leads to increased mitophagy and decreased pyruvate flux into the TCA cycle, resulting in an increased reliance on glutamine catabolism and reductive carboxylation to generate citrate and acetyl-CoA, necessary for fatty acid synthesis[19].

HIF-1 and glucose metabolism are potential targets for improving cancer treatment, and there are ongoing clinical trials using dichloroacetate and 2-deoxy-D-glucose to target PDK and glycolysis, respectively. Moreover, radiation therapy can affect mitochondrial DNA, leading to an increase in the number of mitochondria, the number of DNA copies, and the production of more ROS, which can cause DNA damage and radiation-induced chromosomal instability. However, further research is necessary to understand the roles of mitochondrial alterations and cell survival following irradiation[59,60].

A peptide unrelated to cellular energy metabolism but important for the response of the organism to hypoxia is hepcidin which plays a critical role in iron metabolism and homeostasis[61]. It inhibits both iron absorption in the small intestine and macrophage recycling of iron by binding to ferroportin, which degrades it internally, limiting iron export[62]. Hepcidin upregulation is associated with anemia of chronic disease during chronic inflammation, while hemochromatosis is linked with hepcidin downregulation. The association between oxygen transport, erythropoiesis, and iron metabolism implies a potential connection between the physiology of the hypoxic response and the regulation of iron availability.

The HIF transcription factors are crucial for the response to hypoxia. The VHL pathway, associated with tumor suppression, may also regulate hepcidin levels, as iron deprivation and hypoferric anemia result in poor tissue oxygenation, and the VHL protein regulates the rate of HIF transcription factor degradation. Remarkably, the HIF hydroxylases also strictly require iron for enzymatic activity[63].

1.5 Hypoxia and radiation response

Radiation therapy is a widely used treatment for cancer. However, its effectiveness can be affected by the level of oxygen in the tumor cells. Studies in the early 1990s found that areas with less blood flow were less responsive to radiation therapy, indicating the importance of a sufficient blood supply[64–66]. Further research confirmed that oxygen deficiency is one of the

main reasons for radiation therapy failure, as oxygen is crucial for stabilizing DNA damage caused by ionizing radiation[67–70].While oxygen enhances DNA damage induced by ionizing radiation, hypoxia triggers metabolic reprogramming that results in the production of molecules that protect cells against IR while promoting their survival[71–74]. This metabolic switch produces specific antioxidant molecules that reduce the effects of radiation on DNA and increase cell survival. In hypoxia, for instance, the abundance of lactate enables the scavenging of ROS molecules generated by radiation exposure because lactate has antioxidant properties[72,75–77]. HIF proteins, which are involved in radiotherapy-induced apoptosis, promote endothelial cell survival by increasing VEGF levels[78]. However, the excessive VEGF signal causes tumor vessels to be leaky and poorly functioning, resulting in a further reduction in oxygen supply to tumor cells[79]. Solid tumors with hypoxic regions have demonstrated radioresistance, with radiation targeting well-oxygenated tumor cells since sensitivity to radiation requires oxidation, making oxygenated cells 2.5- to 3-times more sensitive than hypoxic cells[80]. After the death of oxygenated radiosensitive cells, oxygen diffuses to the surviving hypoxic regions, causing reoxygenation of hypoxic tumor cells. Reoxygenation can generate oxidative stress and ROS, which may contribute to stabilizing normoxic HIF. Additionally, ROS can generate NO in tumor associated macrophages (TAMs) and lead to the S-nitrosylation of HIF-1[81–83]. The phosphatidylinositol 3 kinase (PI3K)/protein kinase-B (Akt) pathway can promote HIF-1 accumulation in irradiated tumors in a glucose- and reoxygenation-dependent manner, leading to HIF-1 upregulation in tumors[84]. HIF-1 also plays a role in the survival and repopulation of tumor cells. Perinecrotic tumor cells from hypoxic areas that survive radiation treatment may migrate to proximal regions of tumor blood vessels in an HIF-1-dependent manner. Upregulation of HIF-1 following radiation treatment promotes epithelial-mesenchymal transition (EMT) and cell translocation, as HIF-1 is involved in the induction of cell migration[85]. The radiosensitivity of cells is influenced by their distribution throughout the cell cycle. Cells are more resistant to radiation in the late S phase when they are actively synthesizing DNA and in the early G1 phase when proliferation slows down. The activation of cell cycle regulators by hypoxia plays a role in this process[86,87]. Hypoxia induces the expression of cyclin-dependent kinase (CDK) inhibitors p21 and p27, leading to cell cycle arrest[88]. The impact of HIF-1 upregulation on radiosensitivity is multifaceted. On one hand, HIF-1 acts as an anti-apoptotic factor, enhancing tumor cell radioresistance through vascular protection[89]. On the other hand, HIF-1 possesses pro-apoptotic properties that can increase radiosensitivity in tumor cells. HIF-1 induces p53 phosphorylation in irradiated cells, promoting apoptosis[90]. Additionally, HIF-1 can enhance the metabolism and proliferation of

cancer cells, thereby sensitizing irradiated cells to radiation. Chronic hypoxia, but not acute hypoxia, has been found to heighten cellular radiosensitivity by inhibiting the expression of DNA damage repair genes[91]. Overall, it is believed that the impact of HIF-1 stabilization on radioresistance outweighs the potential benefits of increased radiosensitivity.

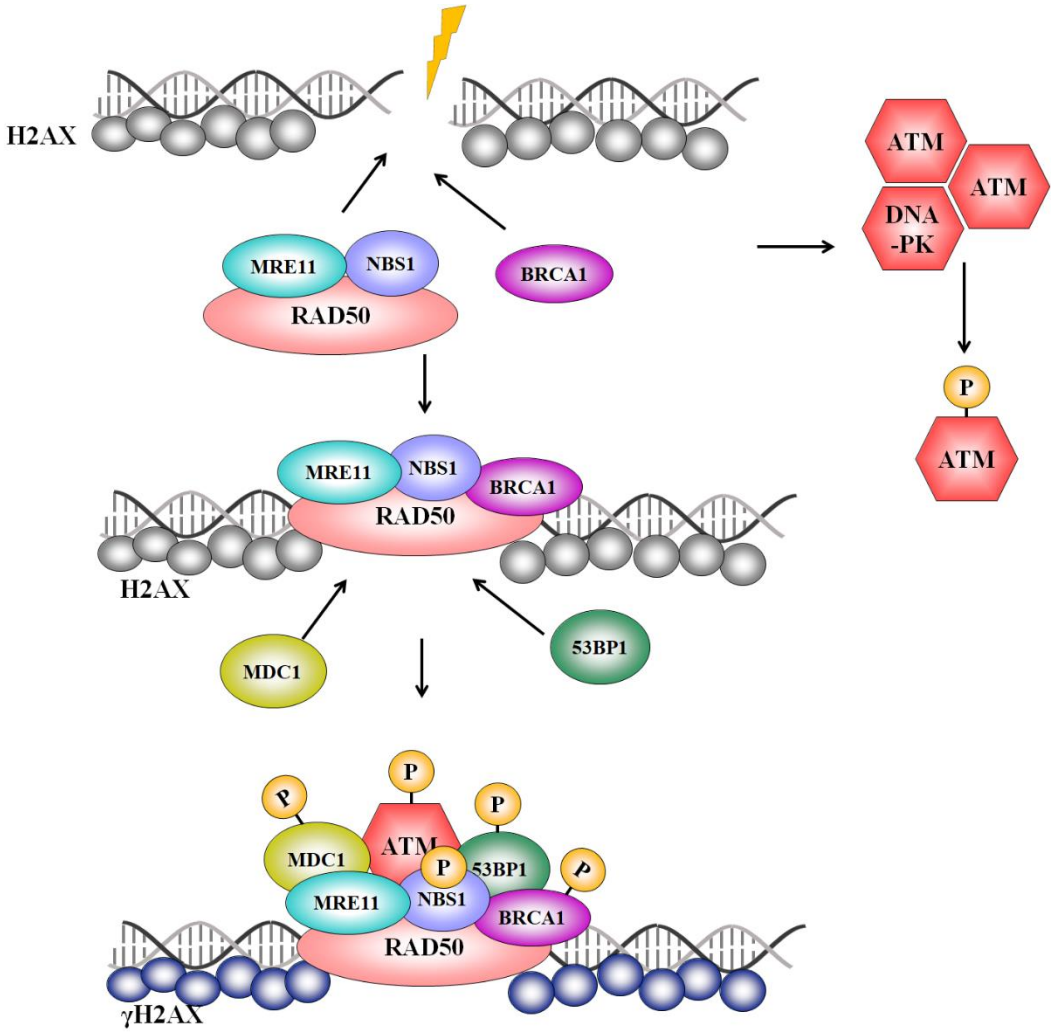

Figure 4 : Detection of IR-induced DSBs. DSBs activate the ataxia telangiectasia mutated kinase (ATM), ataxia telangiectasia and Rad3-related kinase (ATR), and DNA-PK. Histone variant H2AX is phosphorylated by ATM on serine 139, which recruits other repair components. The MRE11-RAD50-Nijmegen breakage syndrome protein 1 **(**NBS1) complex binds to the DSB site, attracting breast cancer protein 1 (BRCA1), mediator of DNA damage checkpoint (MDC1), and p53 binding protein 1 (53BP1). These proteins are phosphorylated in an ATM-dependent manner and co-localize with phosphorylated histone protein H2AX (γH2AX). The cell-cycle-dependent antagonistic mechanism regulates DSB repair choice: 53BP1 mediates end protection and favors non-homologous end joining (NHEJ), whereas BRCA1 mediates end resection and HR.ATR: ataxia telangiectasia and Rad3-related, ATM: ataxia

telangiectasia mutated BRCA1: breast cancer 1, MDC1: mediator of damage checkpoint 1, 53BP1: p53-binding protein 1, P: phosphorylation, NHEJ: non-homologous end-joining, HR: homologous recombination, DNA-PK: DNA-dependent protein kinase.

DNA repair mechanisms have evolved to fix different types of DNA damage. Mismatch repair (MMR) repairs mismatches, insertions, or deletions, while base excision repair (BER) fixes chemical alterations of DNA bases[92,93]. Nucleotide excision repair (NER) fixes more complex DNA damage such as pyrimidine dimers and intrastrand crosslinks[94]. Ionizing radiation (IR) causes DNA single-strand and double-strand breaks (DNA SSBs and DNA DSBs).

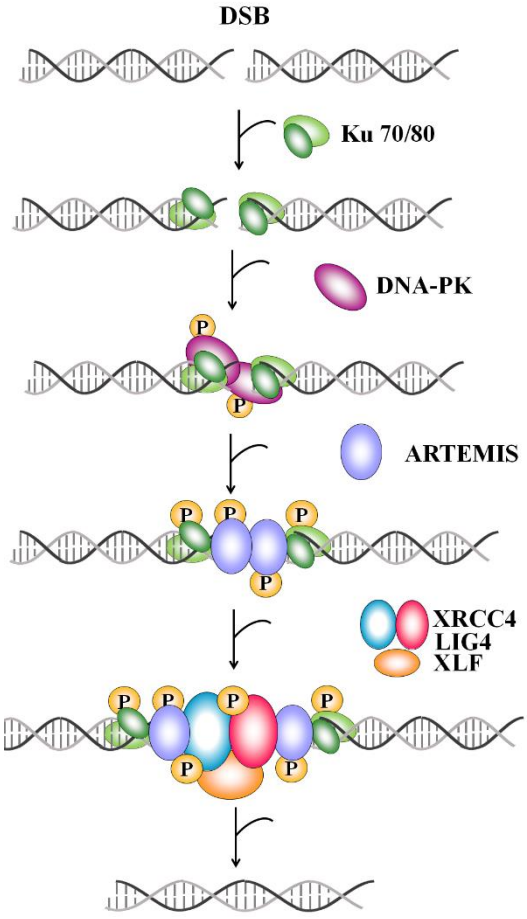

Figure 5: Non-homologous end-joining (NHEJ) pathway. The core NHEJ pathway starts with binding the ends at the DSB by the Ku70/80 heterodimer. This complex then recruits and activates DNA-PK's catalytic subunit (DNA-PKcs), which juxtaposes the two ends of DNA. A ligase complex (XRCC4/XLF-LIGIV/PNK) is then recruited by the DNA-PK complex to promote the final ligation[95].

Single-strand breaks are repaired using single-strand break repair (SSBR) mechanisms, while DSBs are repaired using one of four mechanisms: classical non-homologous end-joining (c-

NHEJ), alternative-NHEJ (alt-NHEJ), single-strand annealing (SSA), and homologous recombination (HR). HR and NHEJ are the primary mechanisms for DSB repair, while alt-NHEJ and SSA are backup mechanisms[96,97]. DSBs activate ATM, DNA-PK, and ATR, which phosphorylate γH2AX and other DNA repair proteins[98–100] (Figure 4). γH2AX acts as a marker for DNA damage at DSB sites and co-localizes with several proteins involved in DSB repair. ATM-dependent phosphorylation activates BRCA1, 53BP1, and MDC1, which are responsible for sensing and repairing DNA damage[101,102]. NHEJ is an error-prone but quick mechanism that works in all cell cycle phases. It involves the Ku70/80 heterodimer, which attaches to the ends of DSBs and recruits DNA-PKs to the DSB site[103,104] (Figure 5). DNA-PK autophosphorylates and activates ARTEMIS, which is required for hairpin opening and overhang processing[105,106]. Ku70/80 also recruits DNA polymerases μ and λ for gap-filling. XLF is recruited to initiate DSB rejoining via XRCC4/LIG4 at the two ends of DNA, and a ligase complex (XRCC4/XLF-LIGIV/PNK) is recruited by the DNA-PK complex to promote the final ligation[107–110]. During the late S and G2 phases of the cell cycle, sister chromatids play an essential role in HR - another critical DNA damage response (DDR) mechanism. The Mre11-Rad50-NBS1 (MRN) complex recognizes and stabilizes DSBs, and NBS1 interacts with ATM and C-terminal binding protein-interacting protein (CtIP) to initiate end resection, generating 3'-single-stranded DNA (ssDNA) overhangs[111]. DSB resection stimulates the accumulation of replication protein A (RPA), stabilizing ssDNA regions by preventing hydrolysis and nucleolytic degradation[112]. Following this, BRCA2 is recruited to the DSB via BRCA1, which facilitates loading of RAD51 on ssDNA, replacing RPA[113] and forming RAD51 nucleoprotein filaments. Immunofluorescence microscopy reveals these filaments as sub-nuclear RAD51 foci[114]. RAD51 filaments invade the sister chromatid's homologous sequence, forming a displacement loop structure[115]. The interplay between 53BP1 and BRCA1 determines the choice between NHEJ and HR[116]. While 53BP1 increases chromatin mobility and facilitates NHEJ[117], BRCA1 interacts with RAD51 to promote efficient DSB repair during HR[118,119] (Figure 6). In the G1 phase, 53BP1 can suppress ATM-dependent resection, favoring NHEJ repair, whereas BRCA1 can remove 53BP1 from replication-associated breaks[120]. Hypoxia can activate the ATR checkpoint, leading to a G1 and intra-S phase arrest[74]. In response to hypoxia, ATR activation causes phosphorylation of p53 and H2AX[121]. Additionally, hypoxia triggers the phosphorylation of CHK2 kinase by ATM, initiating the phosphorylation of multiple downstream target proteins required for cell cycle arrest in the G2

phase[122]. HIF-1 has also been suggested to downregulate the Myc-activated gene BRCA1 and to have a role in c-NHEJ[123,124].

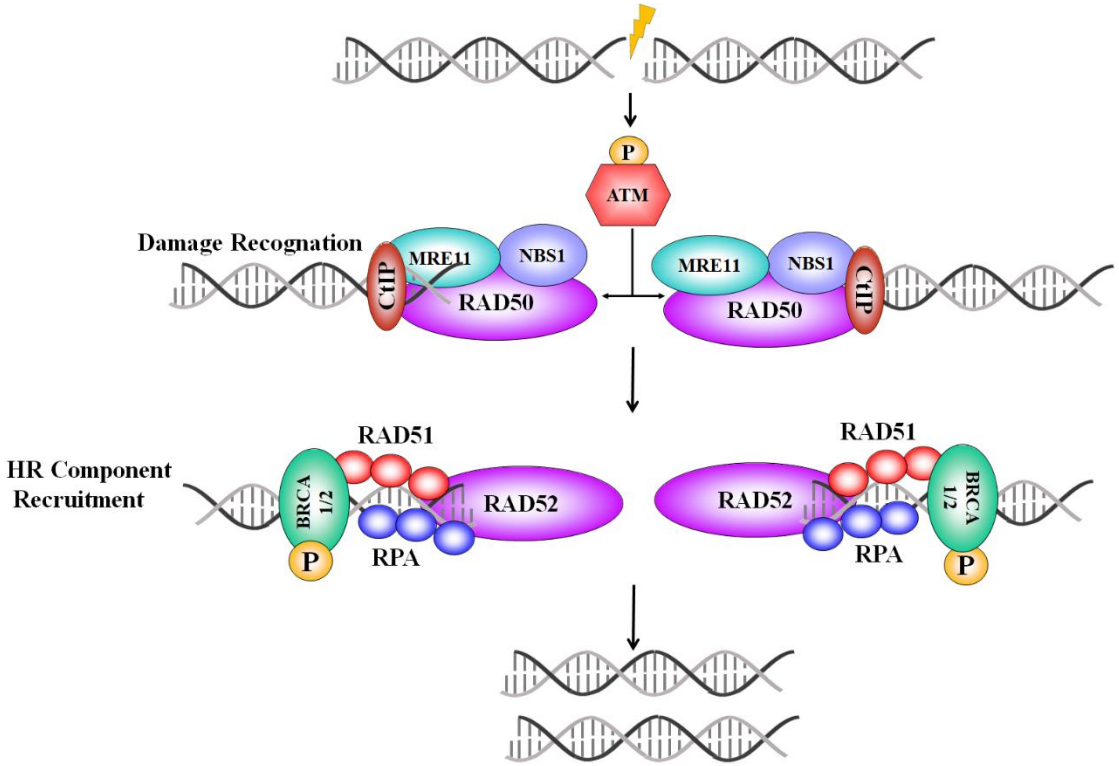

Figure 6: Homologous recombination (HR) repair pathway of DSBs. MRN complex composed of Mre11, RAD50, and NBS1 binds to the DSB ends, together with CtIP and BRCA1, mediates the initiation of DSB end resection in an ATM-dependent manner. The resulting ssDNA open ends are coated by RPA. BRCA1 recruits BRCA2 to the DSB site, which mediates replacing RPA through RAD51 monomers on ssDNA ends. RAD51 filaments induce a strand invasion into homologous DNA sequences and DNA synthesis. ATM: ataxia telangiectasia mutated, CtIP: C-terminal binding protein-interacting protein, RPA: replication protein[125].

Preclinical investigations have shown that blocking both HIF-1 and HIF-2 can slow tumor growth and enhance local control, and that suppressing HIF-1 can improve radiation treatment efficacy[126–130]. However, HIF-1-deficient cells may be more sensitive to changes in redox activity and glucose deprivation, suggesting a protective role in tumors under stress conditions. In hypoxic conditions, cancer cells may increase glycolytic rate, resulting in an extracellular acidic pH and increased therapy resistance[131–134].The production of lactate in hypoxic environments can increase due to HIF-1 and HIF-2 binding to the LDH-A promoter region in human pancreatic cancer cells. This lactate formation helps to scavenge ROS molecules and

has antioxidant characteristics[72,76,77,135,136]. However, lactate accumulation in cancer can lead to increased tumor aggressiveness by increasing epithelial-mesenchymal transition [137]. HIF-1 activation in tumor cells modifies the metabolic response to radiation by influencing lactate generation and mitochondrial function, leading to radiation resistance[138].

HIF-2 expression has been shown to be critical in promoting an aggressive phenotype and tumor progression in clear cell renal cell carcinoma (ccRCC) and neuroblastoma[139–141]. Additionally, radiation can promote HIF-1 stability, leading to its binding to the CXC-motif chemokine receptor 4 (CXCR4) promoter, causing non-small cell lung carcinoma (NSCLC) cells to become invasive and metastatic[142]. The regulatory mechanism of HIF-1 and HIF-2 regulating NSCLC responses to radiation therapy needs further investigation[143]. HIF-2 overexpression in cancer stem cells explains the radio-resistant phenotype of lung cancer, and it has a poor correlation with prognosis in radiation patients. HIF-1 and HIF-2 expression have distinct effects on patient prognosis and other clinicopathological aspects in various malignancies, including NSCLC[144].

2 Thesis outline

Given the complex, in part mutual interactions between hypoxia, HIF regulation, cellular metabolism and radiation sensitivity in particular with respect to hepatocyte physiology, we defined the following aims of our study:

1. Establishing a long-term culture method: Develop a reproducible and long-lasting culture method for transduced murine hepatocyte-derived cells (mHDC) as an *in vitro* model system, providing an essential tool for studying hepatocyte biology and exact function of HIF-1α. This aim addresses the need for a reliable and accessible model due to the limited availability of primary human hepatocytes and the rapid de-differentiation of rodent hepatocytes *in vitro*.
2. Investigating hypoxia and metabolic flux: Analyze the metabolic changes in response to hypoxia, examining the impact of HIF-1α deletion on cellular respiratory metabolism. This aim is intended to enhance our understanding of the molecular mechanisms underlying cellular adaptation to hypoxia and shed light on the role of HIF-1α in regulating metabolic processes.
3. Exploring the role of HIF-1α in ionizing radiation response: Examine the effects of HIF-1α knockout on cellular radiation response to gain insights into the involvement of this transcription factor in radiation-induced signaling pathways and DNA damage repair mechanisms. This objective aims to improve our understanding of the interplay between HIF-1α and ionizing radiation, potentially leading to the development of novel therapeutic strategies for radiation-related conditions.

3 Materials and methods

3.1 Materials

3.1.1 Technical equipment

Table 1: Utilized technical equipment

Device	Manufacturer
Analytic scale ABT 120-4	Kern (California, USA)
Biological irradiator X-RAD 320	Precision X-Ray (North Branford, USA)
Blotting chamber Trans-Blot®	Bio-Rad (Munich, Germany)
CellometerTM Auto T4	Nexcelom Bioscience (Lawrence, USA)
Centrifuge 5810 R	Eppendorf (Hamburg, Germany)
Centrifuge Mikro 220 R	Hettich Zentrifugen (Hettich, Germany)
Fusion-FX7 chemoluminescence documentation system	Peqlab (Erlangen, Germany)
Extracellular flux analyzer Seahorse XFe96	Agilent Technologies (California, USA)
C1000 Touch Thermal Cycler CFX96 Real-Time System	Bio-Rad (Munich, Germany)
Incubator	Memmert (Schwabach, Germany)
Hypoxic chamber	Toepffer Lab System (Göppingen, Germany), Baker Ruskinn (Leicestershire, United Kingdom)
Laminar-flow bench	Bio Flow Technik (Meckenheim, Germany)
Magnetic separation rack MagnaRack™	Thermo Fisher Scientific (Waltham, USA)
Microplate reader BioTec® Synergy™	BioTek (Bad Friedrichshall, Germany)
Take3 Micro-Volume Plate	BioTek (Bad Friedrichshall, Germany)
Orbital shaker MTS 2/4	IKA-Werke (Breisgau, Germany)
Microm HM 340E Microtome	Thermo Fisher Scientific (Waltham, USA)
Pipette controller ErgoOne® FAST	STARLAB (Hamburg, Germany)
Power supply PowerPac HC	Bio-Rad
Protein electrophoresis system	Bio-Rad (Munich, Germany)
Light Microscope ScanScope	Leica biosystems (Wetzlar, Germany)

Thermal cycler T100	Bio-Rad (Munich, Germany)
Vortexer VTL 3000 L	Heidolph (Schwabach, Germany)

3.1.2 Consumables

Table 2: Consumable material

Item	Manufacturer
0.1 µm filter	Sartorius
CASYcups	OMNI Life Science
Cell culture dishes	Sarstedt
Cell culture flasks	Sastedt
Centrifuge tubes	Sarstedt
Cryo tubes	Sarstedt
PVDF membrane	Roth
qPCR seal	4titude
Seahorse XF96 cell culture microplates	Agilent Technologies
Seahorse XF96 sensor cartridges	Agilent Technologies
6-well plates	Eppendorf
384-well qPCR plates	4titude
96-well plates	TPP

3.1.3 Kits and PCR oligonucleotides

Table 3: Utilized commercial kits

Kit	Manufacturer
BaseScope™ Assay Kit	ACDBio (Newark, USA)
Pierce™ BCA Protein Assay Kit	Thermo Fisher Scientific
Direct PCR Kit	highQu (Kraichtal, Germany)
Mouse acetylcholinesterase Assay Kit	Mybiosource (California, USA)

qPCR MasterMix for SYBR® Green I	Eurogentec (Liège, Belgium)
QuantiTect® Reverse Transcription Kit	Qiagen (Hilden, Germany)
RNeasy® Mini Kit	Qiagen (Hilden, Germany)
Seahorse XF Cell Phenotype Test Kit	Agilent Technologies
Seahorse XF Glycolysis Stress Test Kit	Agilent Technologies
Seahorse XF Mito Stress Test Kit	Agilent Technologies
SuperSignal West Femto Maximum Sensitivity Substrate	Thermo Fisher Scientific (Waltham, USA)
Trans-Blot® Turbo™ RTA Transfer Kit	Bio-Rad (Munich, Germany)

All oligonucleotides in table 4 and 5 were purchased from Sigma (USA).

Table 4: PCR primers used for cell genotyping

Primer	Sequence 5´-3´	fragment length [bp]	T_{ann} [°C]
Rosa26-Cre-ER for	TGAGCTACACCAGAGACGGA	120 (knock-in)	65
Rosa26-Cre-ER rev	TTGGCAGAACGAAAACGCTG		
mHIF-1α_E2seq for	CTAGTACTAGATAACCAGTG	1405 (wt)	50
mHIF-1α_E2seq rev	GGTAAACCAAAACAACTTAC	681 (E2 junction)	
mHIF-1α_flox for	GGAGCTATCTCTCTAGACC	200 (HIF-1α wt)	57
mHIF-1α_flox rev	GCAGTTAAGAGCACTAGTTG	250 (HIF-1$\alpha^{fl/fl}$)	
mHepc_ for	ATGATGGCACTCAGCACTCG	200	60
mHepc_rev	GGTATCGCAATGTCTGCCCT	250	

Table 5: Primer used for qPCR gene expression assay

Primer	Sequence 5´-3´	fragment length [bp]
RT_mHIF-1α for	GAAATGGCCCAGTGAGAAA	119
RT_mHIF-1α rev	CTTCCACGTTGCTGACTTGA	
RT_mGLUT-1 for	GGATCCCAGCAGCAAGAAGGT	81
RT_mGLUT-1 rev	TAGCCGAACTGCAGTGATCC	
RT_mPFK for	GAACTACGCACTTGACCAT	119
RT_mPFK rev	CTCCAAAACAAAGGTCCTCTGG	
RT_mHK2 for	CGGCCGTGCTACAATAGG	122
RT_ mHK2 rev	CTCGGGATCATGTGAGGG	

RT_mNOS3 for	CCTTCCGCTACCAGCCAG	
RT_ mNOS3 rev	CTCGGGATCATGTGAGGG	
RT_mBNIP3 for	CCCAGACACCACAAGATACCA	81
RT_mBNIP3 rev	CAGAGATCTTCACTGGATTGGCT	
RT_mB2M for	GGCTCACACTGAATTCACCC	102
RT_mB2M rev	ATGTCTCGATCCCAGTAGACG	

3.1.4 Chemicals

Table 6: Chemicals

Chemical	Manufacturer
Acrylamide solution (Rotiphorese® Gel 30)	Carl Roth
4-(2-hydroxyethyl)-1-piperazineethanesulfonic acid (HEPES)	Carl Roth
Ammonium persulfate (APS)	Carl Roth
Bovine serum albumin (BSA)	Carl Roth
Bromphenol blue	Carl Roth
Coomassie brilliant blue	Sigma-Aldrich
Collagen type I from rat tail	Sigma Aldrich
Crystal violet	Carl Roth
Dimethyl sulfoxide (DMSO)	Sigma-Aldrich
ECL™ Prime Reagent	GE Healthcare Life Sciences
Ethylendiaminetetraacetic acid (EDTA)	Sigma-Aldrich
Fetal Bovin Serum (FbS)	Gibco
Glutar aldehyde	Carl Roth
Hoechst 33342	Thermo Fisher Scientific
Non-fat dry milk	Carl Roth
Paraformaldehyde	Sigma-Aldrich
Sodium chloride (NaCl)	Merck Millipore
Sodium citrate	Carl Roth

Sodium dodecyl sulfate (SDS)	Carl Roth
Sodium pyrophosphate	Sigma-Aldrich
Tamoxifen	Sigma
Tetramethylethylenediamine (TEMED)	Carl Roth
Tetramethylrhodamine ethyl ester (TMRE)	Thermo Fisher Scientific
Trypsin-EDTA (0.05 %)	Biochrom
Tris(hydroxymethyl)aminomethane (Tris)	Carl Roth
Triton X-100	Sigma-Aldrich
Tween-20	Sigma-Aldrich
β-mercaptoethanol	Merck Millipore

3.1.5 Buffers and solutions

Table 7: Composition of buffers and solutions for protein analysis

Buffer/Solution	Components	Amount/Concentration
Agarose gel (3 %)	Agarose	3 %
	TAE	75 ml
RIPA lysis buffer	Tris HCl (pH 7.4)	50 mM
	NaCl	150 mM
	NP-40	1 % (v/v)
	sodiumdesoxycholate	0.5 % (w/v)
4x SDS sample buffer	Glycerol	40 % (v/v)
	Tris-HCl (pH 6.8)	240 mM
	SDS	8 % (w/v)
	Bromphenol blue	0.04 % (w/v)
	β-mercaptoethanol in H_20	10 % (v/v)
12 % SDS PAGE resolving gel (for 1 gel)	H_2O	3.4 mL
	Acrylamid (30 %)	7.5 mL
	Tris-HCl (1.5 M, pH 8.8)	3.8 mL
	SDS (10 %)	0.150 mL
	APS (10 %)	0.150 mL
	TEMED	0.006 mL

10 % SDS PAGE resolving gel (for 1 gel)	H2O Acrylamid (30 %) Tris-HCl (1.5 M, pH 8.8) SDS (10 %) APS (10 %) TEMED	5.9 mL 5 mL 3.8 mL 0.150 mL 0.150 mL 0.006 mL
5 % SDS PAGE stacking gel (for 1 gel)	H2O Acrylamid (30%) Tris-HCl (1 M, pH 6.8) SDS (10%) APS (10%) TEMED	3.4 mL 0.83 mL 0.63 mL 0.05 mL 0.05 mL 0.005 mL
10x SDS running buffer	Tris-HCl Glycine SDS in H_20; adjusted to pH 8.3	250 mM 192 mM 1 % (w/v)
10x Transfer buffer	Tris-HCl Glycine in H_2O; adjusted to pH 8.3	250 mM 192 mM
TBS-T	TBS Tween 20	1x 0.05 % (v/v)
TBS	Tris (pH 7.4) NaCl	20 mM 137 mM
TAE	Tris (pH 7.4) Acetic acid EDTA	40 mM 20 mM 1 mM
Blocking solution	Non-fat dry milk in 1x TBS-T	5 % (w/v)

Table 8: Composition of buffers and solutions for Caspase assay

Buffer/Solution	Components	Amount/Concentration
Caspase lysis buffer pH 7.3	Tris (pH 7.4) NaCl NP-40	50 mM 150 mM 1 % ‘(v/v)
Caspase substrate buffer	HEPES NaCl Saccharose	20 mM 100 mM 10 % (w/v)

	CHAPS	0.1 % (w/v)
	DTT	10 mM
	DEVD-AMC	66 µM
PBS	Tris (pH 7.4)	138 mM
	Na_2HPO_4	8.1 mM
	KCl	2.7 mM
	KH_2PO_4	1.5 mM
PFA pH 7.4	PFA	4 % (w/v)
	PBS	1x
	NaOH	1 M

Table 9: Composition of staining solutions for cell survival assays

Staining solution	Component	Amount/Concentration
Coomassie brilliant blue staining solution	Coomassie brilliant blue Methanol Acetic acid	0.05 % (w/v) 20 % (v/v) 7.5 % (v/v)
Crystal violet staining solution	Crystal violet in PBS	0.1 % (w/v)

Table 10: Composition of assay media for Seahorse XF cellular bioenergetics tests

Test	Component	Amount/Concentration
Mito stress test	Seahorse XF Base Medium Pyruvate L-glutamine D-glucose adjusted to pH 7.4	 1 mM 2 mM 10 mM
Glycolysis stress test	Seahorse XF Base Medium L-glutamine adjusted to pH 7.4	 2 mM

3.1.6 Antibodies

Table 11: Primary antibodies

Antibody	MW [kDa]	Origin	Catalog number, Manufacturer	Dilution
Albumin	66	mouse	A90-134A, Biomol	1:1000 (WB)

Cytokeratin 8 (+KRT18)	54	Guinea pig	810301, Origene	1:50 (IHC)
HIF-2α	110	rabbit	NB100-122, Novus (USA)	1:1000 (WB)
mHIF-1α	110	mouse	10006421, Cayman Chemical Company (USA)	1:1000 (WB) 1:100 (IHC)
PARP-1	116 89 cleaved	rabbit	9542S Cell Signaling (USA)	1:1000 (WB)
ß-actin	24	mouse	ab6276, abcam (UK)	1:6000 (WB)

Table 12: Secondary antibodies

Antibody	Host	Specificity	Catalog number, company	Dilution
IgG/HRP	goat	anti-mouse	P0447, Dako (Denmark)	1:3000 (WB)
IgG/HRP	goat	anti-rabbit	P0448, Dako (Denmark)	1:3000 (WB)
IgG Alexa 488	goat	anti-rabbit	A11070, Invitrogen (Germany)	1:500 (IF)
IgG Alexa 488	goat	anti-mouse	A11017, Invitrogen (Germany)	1:500 (IF)
IgG Alexa 488	goat	anti-Guinea pig	A11073, Invitrogen (Germany)	1:500 (IF)
IgG Alexa 594	goat	anti-mouse	A11005, Invitrogen (Germany)	1:500 (IF)

3.1.7 Software and tools

Table 13: Applied software and tools

Software	Developer
ImageJ	National Institutes of Health
Fusion- FX7	Peqlab (Erlangen, Germany)
GraphPad Prism 6	GraphPad Software Inc.
Wave Desktop 2.3	Agilent Technologies (Santa Clara, USA)
Open Comet v1.3.1	B. M. Gyori and G. Venkatachalam
QuPath-0.4.3	Pete Bankhead (open source)
ZEN imaging software	Carl Zeiss (Wetzlar, Germany)

3.2 Methods

3.2.1 Administration of tamoxifen to cultured murine hepatocyte derived cells

In collaboration with upcyte technologies GmbH (Hamburg, Germany), an attempt was made to establish cell cultures of differentiated murine hepatocytes with a deletion of HIF-1α. This was acieved by breeding C57BL/6-Gt(ROSA)26Sortm9(Cre/ESR1)Arte mice (Model 10471, Taconic Biosciences, Lille Skensved, DK)[145] that bear global tamoxifen inducible Cre recombinase expression to mice that carry loxP sites flanking exon 2 of HIF-1α[146]. The isolation of hepatocytes, lentiviral transduction and the establishment of cell culture were carried out commercially by upcyte technologies. Three Cre negative mice (mouse 17, 23, and 24) which served as controls and three heterozygous ROSA_CreERT2 mice (mouse 16, 21, and 22) were used to isolate the hepatocytes.

The hepatocytes were extracted from the liver using of a two-step collagenase perfusion technique. After isolating the hepatocytes, the cells were enumerated and plated at a subconfluent density that allowed for initial growth in cell culture vessels coated with collagen. The hepatocytes were then transduced with lentiviral particles containing the papilloma virus genes E6 and E7, which induced expression of the oncostatin M receptor[147]. The lentiviral particles were used at a multiplicity of infection (MOI) of 1 or 2, 24 hours after isolation. The resulting Upcyte® hepatocytes are not fully immortalized, as they retain their typical cobblestone morphology and form a confluent monolayer both before and after transduction. The Upcyte® mouse hepatocytes, following initial passages, were transferred to our laboratory, and carefully thawed using the recommended thawing medium. They were then seeded at a density of 10000 cells per square centimeter in flasks coated with collagen type I, and grown in a medium called Hepatocyte Culture Medium (HCM) that contained supplement A and B specifically tailored for mouse, 2 millimoles per liter of L glutamine (Upcyte), 100 units per milliliter of penicillin, 100 micrograms per milliliter of streptomycin, and 5% fetal bovine serum (FBS). The medium was changed every 2 to 3 days.

After achieving confluence, the cells were subcultivated by means of a trypsin/EDTA solution and then reseeded. To inhibit cell proliferation, the hepatocytes were grown in a High Performance Medium (HPM), which is a modified version of the standard culture medium (HCM), for a period of three days prior to conducting endpoint experiments. All of the culture, high performance, and thawing mediums were obtained from Upcyte Technologies. The cells were maintained under standard *in vitro* conditions, including a temperature of 37 °C, a carbon dioxide concentration of 5%, and a humidity level of 95% in a cell culture incubator. These

conditions were also applied to control cells during normoxic incubation. Hypoxia treatments were implemented by exposing the cells to low oxygen conditions in specialized chambers, (Toepffer Lab System from Goeppingen, Germany or the InVivo400 from Baker Ruskinn in Bridgend, UK) which contain a composition of 1% oxygen, 5% CO_2 and balance nitrogen. The Cre-mediated deletion of the HIF-1α gene was activated by the addition of 500 nM 4H-tamoxifen to the hepatocyte cultures for a period of three days. Following this induction, the tamoxifen was removed by replacing the culture medium and it was not used again at any subsequent time point.

3.2.2 Measurement of acetylcholine esterase

The colorimetric method (ELISA) was used to measure the concentration of acetylcholine esterase (AChE). The ELISA protocol was modified for use with 96-well plates, with a final assay volume of 100 µL. A commercial kit from Mybiosource was utilized for the detection of AChE. To initiate the experiment, mHDC cells were subjected to hypoxic and normoxic conditions for 48 hours. After the incubation period, the supernatant was collected from each sample, and 200 µL of the supernatant was transferred to a round-bottom 96-well plate. The plate was then centrifuged at 2500 rpm for 5 minutes at 4 °C to remove any cellular debris. Subsequently, AChE concentration was determined using a colorimetric approach by measuring the absorbance at 450 nm within a 10-minute timeframe. The absorbance readings were obtained using a microplate reader. Based on the absorbance values obtained from the samples, the concentration of AChE in each sample was calculated using the standard curve equation.

3.2.3 SDS-PAGE

Sodium dodecyl sulfate polyacrylamide gel electrophoresis (SDS-PAGE) was used to separate proteins based on their molecular weight. When the cells reached 70-80% confluence, cells were scraped off the culture dish and washed with ice-cold phosphate-buffered saline (PBS). The cells were lysed in radioimmunoprecipitation assay (RIPA) lysis buffer containing proteinase/phosphatase inhibitors (Cell Signaling) at 4 °C for 30 minutes. The lysate was centrifuged at 14000 rpm and 4 °C for 3 min and thereafter the supernatant was stored at -80 °C. Protein concentration was determined using the BCA Protein Assay Kit (Thermo Fisher Scientific), measuring absorbance at 562 nm after a 20-minute incubation at 37 °C. 30 µg of protein was mixed with SDS sample buffer and 1 µl of dithiothreitol (DTT), and then boiled for 5 minutes at 95 °C. A pre-stained protein standard was also added to each gel to follow

protein separation and to determine protein weight for detection. Proteins were separated on 5 – 12.5 % SDS-PAGE gels with 5 % stacking gels, which was then run in 1x SDS running buffer at 120 V for approximately 45 minutes.

3.2.4 Western blotting (WB)

Trans-Blot Turbo Transfer System with Trans-Blot® Turbo™ ready-to-assemble (RTA) Transfer Kit (Bio-Rad) was used to transfer proteins from SDS-PAGE gels onto methanol activated polyvinylidene fluoride (PVDF) membranes. Electrophoretic transfer was performed in 1x transfer buffer at 1.5 A for 1.5 hours. To block unoccupied binding sites, the PVDF membrane was incubated in blocking solution containing 5 % non-fat milk in Tris-buffered saline (TBS-T) for 1 h at room temperature. Incubation with appropriate dilutions of primary antibodies in 1x TBS-T containing 5 % BSA was carried out at 4 °C overnight. Following three washing steps with 1x TBS-T for 15 minutes, the membrane was incubated with horseradish peroxidase-conjugated secondary antibody 1:2000 dilution for 1 hour at room temperature. After three additional washing steps with 1x TBS-T, the HRP-conjugated secondary antibody was detected with SuperSignal West Femto Maximum Sensitivity Substrate (Thermo Fisher Scientific) using an FX7 chemiluminescence imager and Fusion software (Peqlab/VWR International, Erlangen).

3.2.5 Cell genotyping

3.2.5.1 DNA extraction

DNA extraction was performed with Direct PCR Kit (highQu, Kraichtal, Germany) by adding of 70 µl nuclease-free water, 10 µl protease buffer and 20 µl lysis buffer to the sample as instructed by the manufacturer. To prepare the lysate, the samples were incubated for 5 min at 75 °C on a shaker. Following the incubation, the protease was inactivated by heating the samples to 95 °C for 10 minutes. The samples were diluted 1:10 in nuclease-free water and stored at -20 °C.

3.2.5.2 PCR for genotyping

DNA fragment amplification was performed using the Direct PCR Kit (highQu, Kraichtal, Germany). The polymerase chain reaction (PCR) setting was as follows: 1x (initial denaturation: 2 min, 95 °C), followed by 40 cycles of: denaturation (15 sec at 95 °C), annealing (15 sec at 55-65 °C (depending on the length of the amplicon)) and extension (90 sec at 72 °C). For analysis of Cre-ER knockin cell genotype was used ROSA26-Cre-ER oligonucleotides.

mHIF-1α_flox primer were used to determine the status of heterozygous or homozygous HIF-$1\alpha^{flox}$ mice (Table 4).

3.2.5.3 Agarose gel electrophoresis

The PCR products were analyzed by DNA fragment separation on 1% agarose gels The DNA dye SYBR Green was added directly to the gel solution. Gel electrophoresis was performed in TAE buffer for 45 minutes at room temperature with 75 V. Then, the DNA amplicons were visualized using a Fusion-FX7 system (Peqlab).

3.2.6 RNA isolation

In purification of RNA from biological samples, the presence of ribonuclease made this procedure difficult. An important part of RNA isolation is to create an RNase-free environment and inactivate the RNases. Following 48 hours incubation in normoxia or moderate hypoxia, RNA isolation was performed using RNeasy® Mini Kit (Qiagen) according to the manufacturer's protocol. To prevent RNase contamination, disposable plasticware and sterile RNaseA-free reagents were used. RNA concentration was assessed using a Nanodrop spectrophotometer (Biotech).

3.2.7 cDNA synthesis

Generating complementary DNA (cDNA) from an RNA template, is a process termed reverse transcription (RT) which was performed as recommended by the manufacturer of QuantiTect Reverse Transcription Kit (Qiagen). The RT reaction mixture was prepared by combining 4 µl of 5X Reaction Mix, 2 µl of Maxima Enzyme Mix, 1 µg of the RNA template and nuclease-free water to a final volume of 20 µl. The mixture was gently mixed, centrifuged and then incubated for 10 min at 25 °C, followed by 15 min at 50 °C. The reaction was then terminated by heating at 85 °C for 5 min. The cDNA samples were subsequently stored at -20 °C for further analysis.

3.2.8 RT-qPCR

Real-time polymerase chain reaction (qPCR) monitors the amplification of a targeted DNA molecule during the PCR. One important difference between qPCR and normal PCR is the fluorescent reporter dye, which increases more rapidly in proportion to the target concentration in the cDNA. The RT-qPCR reaction mixtures were prepared according to the manufacturer's recommendations for MESA Green qPCR^{TM} Mastermix Plus for SYBR Assay (Eurogentec) (Table 14).

Table 14 : Composition of qRT-PCR reaction mixtures

Component	Volume
cDNA	5 µl (50 ng)
2x reaction buffer	10 µL
Primer forward	0.6µL
Primer reverse	0.6 µL
DEPC water	Total volum 20 µl

qRT-PCR was carried out using the C1000 Touch Thermal Cycle CFX96 Real-Time System (BioRad). The cycling conditions are shown in (Table 15).

Table 15: qRT-PCR cycling conditions

Step	Temperature	Time	Cycles
DNA polymerase activation	95 °C	5 min	1
Denaturation	95 °C	15 s	30
Annealing and extension	60 °C	1 min	30
Melting curve analysis	60-95 °C	+ 0.5 °C every 3 s	

RT_mB2M (ß2-microglobulin) was used as a housekeeping genebecause it is expressed more stably compared to other frequently used reference genes[148]. The normalized target gene expression was related to the ct value for B2M using the ΔΔct method. The logarithm base 2 of this value ($2^{-\Delta\Delta ct}$) was used to determine the expression fold change[149].

$$2^{-\Delta\Delta ct} = 2^{-(\Delta ct(GOF_{sample} - B2M_{sample}) - \Delta ct(GOF_{control} - B2M_{control}))}$$

3.2.9 BaseScope assay

BaseScope™ a novel in situ hybridization manual assay that enables the visualization of a specific RNA locus at the single-cell level through the use of a novel probe design strategy and a hybridization-based signal amplification system. This system simultaneously amplifies signals and suppresses background. Many of the steps in RNAscope are comparable to those in immunohistochemistry (IHC). The RNAscope method can be applied to archival formalin-fixed, paraffin-embedded (FFPE) tissue samples on glass slides, and the stained slides can be viewed using either a bright-field microscope (with chromogenic labeling) or an epifluorescent microscope (with fluorescent labels). The RNAscope approach enables multiplex detection for up to four target genes (limited by the number of spectrally discernible fluorescent dyes) (Figure 10).

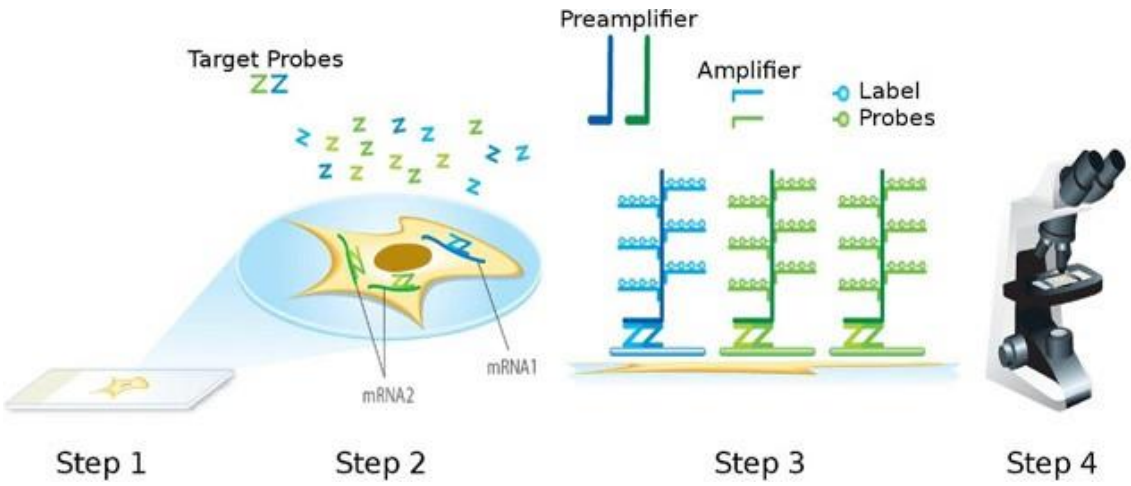

Figure 7: Schematic of the Basescope assay procedure. In step 1, cells or tissues are fixed and permeabilized to allow for target probe access. In step 2, target RNA-specific oligonucleotide probes (Z) are hybridized in pairs (ZZ) to multiple RNA targets. In step 3, multiple signal amplification molecules are hybridized, each recognizing a specific target probe, and each unique label probe is conjugated to a different fluorophore or enzyme. In step 4, signals are detected using an epifluorescent microscope (for fluorescent labelling) or standard bright-field microscope (for enzyme labelling)[150].

BaseScope assays were conducted following the supplier's guidelines provided by Advanced Cell Diagnostics, Newark, CA. Sections were cut at a thickness of 5 μm onto Superfrost Plus slides and left to dry overnight at room temperature (RT). Subsequently, the sections were baked at 60 °C for 1 hour before deparaffinizing in xylene (2 × 5 min) and ethanol (2 × 2 min), followed by drying through baking at 60 °C for 2 min. Pretreat 1 (hydrogen peroxide) was applied for 10 minutes at room temperature. Pretreat 2 (target retrieval) was performed for 15

minutes at 100 °C and Pretreat 3 (protease) was carried out for 30 min (for tissue sections) or 15 min (for cell pellets) at 40 °C, with two rinses in distilled water between pretreatments. Afterwards, BaseScope probes were utilized for 2 hours at 40 °C in a HybEZ oven, followed by incubation with reagents AMP0 (30 min at 40 °C), AMP1 (15 min at 40 °C), AMP2 (30 min at 40 °C), AMP3 (30 min at 40 °C), AMP4 (15 min at 40 °C), AMP5 (30 min at RT), and AMP6 (15 min at RT). The slides were rinsed with wash buffer (2 × 2 min) between each AMP incubation. Finally, the slides were incubated with Fast Red for 10 minutes at room temperature in the dark. Slides intended for sequential staining were kept in PBS at 4 °C overnight before proceeding to the next protocol. Slides that were not used for further staining were counterstained with Gill's hematoxylin, dried for 15 minutes at 60 °C, and mounted in VectaMount permanent mounting medium (Vector labs, Burlingame, CA).

3.2.10 Analysis of cellular energy metabolism

The Seahorse XF Extracellular Flux technology is a tool used for analyzing the metabolic activities of cells. It measures two crucial energy-generating pathways: glycolysis and mitochondrial respiration, by analyzing the extracellular acidification rate (ECAR) and the oxygen consumption rate (OCR). This technology enables the comparison of cellular metabolic responses under different conditions of basal and energetic stress.

3.2.10.1 Seahorse XF mito stress test

The Seahorse XF mito stress test measures mitochondrial function in cells by analyzing changes in the OCR in response to sequential injections of different respiration modulators (Figure 8). These modulators target various components of the electron transport chain (ETC) and are used to determine different parameters of mitochondrial function. The test begins by measuring basal respiration, followed by the addition of oligomycin, an inhibitor of ATP synthase (complex V). Next, FCCP (Carbonyl cyanide p-(trifluoromethoxy) phenylhydrazone), an uncoupler of oxidative phosphorylation, is added to collapse the inner membrane gradient and drive maximal oxygen consumption by complex IV. The maximal respiratory capacity is then calculated by subtracting the non-mitochondrial respiration from the FCCP OCR. Finally, rotenone, an inhibitor of complex I, and antimycin A, a complex III inhibitor, are added to determine the non-mitochondrial O_2 consumption. The mitochondrial reserve capacity is calculated as the difference between the maximal respiratory capacity and the basal respiration.

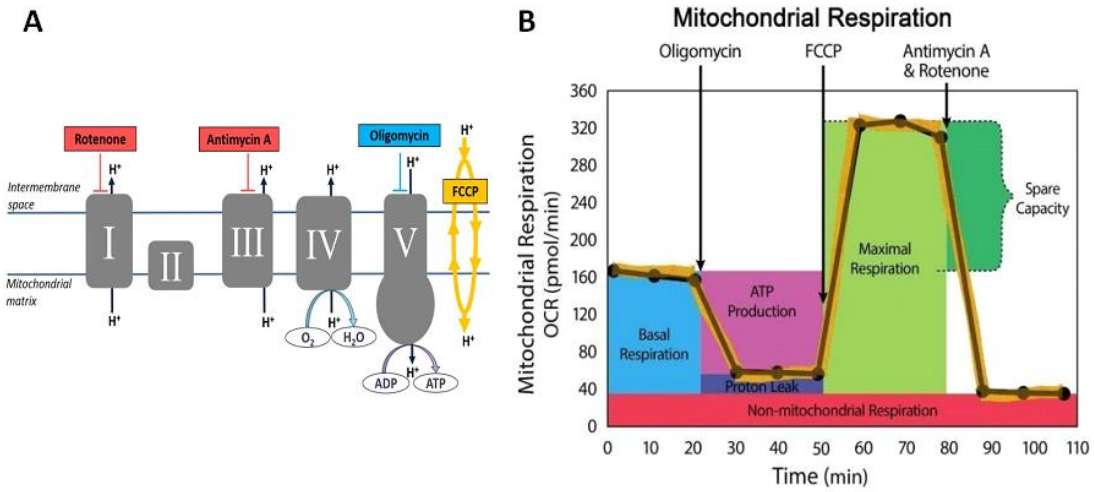

Figure 8: Seahorse XF mito stress test and their effect on the cellular profile of key parameters of mitochondrial respiration. A) Oligomycin inhibits ATP synthase (complex V), FCCP uncouples oxygen consumption from ATP production, antimycin A, and rotenone inhibit complexes I and III, respectively. B) Key parameters of mitochondrial function, in particular ATP production, non-mitochondrial respiration and maximal respiration, are assessed by measuring changes of the OCR in response to compound injection [151].

3.2.10.2 Seahorse XF glycolysis stress test

The Seahorse XF glycolysis stress test measures the key parameters of glycolytic flux in cells. In this test, cells are incubated in an assay medium without glucose or pyruvate, and then glucose is injected. As the cells break down glucose to produce pyruvate, ATP, NADH, water, and protons, the extrusion of protons is measured as an increase in the ECAR, which represents the glycolysis rate under baseline conditions. The addition of oligomycin, which shuts down mitochondrial ATP production, shifts cellular energy production to glycolysis and reveals the maximal ECAR, or glycolytic capacity. The glycolytic reserve is calculated as the difference between the glycolytic capacity and the glycolysis rate under baseline conditions. Finally, the injection of 2-deoxy-glucose, an inhibitor of glucose hexokinase, results in a decrease in ECAR, confirming that the protons produced and ECAR measured in the experiment were solely due to glycolysis (Figure 9).

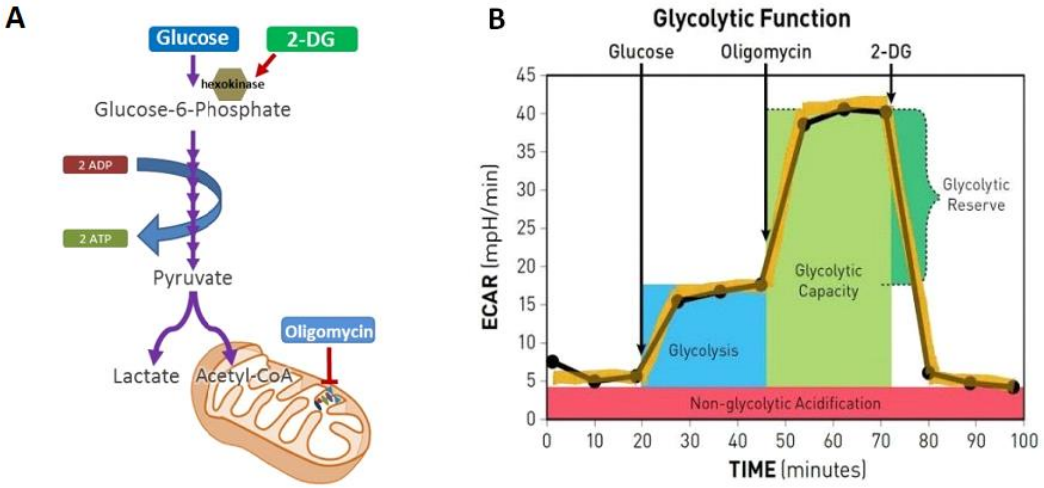

Figure 9: Seahorse XF glycolysis stress test profile of key parameters of glycolysis. A) Glucose fuels glycolysis and triggered in response to ATP synthase inhibitor oligomycin. 2-DG is a glucose analog and inhibits glycolysis by binding to glucose hexokinase B) Measuring glycolysis, glycolytic capacity, and enable calculation of glycolytic reserve and nonglycolytic acidification by sequential compound injections[151].

3.2.11 Irradiation of cells

Irradiation of cells was performed with an X-ray irradiating machine X-RAD 320 (Xstrahl Ltd), operated at 320 kV and 12.5 mA, with a 1.65 mm aluminium filter at a distance of 50 cm. The dose rate was ~2.76 Gy/min, with an effective photon energy of ~90 kV. For irradiation of hypoxic cells, the culture flasks and plates were tightly sealed with parafilm in the hypoxic chamber, transported to the irradiation machine and returned to the hypoxia chamber immediately after irradiation.

3.2.12 Cell viability and colony formation assay

To determine cell viability, MTT assays were performed as previously described[152]. In brief, 2 $\times 10^3$ cells were plated into 96-well plates, subjected to the intended treatment, and incubated for 72 h. The cells were then incubated with 3-(4,5-dimethylthiazol-2-yl)-2,5-diphenyltetrazolium bromide (MTT) for 4 h at 37 °C. Subsequently, the cells were lysed, and the absorbance of formazan was measured at 540 nm by photometry (Synergy HT, BioTek, Bad Friedrichshall, Germany). This assay is relies on the capacity of individual cells to form colonies after exposure to increasing doses of radiation. Cells were seeded in triplicates at

various concentrations in T25 flasks, incubated for 48 h in normoxia and then exposed to hypoxia for 24 hours. Subsequently, cells were irradiated with doses of 0-10 Gy and incubated in hypoxia for another 24 hours. After incubation, the cells were trypsinized and seeded in 6-well plates at various densities (100-6400 cells per well). They were then incubated for 8-10 days under normoxic conditions. Once sufficiently large colonies (≥50 cells) had formed in the untreated controls, the medium was removed. The cells were fixed by incubating them with 1% paraformaldehyde (PFA) for 10 minutes and permeabilized with 70% ethanol for 10 minutes. Subsequently, the cells were stained with Coomassie Brilliant Blue solution for 1 hour. After removing the staining solution, the plates were rinsed with water and allowed to dry. Colonies containing more than 50 cells were counted using ImageJ and a colony area plug-in. The plating efficiency (PE) was calculated according to numbers of counted colonies and seeded cells in untreated normoxia and hypoxia controls:

PE (%) = (counted cell number / seeded cell number) x 100

Survival fractions (SF) were quantified as number of colonies divided by the plating efficiency (PE) multiplied with the number of cells seeded.

SF = (counted colonies / (plating efficiency (PE) x seeded cell number))

3.2.13 Caspase assays

In order to quantify apoptosis, caspases-3 activity was measured as described previously[153]. The assay is based on the caspase-3 specific cleavage of a substrate called N-acetyl-Asp-Glu-Val-Asp (DEVD) from N-acetyl-Asp-Glu-Val-Asp-7-amino-4-methylcoumarin (DEVD-AMC), resulting in the release of a fluorescent compound called 7-amino-4-methylcoumarin (AMC). Therefore, the fluorescence intensity of AMC is directly proportional to the activity of caspase 3. To perform this assay, cells were lysed in caspase-3-lysis buffer containing 50 mM Tris (pH 7.3), 150 mM NaCl, and 1% (v/v) Nonidet P40. The protein content in the sample was determined using a BCA Kit (Thermo Fisher Scientific). Ac-DEVD-AMC (66 µM), was then added to a sample containing 10 µg of protein, along with 10 mM DTT in caspase-3 substrate buffer (20 mM HEPES (pH 7.3), 100 mM NaCl, 10 % (w/v) saccharose (w/v), 0.1 % (w/v) CHAPS). The mixture was incubated at 37 °C, and the level of caspase-3 activity was determined by measuring the fluorescence of AMC at 430 nm over a period of 4 hours, with measurements taken every 10 minutes. Western blotting was also used as an independent method to assess the cleavage of PARP, another marker of apoptosis. The results obtained from the linear range of the reaction were used for analysis.

3.2.14 Immunofluorescent staining

Cytokeratin 8 and 18 are considered specific markers for hepatocytes. To determine the expression of cytokeratin 8/18, approximately 80 % confluent cultures of hepatocytes were utilized. The cells were fixed with 1 % paraformaldehyde in phosphate-buffered saline for 10 minutes and then stained with primary antibodies diluted in 2 % bovine serum albumin for 1.5 hours. Subsequently, the cells were incubated with a 1:500 dilution of Alexa Fluor 488-conjugated fluorescent secondary antibodies. Counterstaining was performed using Hoechst 33342 (Sigma-Aldrich) at a concentration of 1.5 µM and the coverslips were mounted with mounting medium (Dako). Fluorescent images were captured using a Zeiss LSM 510 confocal microscope with a 63x/1.2 oil immersion lens (Carl Zeiss, Oberkochen, Germany) and were analyzed using the ZEN software package (Carl Zeiss). To evaluate nuclear DNA repair proteins, 10000 cells were plated on glass cover slides coated with collagen type I in a 24-well plate. The cells were then subjected to moderate hypoxia (1% O_2) for 48 hours and irradiated with 5 Gray (Gy). Samples were collected at various time points (1, 6 or 24 hours) following the same staining protocol as described above using the appropriate primary antibody. The confocal microscope used in this case was a Leica TCS-SP5 (Leica Microsystems, Wetzlar, Germany).

3.2.15 Neutral comet assay

The comet assay, also called single cell gel electrophoresis (SCGE), is a relatively simple, fast, and sensitive method for detecting DNA damage in individual eukaryotic cells. This assay can detect damage ranging from approximately 50 to 10000 breaks per diploid mammalian cell. Cells are first embedded in agarose, lysed, and then subjected to an electric field. Following this step, a fluorescent DNA binding dye is used to stain the cells. Damaged DNA moves towards the positive electrode, forming the tail of a "comet," while undamaged DNA remains in the head of the "comet." For this experiment, cells were seeded at a density of 1 x 10^5 cells/cm^2 and grown under either normoxia or hypoxia conditions for 24 hours. After exposure to irradiation, the cells were trypsinized and embedded in a low-melting agarose solution with a concentration of 1 % agarose. Cold lysis was then performed using the Olive protocol[154], which involves a lysis buffer containing 2 % sodium lauryl sulfate, 0.5 mM Na_2EDTA, 0.5 mg/ml proteinase K, and a pH of 8. The cells were stored overnight at 4 °C in the dark, followed by an additional 24-hour incubation in a high-salt buffer composed of 1.85 M NaCl, 0.15 M KCl, 5 mM $MgCl_2$, 2 mM EDTA, 4 mM Tris, and 0.5 % Triton X-100 at pH 7.5. Subsequently, the slides were incubated in cold electrophoresis buffer, consisting of 90 mM Tris buffer, 90

mM borate, 2 mM Na_2EDTA, and pH 8.5, at room temperature for 20 minutes. Electrophoresis was then performed at 20 V, 300 mA for 25 minutes, followed by staining with SYBR gold (Invitrogen). The analysis of the comets was conducted using the OpenCometv1.3.1 image analysis software. In this analysis, 50 cells were counted per slide, and two slides were counted per condition for each experiment (Figure 7).

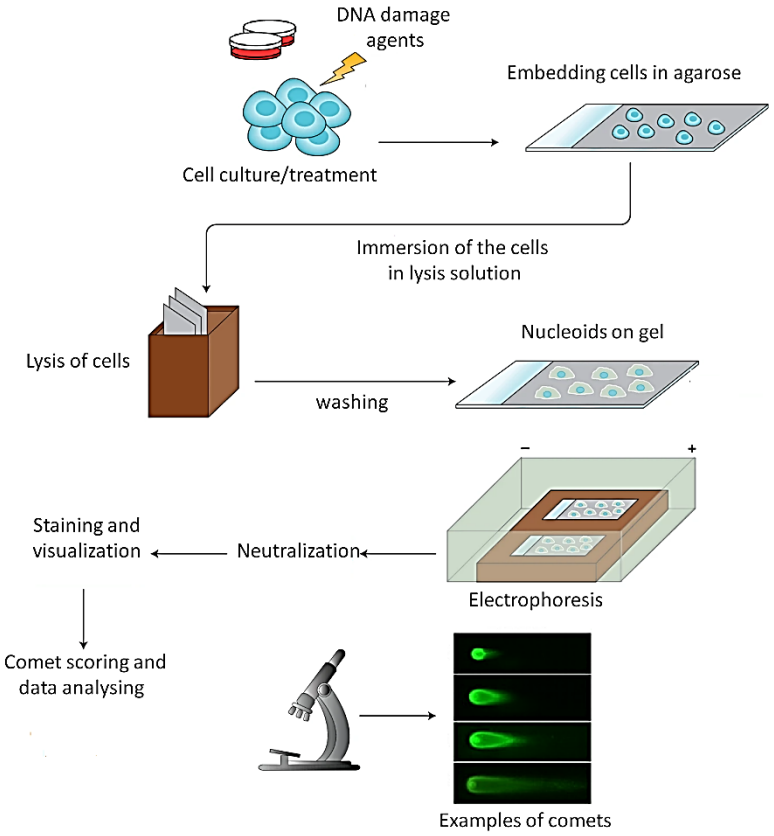

Figure 10: The comet assay procedure. 1) Mix cells with low melting agarose 2) Immobilize cells on a slide 3) Remove cellular proteins with lysis solution 4) Unwind and denature DNA 5) Electrophoresis 6) Stain with fluorescent dyes and image [155].

3.2.16 Statistical analysis

Experiments were typically conducted at least three times. The data were presented as mean ± standard deviation (SD), unless otherwise specified. All statistical analyses were performed using GraphPad Prism 6 software. The images were analyzed by ImageJ and QuPath 0.4.3 software. The groups of data were analyzed for statistical significance using either one-way or two-way analysis of variance (ANOVA) with a post-hoc Bonferroni test. Significance levels were indicated with asterisks as follows: *$p < 0.05$, **$p < 0.01$, ***$p < 0.001$, ****$p<0.0001$.

4 Results

4.1 *Establishment of mouse hepatocytes in vitro system*

4.1.1 Tamoxifen-inducible HIF-1α knockout mouse model

A global knockout of HIF-1α, wherein the gene is completely eliminated from all cells in the body, leads to embryonic death. This implies that the developing embryo cannot survive without the presence of HIF-1α. The precise mechanisms behind this lethality are not fully understood. However, it is likely that the absence of HIF-1α disrupts the normal processes of angiogenesis, metabolism, and cell survival, which are crucial for proper embryonic development[126,156]. To investigate the role of HIF-1α, previous studies in our group employed a conditional knockout approach. This approach involved crossbreeding two mouse strains:

Sequence of HIF-1α from exon 1 to exon 3

exon 1:

```
  1 cgcgaggact gtcctcgccg ccgtcgcggg cagtgtctag ccaggccttg acaagctagc
 61 cggaggagcg cctaggaacc cgagccggag ctcagcgagc gcagcctgca cgcccgcctc
121 gcgtcccggg ggggtcccgc ctcccacccc gcctctggac ttgtctcttt ccccgcgcgc
181 gcggacagag ccggcgttta ggcccgagcg agcccggggg ccgccggccg ggaagacaac
241 gcgggcaccg attcgccatg gagggcgccg gcggcgagaa cgagaagaaa aa
```

exon 2:

```
  1 gatgagttct gaacgtcgaa aagaaaagtc tagagatgca gcaagatctc ggcgaagcaa
 61 agagtctgaa gttttttatg agcttgctca tcagttgcca cttccccaca atgtgagctc
121 acatcttgat aaagcttctg ttatgaggct caccatcagt tatttacgtg tgagaaaact
181 tctggatgcc g
```

exon 3:

```
  1 gtggtctaga cagtgaagat gagatgaagg cacagatgga ctgtttttat ctgaaagccc
 61 tagatggctt tgtgatggtg ctaacagatg acggcgacat ggtttacatt tctgataacg
121 tgaacaaata catggggtta actcag
```

Sequence of HIF-1α from exon 1 to exon 3 after E2 excision

exon 1:

```
  1 cgcgaggact gtcctcgccg ccgtcgcggg cagtgtctag ccaggccttg acaagctagc
 61 cggaggagcg cctaggaacc cgagccggag ctcagcgagc gcagcctgca cgcccgcctc
121 gcgtcccggg ggggtcccgc ctcccacccc gcctctggac ttgtctcttt ccccgcgcgc
181 gcggacagag ccggcgttta ggcccgagcg agcccggggg ccgccggccg ggaagacaac
241 gcgggcaccg attcgccatg gagggcgccg gcggcgagaa cgagaagaaa aa
```

exon 3:

```
  1 gtggtctaga cagtgaagat gagatgaagg cacagatgga ctgtttttat ctgaaagccc
 61 tagatggctt tgtgatggtg ctaacagatg acggcgacat ggtttacatt tctgataacg
121 tgaacaaata catggggtta actcag
```

Figure 11: HIF-1α mRNA sequence exon 1 to exon 3 before and after exon 2 excision. From GenBank (AH006789.2) created by Alexandra Wolf.

C57/BL6 mice which a conditional knockout of HIF-1α[157] and ROSA26 CreERT$^{ki/ki}$ mice. The HIF-1α $^{fl/fl}$ mice carried loxP sites flanking the second exon, which encodes the helix-loop-helix/PAS motif necessary for DNA binding and dimerization with ARNT following transcriptional activation (Figure 11).

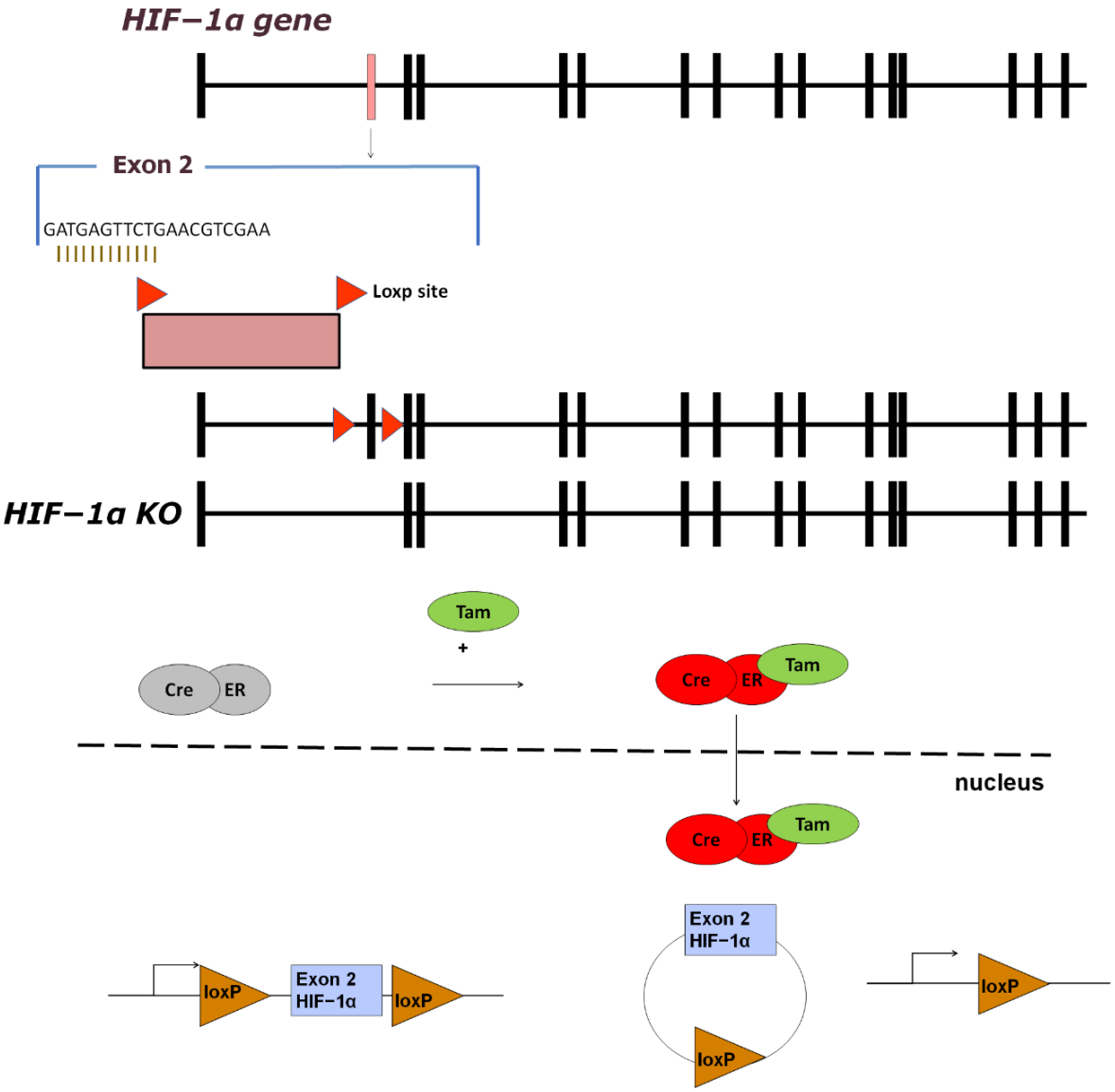

Figure 12: Developing a Conditional Knockout Strategy for Hif1a. Mice were used which carry LoxP sites flanking exon 2 (E2) of HIF-1α[146]. Recombination was achieved by inducing the expression of Cre recombinase through tamoxifen administration, utilizing the ROSA26_CreERT2 locus. The deletion of exon 2 led to the functional impairment of HIF-1α, preventing its binding to DNA, and subsequently affecting the interaction with HIF-1β[158].

The Cre-ER$^{ki/ki}$ mice carried the knock-in (ki) mutation of the Cre recombinase fused to the mutated estrogen receptor, which can be activated by the estrogen receptor ligand tamoxifen.

Consequently, the application of tamoxifen induced E2 excision, thereby preventing the functional activation of HIF-1α (Figure 12).

4.1.2 Isolation of mouse hepatocytes from HIF-1α knockout mice

In collaboration with Upcyte Technologies, transformed hepatocyte cultures were established using mice generated by our group. The mice were transferred to Upcyte Technologies, where they were anesthetized with ketamine and xylazine via intraperitoneal injection. The livers were then perfused with collagenase and EGTA through the vena cava inferior and portal vein. The resulting liver tissues were manually filtered using a cell strainer. From these preparations, murine hepatocytes were isolated from three HIF-1α $^{fl/fl}$ C57/BL6 mice that were negative for Cre (mouse 17, 23, and 24) serving as controls. Additionally, hepatocytes were isolated from three Cre-positive HIF-1α $^{fl/fl}$ C57/BL6 mice (mouse 16, 21, and 22), which were intended to have HIF-1α deleted upon tamoxifen treatment (Table 16). After the isolation procedure, the cells obtained were counted and 30000 viable cells were seeded per cm^2 in William's E supplemented with 10 % FBS, 2 mM L-glutamine, 1 % penicillin/streptomycin, and 100 nM dexamethasone. For each mouse, three 25 cm^2 flasks were seeded, resulting in a total of 18 cell culture flasks. To remove non-adherent cells, the medium was replaced after 3.5 hours, and the flasks were incubated overnight at 37 °C and 5 % CO_2. The cells were examined under a microscope and displayed typical hepatocyte morphology along with advanced spreading and adhesion. The medium was then changed to Hepatocyte Growth Medium (HGM), which resulted in the formation of a confluent monolayer of cells with a typical hepatocyte morphology.

Table 16: Generated upcyte donors and corresponding animal characteristics

Donor no.	Sex	Age	Genotype	Samples
16	Male	11 weeks	HIF fl/fl Cre+	Control, MOI1, MOI2
17	Male	11 weeks	HIF fl/fl Cre-	Control, MOI1, MOI2
21	Female	11 weeks	HIF fl/fl Cre+	Control, MOI1, MOI2
22	Female	11 weeks	HIF fl/fl Cre+	Control, MOI1, MOI2
23	Female	11 weeks	HIF fl/fl Cre-	Control, MOI1, MOI2
24	Female	11 weeks	HIF fl/fl Cre-	Control, MOI1, MOI2

The resulting cells were counted and seeded in collagen-coated cell culture vessels with hepatocyte growth medium to allow for initial growth. Lentiviral vectors carrying proliferation

inducing genes, were introduced to the cells at MOI 1 and 2, 24 hours after isolation. The hepatocytes maintained their typical cobblestone morphology and formed a confluent monolayer prior to transduction, as observed in (Figure 13).

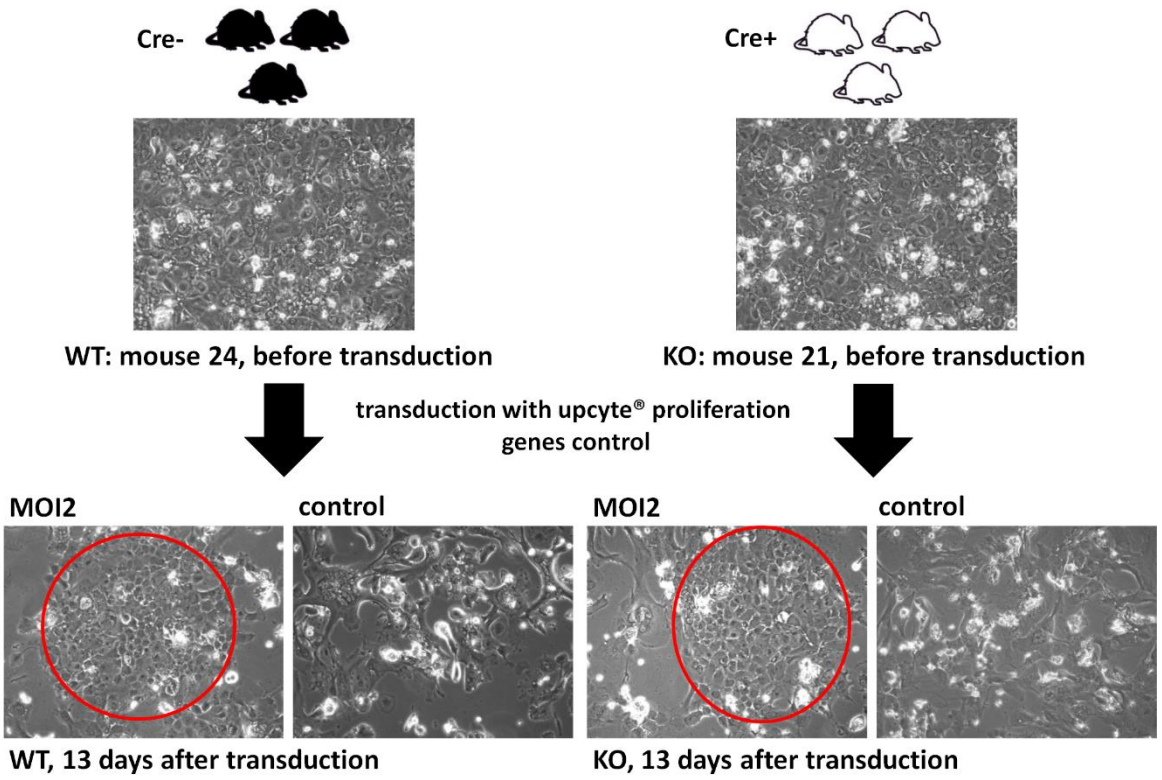

Figure 13: Isolation and upcyting of mouse hepatocytes. Isolated mouse hepatocytes maintained their typical cobblestone morphology and a confluent monolayer before transduction (images provided by upcyte technologies)**.**

4.1.3 Morphological and functional profiling of mHDC

To establish a functional *in vitro* system of murine hepatocytes, it is crucial to ensure that the cultured cells accurately mimic the morphology of hepatocytes observed *in vivo*. Upon transfer of the isolated hepatocytes to our laboratory, we observed a characteristic polygonal morphology with rounded nuclei and a granular cytoplasm, indicating the presence of regular and flat cells (Figure 14). In addition to morphological features, the functional aspects of the hepatocytes in the *in vitro* system should also align with their *in vivo* counterparts. This includes their ability to synthesize essential proteins and enzymes and maintain key metabolic pathways. To assess this, we examined the expression of specific genes that serve as markers for the hepatocyte phenotype. Additionally, we investigated the functional activity of the cell lines by analyzing the secretion of serum proteins, such as albumin and acetylcholinesterase, which are

normally produced by hepatocytes. Western blotting confirmed the production of albumin by all cell lines (Figure 15A). The analysis revealed similar levels of albumin production across the different cell lines, with no significant differences in the intensity of the albumin band.

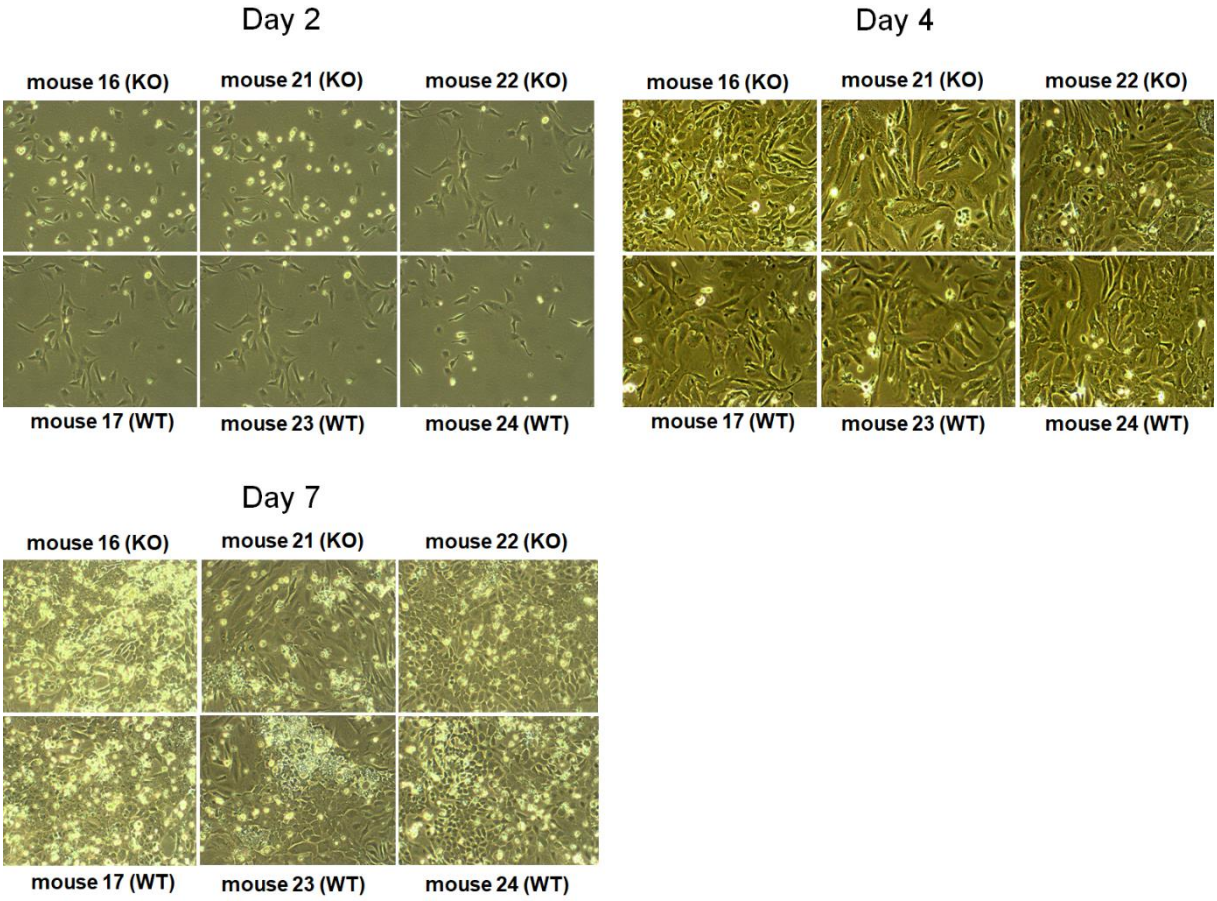

Figure 14: Phase contrast microscopy of nearly confluent cultures of mHDC monolayers. mHDC images at day 2, 4 and 7 by magnification 100x.

Acetylcholinesterase is a serine hydrolase enzyme that catalyzes the breakdown of acetylcholine into choline and acetic acid. It is primarily found at neuromuscular junctions and cholinergic nerve synapses in the central nervous system, where it terminates synaptic transmission by rapidly hydrolyzing acetylcholine. In addition to its role in neurotransmission, hepatocytes are known to produce acetylcholinesterase, which is secreted into the bloodstream. In the liver, acetylcholinesterase plays a role in the clearance of acetylcholine from the blood and the detoxification of certain chemicals. It exists in several molecular forms, including tetramers, dimers, and monomers. The secretion of acetylcholinesterase into the cell culture media of our hepatocyte-derived cells was analyzed using a mouse acetylcholinesterase enzyme-linked immunosorbent assay (ELISA). The results confirmed that all cell lines

exhibited acetylcholinesterase secretion (Figure 15B), which varied likely due to differences in cell density and was not caused by tamoxifen or hypoxia.

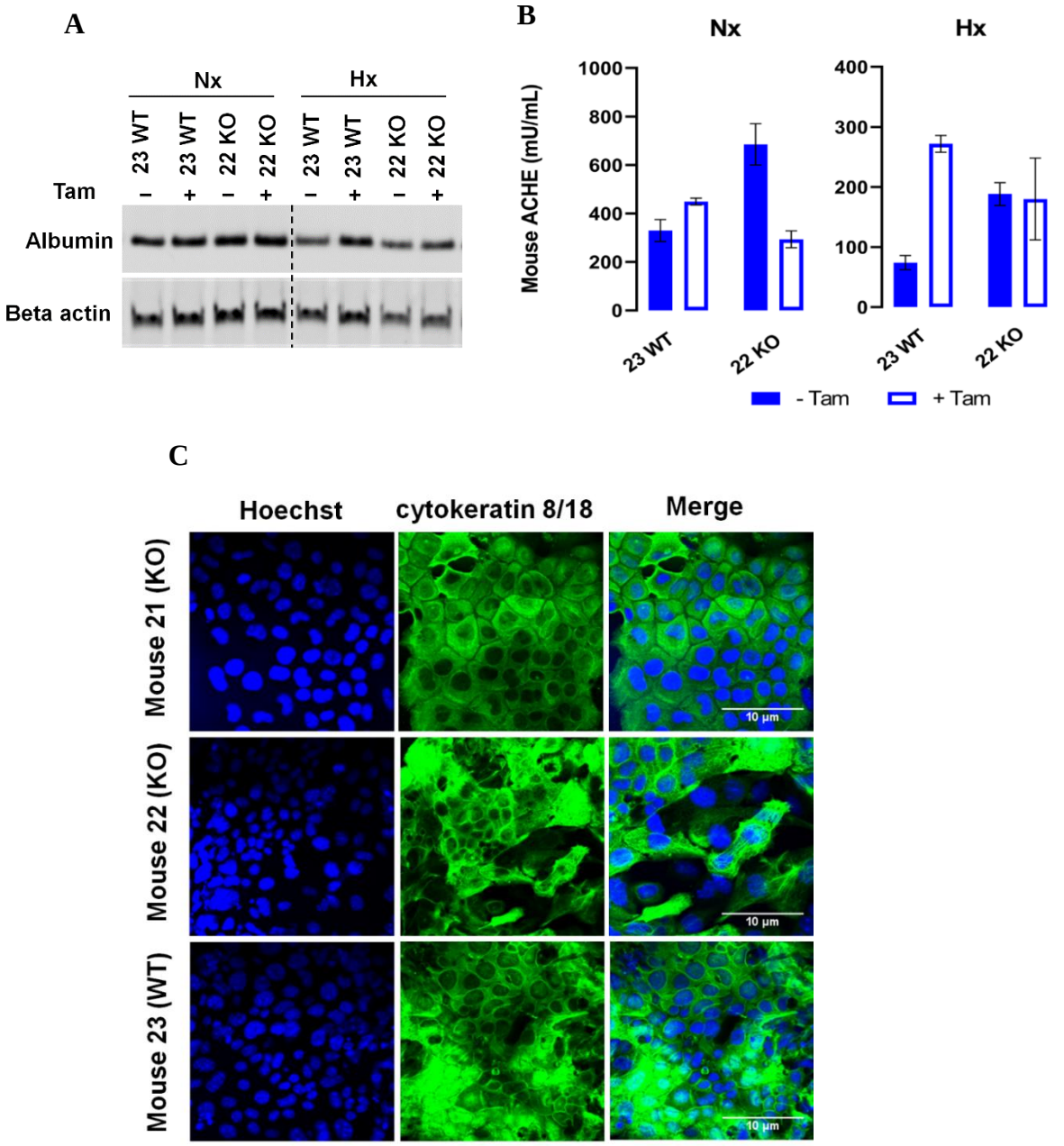

Figure 15: Characterization of mHDC differentiation. A) Protein lysates from mHDC were subjected to Albumin Western blot analysis. (30 µg per lane was loaded onto the gel. Hypoxic incubation lasted for 24 hours). Beta-actin was used as a loading and protein transfer control. B) ELISA was performed to assess the secretion of murine acetylcholine esterase in the cell culture media of mHDC. C) Immunofluorescent staining was conducted to evaluate the expression of CK8/CK18. Hoechst33342162 was used to counterstain the cell nuclei[158].

Cytokeratins are a group of intermediate filament proteins that form part of the cytoskeleton in epithelial cells, including hepatocytes. Specifically, cytokeratins 8 and 18 are expressed in hepatocytes and are commonly used as markers to identify hepatic differentiation and assess liver function. These proteins are essential for maintaining the structural integrity of hepatocytes and are involved in various cellular processes such as cell signaling, metabolism, and apoptosis.

Immunohistochemical staining for cytokeratins 8 and 18 is a widely used method for detecting and quantifying hepatocyte differentiation and function *in vitro* and *in vivo*. Their expression can be affected by various factors, including disease, inflammation, and drug toxicity, making them useful biomarkers for evaluating liver function and disease progression. Immunohistochemistry analysis showed positive expression of cytokeratins 8 and 18 antibodies in all isolated cells, indicating their similarity to hepatocytes (Figure 15C).

4.1.4 Cell genotyping

As mentioned earlier, a conditional knockout of the Hif1a gene was created by introducing Cre recombinase sites (loxP) between exon 1 and exon 3 of the Hif1a gene[146]. To confirm the successful tamoxifen (Tam) treatment, which is essential for the knockout, the mHDC cells were established, characterized, and treated with tamoxifen. To validate the Tam treatment, an end-point PCR was conducted using the ROSA26-Cre-ER primer pair specific for Cre-ER genotyping. This primer pair generates a 120 bp fragment when Cre-ER is present in both knock-in and wild-type cells (Cre(ki): cell lines 16, 21, 22). Conversely, in the absence of Cre-ER in wild-type cells (Cre(-)): cell lines 17, 23, 24), no amplicon is produced.

To confirm the excision of exon 2 in HIF-1$\alpha^{fl/fl}$ E2 after tamoxifen administration, genotyping was performed using the mHIF-1α_E2seq primer pair. The forward primer of this primer pair binds to the sequence in intron 1 while the reverse primer binds to intron 2 of HIF-1α. The PCR results obtained before Tam administration showed the presence of an amplicon of approximately 1400 bp in cell lines 16, 21, and 22. However, after treatment with Tam, the PCR product size in these cell lines was approximately 700 bp shorter, indicating the successful deletion of exon 2. These findings confirm that Tam application induced E2 excision in the HIF-1$\alpha^{fl/fl}$ Cre ERki/wt mice, thus validating the use of this knockout model for further studies.

During the course of this study, unexpected results were observed in the PCR genotyping assays, raising questions about the reliability of our experimental system. Specifically, in the genotyping PCR using the mHIF-1α_E2 seq primer pair, a shorter PCR fragment was observed in some samples that were not expected to undergo exon 2 excision. This was particularly puzzling because exon 2 excision is known to occur only in cells that express Cre recombinase, which is under the control of the tamoxifen-inducible Cre-ER promoter in our system. Surprisingly, the shorter fragment was also observed in some wild-type cells lacking the Cre-ER transgene, suggesting a potential issue with the PCR assay itself.

To address this problem, several possibilities were considered. Firstly, there might have been a technical error during the PCR assay, leading to the formation of non-specific PCR products or primer-dimer artifacts, which could have affected the interpretation of the results. Alternatively, the presence of the observed shorter fragments may indicate a rare, spontaneous event of exon 2 excision that occurred independently of the tamoxifen-induced Cre-ER activity. However, this seems unlikely considering the low frequency of spontaneous excision events and the fact that the shorter fragment was also observed in some wild-type cells lacking the Cre-ER transgene. Another possibility is the presence of a heterozygous loxP allele in some cells, which could have resulted in a mixed population of cells with and without the exon 2 deletion. In support of this, an analysis of the loxP allele using a different set of primers revealed that one of the parents was heterozygous for the lox-flanked allele of HIF-1α. This finding provides a plausible explanation for the presence of the shorter fragment in some samples (Figure 16).

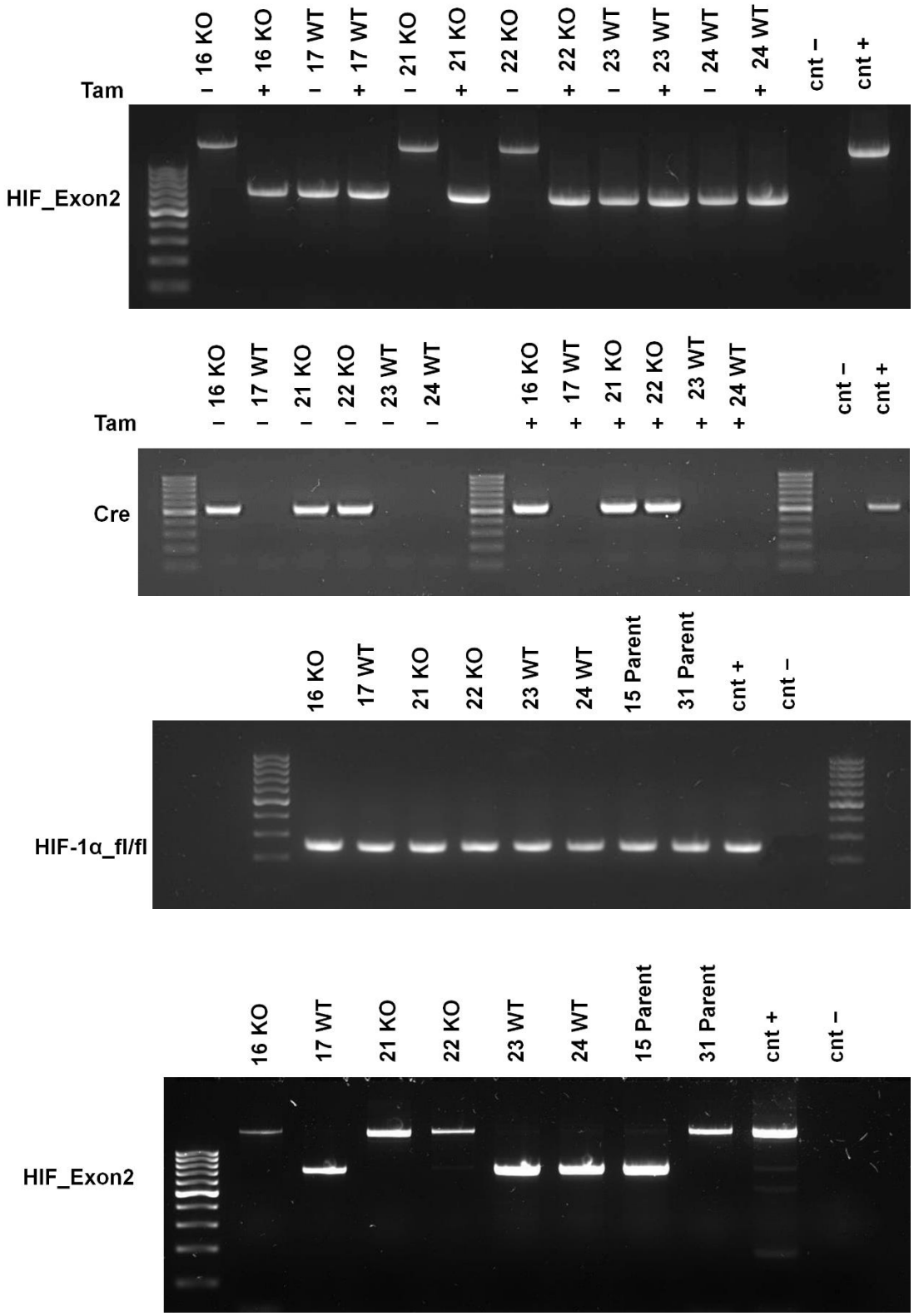

Figure 16: Genotyping phenomenon. Cells with Cre-ER$^{ki/wt}$ (Cre(ki)) genotype had the shortened fragment of HIF-1α PCR after treatment with Tam. Cre-ER$^{wt/wt}$ mice (Cre(-)) demonstrated an unchanged long fragment of HIF-1α without E2 excision (+E2).

4.1.5 Analyzing the efficacy of inducible HIF-1α knockout

To evaluate the effectiveness of the inducible knockout of HIF-1α on a protein level, we conducted a Western blot analysis (Figure 17A). The objective was to determine the impact of removing exon 2 in HIF-1α, which was expected to cause a frame shift in the gene sequence and premature termination of translation due to the presence of a stop codon at the beginning of exon 3. Our observations revealed that under hypoxic conditions (HX, 1 % O_2), cells expressing Cre recombinase exhibited a truncated form of HIF-1α, lacking the DNA binding domain as anticipated. This shortened form of HIF-1α was inactive, confirming the effectiveness of the knockout. Tamoxifen-treated cells showed no detectable levels of full-length HIF-1α. In addition, we examined the expression of HIF-2α in the cell lines and found that all the hepatocyte-derived cells (mHDC) expressed HIF-2α.

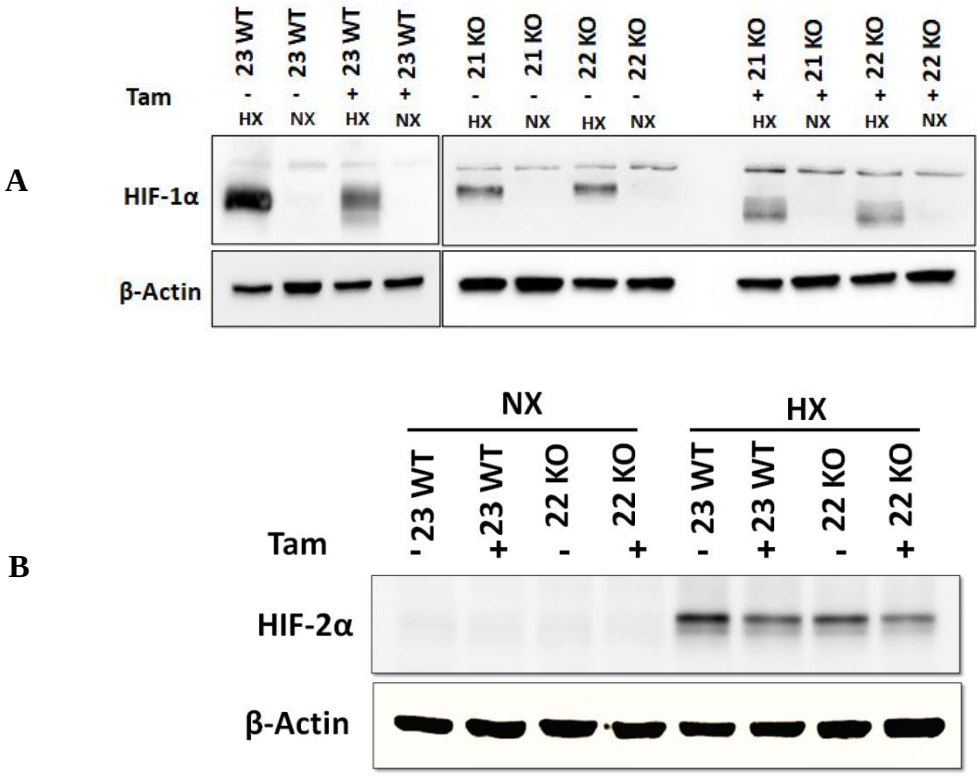

Figure 17: Protein expression of HIF-1α (A) and HIF-2α (B) in mHDC analyzed by Western blotting. Tamoxifen (Tam) was used to induce HIF-1α knockout (KO). The cells labeled as "23 WT" are Cre negative, indicating that Tam does not induce HIF-1α KO in these cells. The Cre-positive cell lines "21 KO" and "22 KO" express a shorter non-functional form of HIF-1α after Tam treatment. The cells were incubated for 4 hours under either normoxic (NX) or moderately hypoxic conditions (HX, 1% O_2). Beta actin was used as a loading control to ensure equal loading and transfer[158].

Furthermore, its expression levels were induced during hypoxic conditions, aligning with expectations. These results demonstrate that the knockout of HIF-1α did not affect the expression of HIF-2α in the cell lines (Figure 17B). To further investigate the effectiveness of the inducible knockout of HIF-1α, we generated complementary DNA (cDNA) from the hepatocyte-derived cells and performed quantitative polymerase chain reaction (qPCR) to quantify the mRNA levels of HIF-1α and its target genes BNIP3, PFK, NOS3, and GLUT-1 in both knockout and control cells. The results indicated a significant downregulation of the mRNA levels of all four target genes in the knockout cells. Furthermore, these genes were no longer responsive to hypoxic conditions (Figure 18). The downregulation of these genes in the knockout cells suggests that HIF-1α plays a critical role in the regulation of the hypoxic response in these cells. Moreover, it confirms that the inducible knockout of HIF-1α effectively suppressed the expression of its target genes.

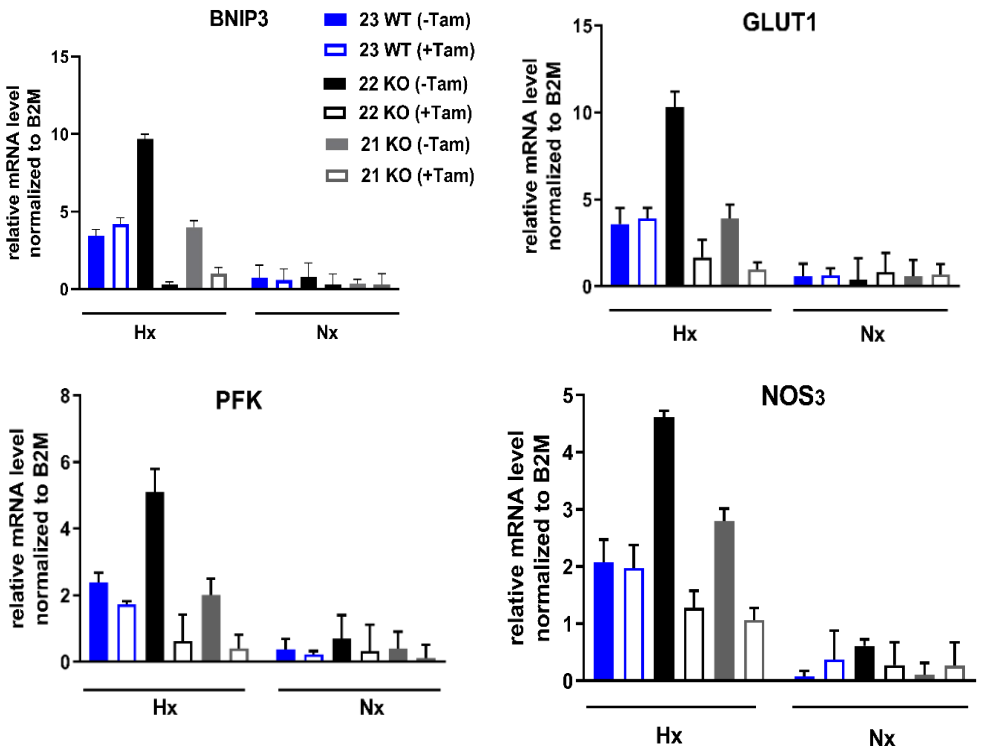

Figure 18: RT-qPCR Analysis of HIF-1α Target Gene mRNA Expression in mHDC Cells. mHDC cells were cultured overnight under normoxic conditions or exposed to hypoxia (1% O_2). The mRNA levels of HIF-1α target genes BNIP3, GLUT-1, PFK, and NOS3 were measured using qPCR and normalized to the mRNA levels of the reference gene ß2-microglobulin (B2M)[158].

To assess the efficacy of HIF-1α knockout, we employed a novel RNA in situ hybridization technique called BaseScope assay. This advanced method allows for the identification of exon

junctions in formalin-fixed paraffin-embedded (FFPE) tissue, offering morphological context. Remarkably, only a single zz probe designed specifically for the target exon junction is required for detection. In our study, we focused on exon 2 of HIF-1α, which is selectively deleted in the HIF-1α$^{fl/fl}$Cre-ER$^{ki/wt}$ allele upon tamoxifen treatment. To facilitate our analysis, we designed three high-sensitivity in situ hybridization probes. The first probe served as a control, targeting an exon junction present in all HIF-1 transcripts (exon junction 3/4). The second probe was designed to detect the exon junction with exon 2 (exon junction 1/2), while the third probe was designed to detect the exon junction with exon 2 skipping (exon junction 1/3) (Table 18).

Table 17: Exon junction-specific single-pair probes

Exon junction	Specificity	
E1E2	no E2 excision	WT
E1E3	E2 excision	KO
E3E4	positive control	positive control

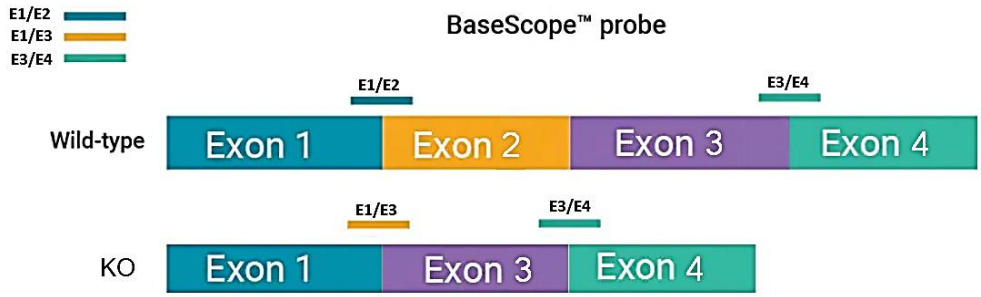

Figure 19: Probe design for the detection of DELΔ2 using the BaseScope™ assay. One ZZ probe (Green), designed to detect the junction between exons 3 and 4, is considered common and will detect both wild-type and DELΔ2 mRNA. A second ZZ probe (Blue) is designed to detect the junction between exons 1 and 2 and will detect only DEL mRNA containing exon 2 (wild type). A third ZZ (Orange) probe is designed to detect the junction between exons 1 and 3 and will detect only DEL exon 2 skipped mRNA (METΔ2). The 3 probes are tested in parallel.

In addition to the qualitative analysis, we employed a macro within the open-source software CellProfiler[159], to enable unbiased quantification of the signals. This pipeline, readily available online, identifies FastRED signals above a predetermined threshold and assigns them to the nearest DAPI-positive nuclei (Figure 20). By combining the BaseScope assay with the CellProfiler pipeline, we successfully detected and quantified the signals from the three probes in both knockout and control cells. As anticipated, the probe designed for the exon junction with exon 2 (exon junction 1/2) was not detected in the knockout cells, affirming the efficiency of the HIF-1α knockout.

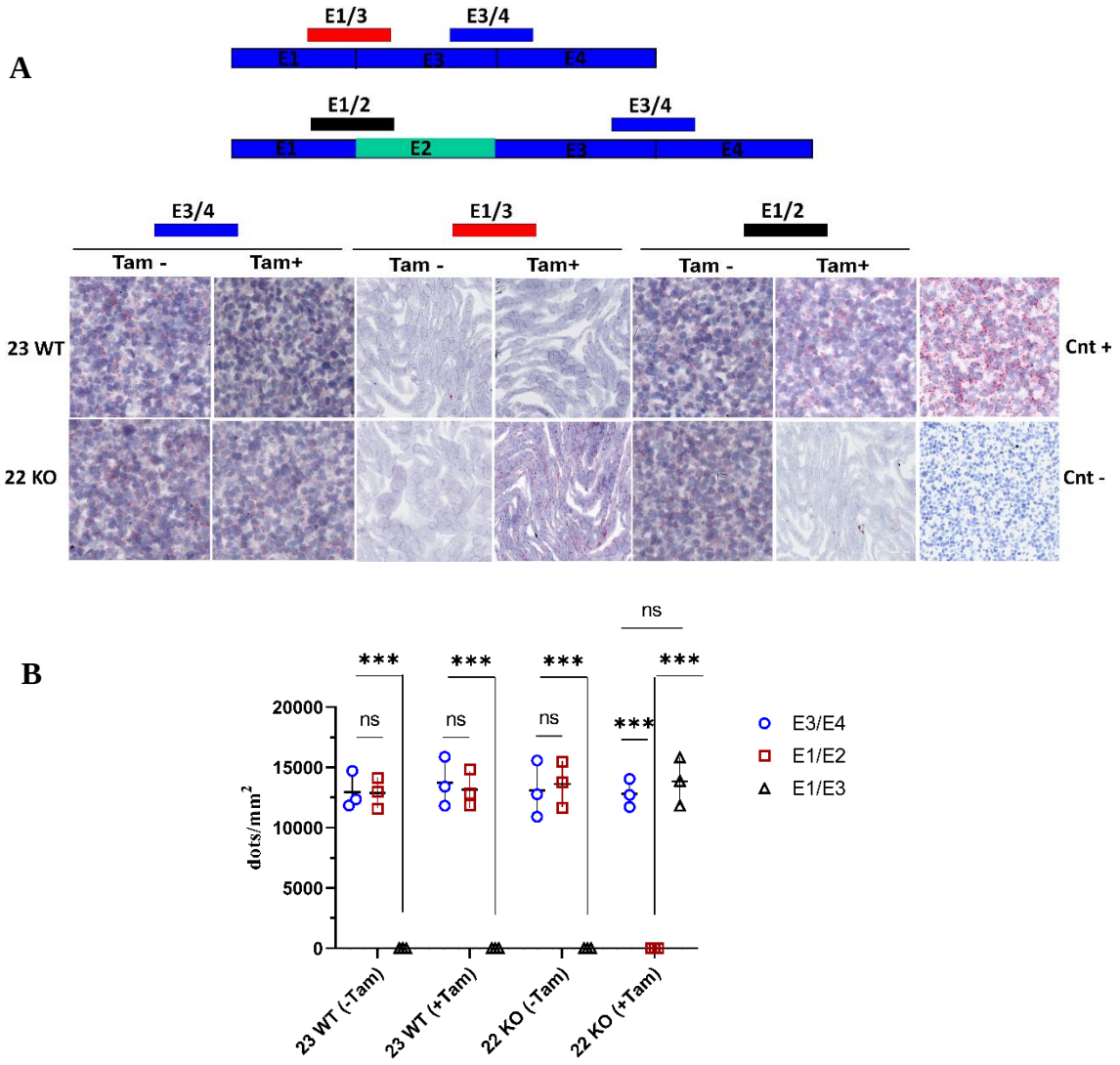

Figure 20: Detection levels for independent probes targeting distinct exon junctions. Expression analysis at a cellular level in the mHDC indicates that approximately 90% of cell nuclei are labeled by single pair E3/E4 probes, as was expected in all cell lines. The signals on sections from WT cells were dramatically higher than in sections from HIF1- KO cells using probes that target the deleted exon 2. ***p<0.001.

Conversely, the probe designed for the exon junction with exon 2 skipping (exon junction 1/3) was detected in the knockout cells. Additionally, the control probe was detected in both the knockout and control cells, indicating the assay's specificity and the presence of HIF-1 transcripts. These findings provide further substantiation for the effectiveness of the inducible knockout of HIF-1α while also showcasing the applicability of the BaseScope assay in detecting and quantifying exon junctions.

4.2 Metabolic Profiling

4.2.1 HIF-1α deficiency alters mitochondrial metabolism

The study aimed to investigate the relationship between hypoxia and metabolic flux and to determine the impact of HIF-1α deletion on cellular respiratory metabolism. In order to accomplish this, we measured the oxygen consumption rate (OCR) and extracellular acidification rate (ECAR) of mHDC cells using the Mito Stress Test Kit. The results were then normalized to Hoechst 33342 fluorescence units (FU) 24 hours after exposing the cells to hypoxia. OCR serves as an indicator of oxidative phosphorylation, which is the process by which cells produce ATP through the electron transport chain in mitochondria. On the other hand, ECAR is an indicator of glycolysis, which is the process by which cells break down glucose to generate ATP in the absence of oxygen. To evaluate the metabolic potential of the cells, we simultaneously measured OCR and ECAR under both basal and energetically stressed conditions.

To assess glycolysis, we inhibited ATP synthase using the oligomycin (1 µM) and introduced the mitochondrial uncoupler FCCP (2 µM) to drive a compensatory increase in glycolysis and reveal the maximum capacity of oxidative phosphorylation, respectively. At specified time points, we also utilized electron transport chain inhibitors such as antimycin A and rotenone (0.5 µM). The results indicated that hypoxia caused a significant decrease in OCR in control cells, suggesting a shift towards glycolysis as the primary ATP source. However, HIF-deficient cells did not exhibit this metabolic switch and maintained high levels of OCR even under hypoxic conditions. These findings suggest that HIF-1α is crucial for the metabolic adaptation to hypoxia by promoting the switch to glycolysis. Regarding ECAR, the absence of HIF-1α proteins did not lead to changes in ECAR regulation under normoxic conditions. However, knockout cells demonstrated a significant reduction in basal ECAR compared to wild-type cells. This decrease in glycolytic activity, as reflected by the reduction in ECAR, potentially affects pH levels or lactic acid production when compared to wild-type cells (Figure 21 A-D).

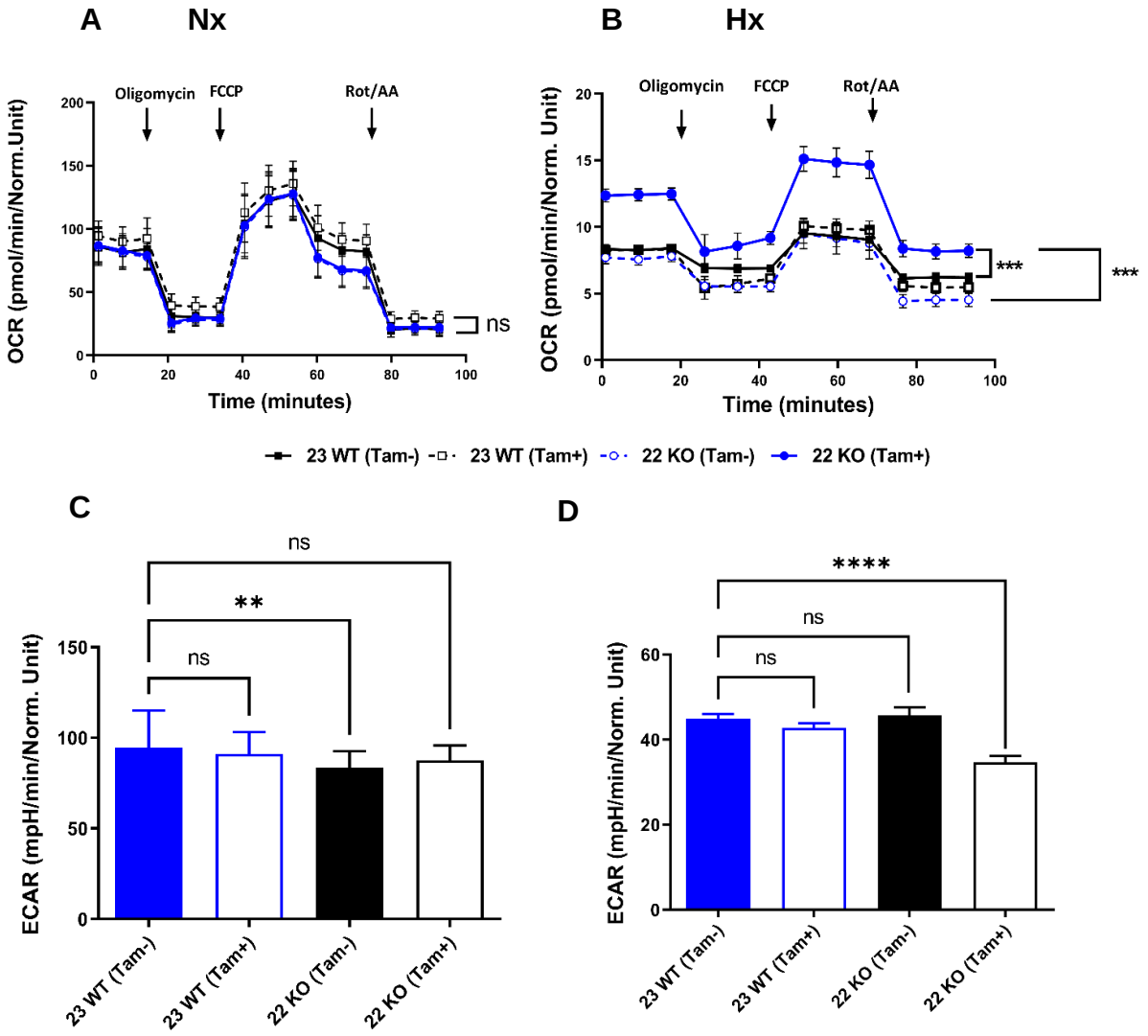

Figure 21: Cellular metabolism. A-B) OCR was measured using Mito Stress Test Kit and normalized to Hoechst 33342 fluorescence units 24 h after treatment with Hx. Real-time injection of oligomycin (Oligo, 1µM), carbonyl cyanide-4-(trifluoromethoxy) phenylhydrazone (FCCP, 2 µM), rotenone (Rot, 0.5 µM) and antimycin A (AA, 0.5 µM). C-D). To investigate the impact of HIF-1α deletion on cellular respiratory metabolism, we measured the ECAR.. Real-time injection of rotenone (Rot, 0.5µM), antimycin A (AA, 0.5µM). Mean values ±SEM are shown, A) and B) from n=12 wells (2 independent experiments); *p < 0.05, ** p<0.01, ****p<0.0001 two-way ANOVA.

4.2.2 HIF-1α deficiency affects mitochondrial morphology

In addition to investigating the effects of HIF-1α deficiency on cellular metabolism, our study also delved into the impact of HIF-1α on mitochondrial morphology. Previous research has demonstrated that exposure to hypoxia, can induce changes in mitochondrial morphology, leading to fragmentation, elongation, and altered distribution within the cell[160]. These alterations in mitochondrial morphology have been associated with modifications in both mitochondrial function and cellular metabolism, including changes in oxidative phosphorylation and glycolysis. To observe mitochondrial morphology, we employed fluorescent microscopy to visualize mitochondria in mHDC cells before and after subjecting them to hypoxic treatment. We utilized ImageJ software to quantify the number of mitochondria in the cells. Interestingly, HIF-1α deficiency resulted in a less pronounced decrease in mitochondrial number after hypoxic treatment. This suggests that HIF-1α may play a role in regulating mitochondrial biogenesis or turnover in response to hypoxia (Figure 22 A-B)[161]. To provide a clearer understanding of the potential role of HIF-1α in regulating mitochondrial morphology, we conducted transmission electron microscopy to measure mitochondrial length and diameter. The maximum distance between any two points within the mitochondrial boundaries was measured to determine mitochondrial length, while the minimum distance between two opposing points of mitochondrial boundaries was used to assess mitochondrial diameter. Interestingly, when comparing cells maintained under hypoxia to those under normoxia, we observed a significant increase in mitochondrial length in the hypoxic conditions. Additionally, the measurements of mitochondrial diameter revealed a noticeable increase between normoxia and hypoxia, indicating mitochondrial swelling following hypoxia. This swelling could potentially be associated with calcium-induced cytochrome-c release from mitochondria during instances of mitochondrial-induced apoptosis[162] (Figure 23 A-C).

Overall, these results suggest that HIF-1α may play a role in regulating mitochondrial morphology in addition to its well-established role in regulating cellular metabolism.

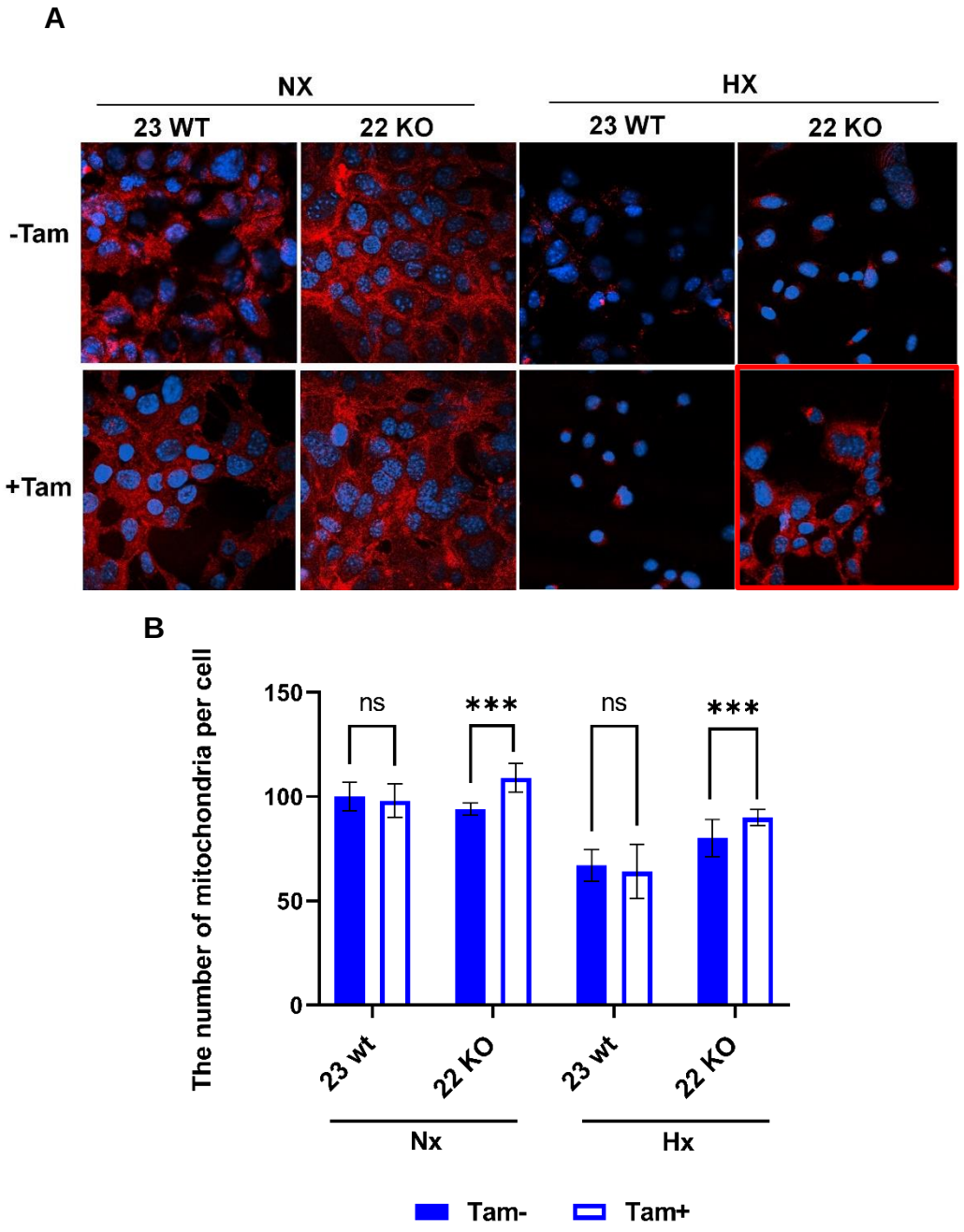

Figure 22: A) Confocal imaging and B) quantification of mitochondrial morphology in mHDC. Cells incubated under hypoxic and normoxic conditions for 72 h and were stained with Mito Tracker deep red (100 nM) and nuclei were stained with Hoechst showing blue fluorescence. Graphs show the number of mitochondria by using Mito-Morphology Macro tool of ImageJ software. Graphs show mean ± SD, groups were compared using two-way ANOVA and Bonferroni post-hoc test, *** $p<0.001$, ns $p > 0.05$.

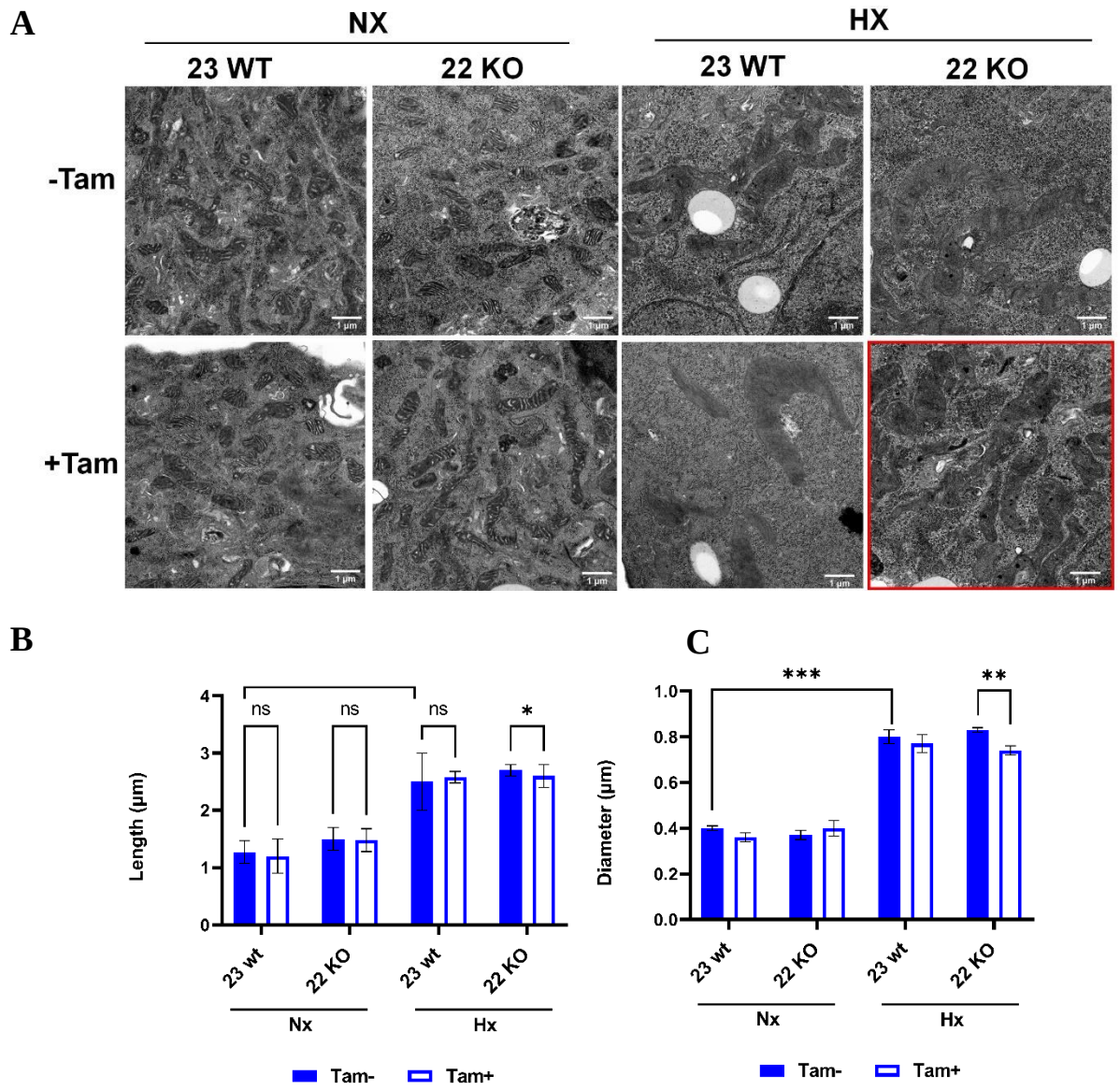

Figure 23: Measurements of mitochondria dimensions. A) Transmission electron micrographs of mHDC, B) mitochondrial length, and C) mitochondrial diameter. Cells incubated under hypoxic and normoxic condition for 72 h. Graphs show the length and diameter of mitochondria by using QuPath-0.43 software. Graphs show mean ± SD, groups were compared using two-way ANOVA and Bonferroni post-hoc test, n=150 for each group * $p < 0.05$, ** $p < 0.01$, *** $p<0.001$, ns $p > 0.05$.

4.2.3 HIF-1α regulates EPO expression in mHDCs

Erythropoietin (EPO) is a hormone that plays a key role in regulating the production of red blood cells in response to changes in oxygen levels. The expression of EPO is tightly regulated by various factors including HIF-1α. In this study, we investigated the effects of HIF-1α KO on EPO expression in mHDC. The results showed that in HIF-depleted cells, EPO expression was reduced under hypoxic condition, indicating that HIF-1α is necessary for the upregulation of EPO expression in response to hypoxia. In contrast, EPO expression was increased in wild-type cells and cells treated with DMOG, a small molecule that stabilizes HIF-1α and mimics the effects of hypoxia, under both hypoxic and normoxic conditions (Figure 24). This suggests that HIF-1α activation leads to an increase in EPO expression, even under normoxic conditions. Interestingly, after treatment with DMOG under normoxic conditions, EPO expression was reduced in HIF knockout cells compared to control cells.

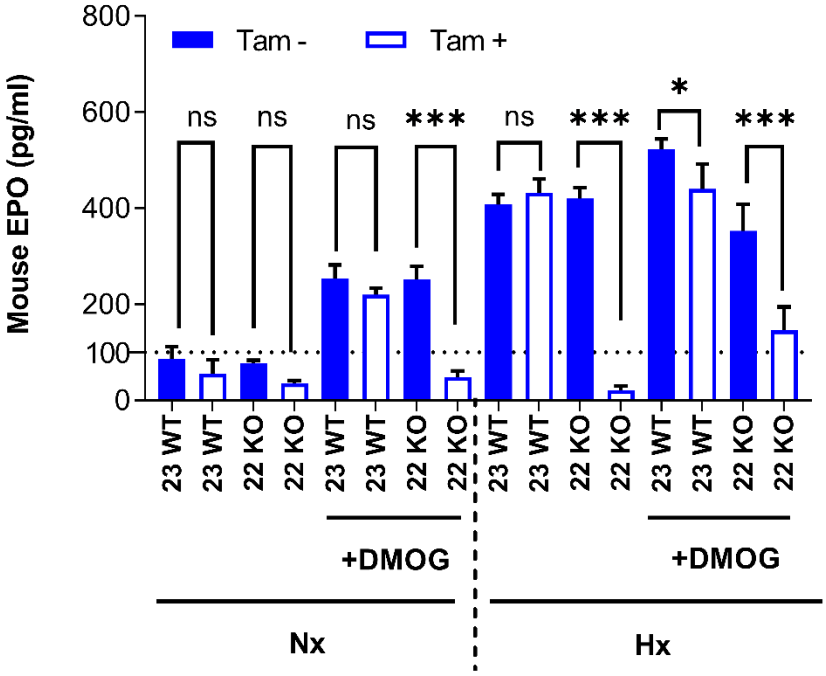

Figure 24: Effect of HIF-1α knockout and DMOG treatment on erythropoietin (EPO) levels. The mHDC were incubated in normoxia or moderate hypoxia for 72 hours. All groups included n=4 independent cultures. The statistical analysis was performed using two-way ANOVA, graphs show mean ± SD and the results were considered significant for *$p < 0.05$ and ***$p < 0.001$.

4.2.4 HIF-1α affects hepcidin expression in mHDC

Hepcidin is a hormone that plays a key role in regulating iron homeostasis in the body. It acts by controlling the amount of iron that is absorbed from the diet and released into the bloodstream. In this study we investigated the impacts of HIF-1α knockout and DMOG treatment on hepcidin expression in mHDC. In order to measure the levels of hepcidin in mHDC culture supernatants, we used the Mouse Hepcidin ELISA Kit. The cells were incubated for 72 hours under both hypoxic (1% O_2) and normoxic conditions, and the results showed that hepcidin levels were completely suppressed by hypoxia. However, interestingly, hepcidin levels increased in hypoxic HIF-1α knockout cells, indicating that HIF-1α is contributing to the suppression of hepcidin expression under hypoxic conditions. Remarkably, under normoxic conditions, DMOG suppressed hepcidin levels almost as efficiently as hypoxia. Again, the smaller fraction of this effect was reversed by HIF-1α knockout. The effects of DMOG and hypoxia in combination were demonstrated not to be additive (Figure 25).

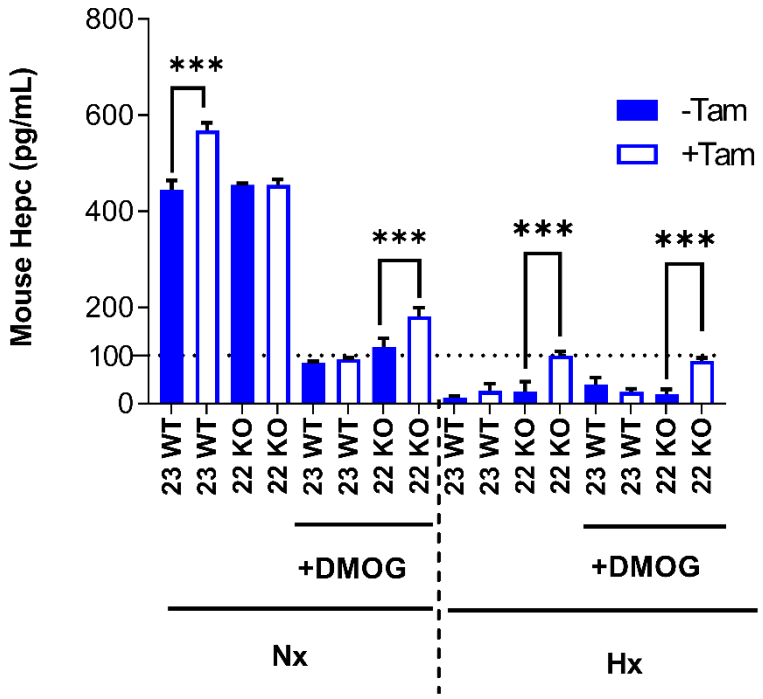

Figure 25: Effect of HIF-1α knockout and DMOG treatment on hepcidin levels. The mHDC were incubated in normoxia or moderate hypoxia for 72 hours. All groups included n=4 independent cultures. The statistical analysis was performed using two-way ANOVA, graphs show mean ± SD and the results were considered significant for ***$p < 0.001$.

In order to validate our ELISA findings, we proceeded to perform qPCR analysis to quantify the mRNA levels of hepcidin in both the HIF-1α knockout (KO) cells and control cells. After incubating the cells for 72 hours under hypoxic (1% O_2) and normoxic conditions, RNA was extracted, converted to cDNA, and finally, the qPCR results were visualized using agarose gel electrophoresis. Our results showed a significant downregulation of hepcidin mRNA levels in the cells under hypoxia, while there was a significant upregulation of hepcidin mRNA levels in the KO cells (Figure 26), thus recapitulating the ELISA results and pointing to a transcriptional mechanism in the hypoxic suppression of hepcidin. Interestingly, we again observed a decrease in hepcidin mRNA levels in cells treated with DMOG. Strikingly, the main results were consistently detectable in a non-quantitative PCR.

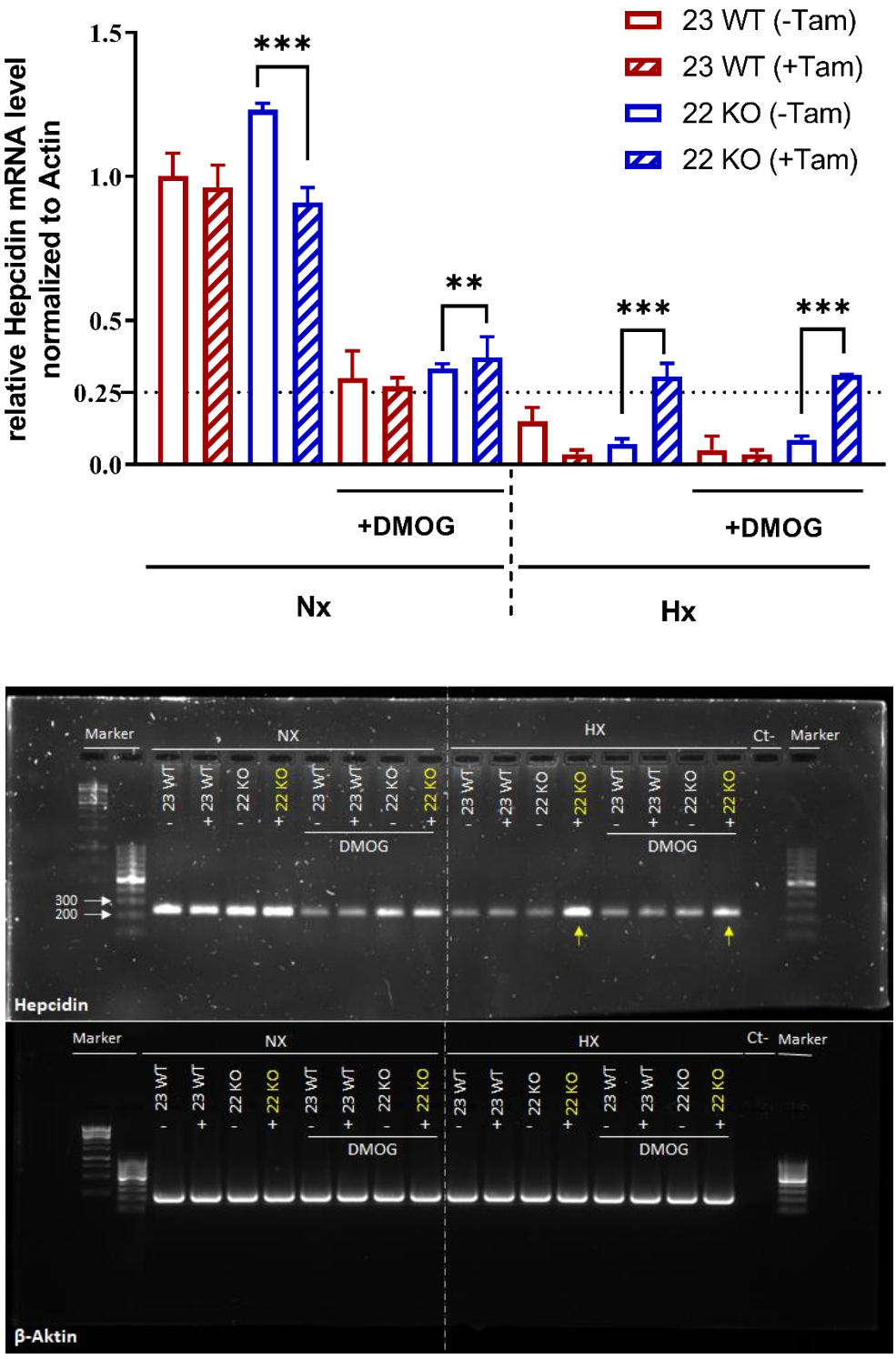

Figure 26: Analysis of Hepcidin mRNA levels in mHDC by RT-qPCR. A) The cells were grown 3 days in normoxia (NX) or hypoxia (HX, 1 % O_2). The cDNA levels of hepcidin gene were analysed by qPCR and normalized to the cDNA levels of the control β-actin (n = 4) and the results were considered significant for **p < 0.01 and ***p < 0.001. B) Agarose gel electrophoresis to visualize the qPCR results.

4.3 The effect of HIF-1α knockout on radiation sensitivity

4.3.1 HIF-1α reduces irradiation effects

When exposed to ionizing radiation, cells undergo significant DNA damage and other detrimental effects, leading to cell death. In this study, the MTT assay was employed to evaluate the viability of mHDC before and after exposure to ionizing radiation. Remarkably, hypoxic HIF-1α depleted cells demonstrated a highly significant decrease in viability 48 hours after radiation treatment, indicating a potential protective effect of HIF-1 in irradiated cells. These results suggest that HIF-1 plays a critical role in protecting cells from radiation-induced damage in mHDC (Figure 27).

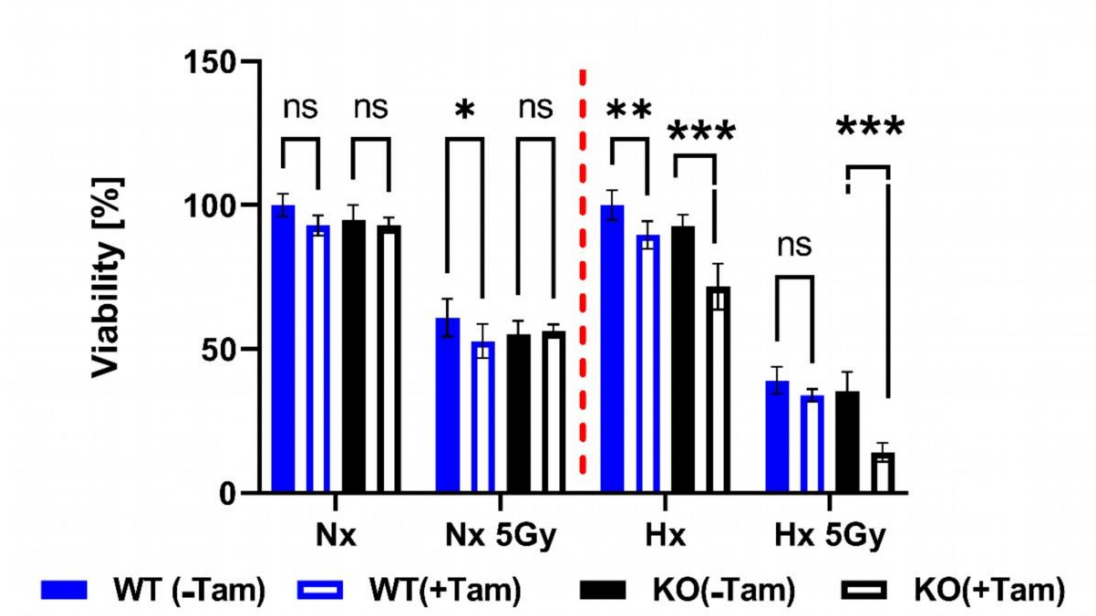

Figure 27: Assessment of cell viability using MTT assays. Cells were cultured for 48 hours under either normoxia or hypoxia and then exposed to 5 Gy of radiation. Control cells underwent the same treatment but were not irradiated. Following irradiation, the cells were returned to either normoxia or hypoxia. After 48 hours, the cells were incubated with MTT and lysed after 4 hours. The absorbance was measured at 540 nm. The reference values, set to 100%, were determined based on Cre negative cells not treated with Tam. A total of 10 samples per group were analyzed using a two-way ANOVA (***$p<0.001$)[158].

In order to investigate the impact of depleting HIF-1α on cell survival in the initial 24-hour period after exposure to radiation, a clonogenic survival assay with delayed plating was conducted. This assay evaluates the ability of single cells to repair DNA damage caused by radiation and subsequently proliferate to form colonies. Specifically, mHDC HIF-1α knockout

cells were subjected to 12 hours of hypoxia, followed by exposure to varying doses of radiation ranging from 0 to 10 Gy. After irradiation, the cells were incubated in a hypoxic environment for 24 hours and then seeded at different densities. The results of the study revealed a decrease in the mean survival fraction of HIF-1α knockout cells following irradiation with 6 Gy. Notably, a significant difference ($p < 0.001$) was observed at the 6 Gy dose, indicating that the absence of HIF-1α affects the mechanisms involved in DDR by hindering the successful repair and ongoing proliferation of irradiated cells. However, no discernible differences were observed between wild-type and knockout cells under normoxic conditions. These findings suggest that HIF-1α plays a critical role in the repair of double-strand breaks (DSBs) induced by ionizing radiation in hypoxia. Consequently, further investigations were conducted to explore the specific impact of HIF-1α on the repair of radiation-induced DSBs (Figure 28).

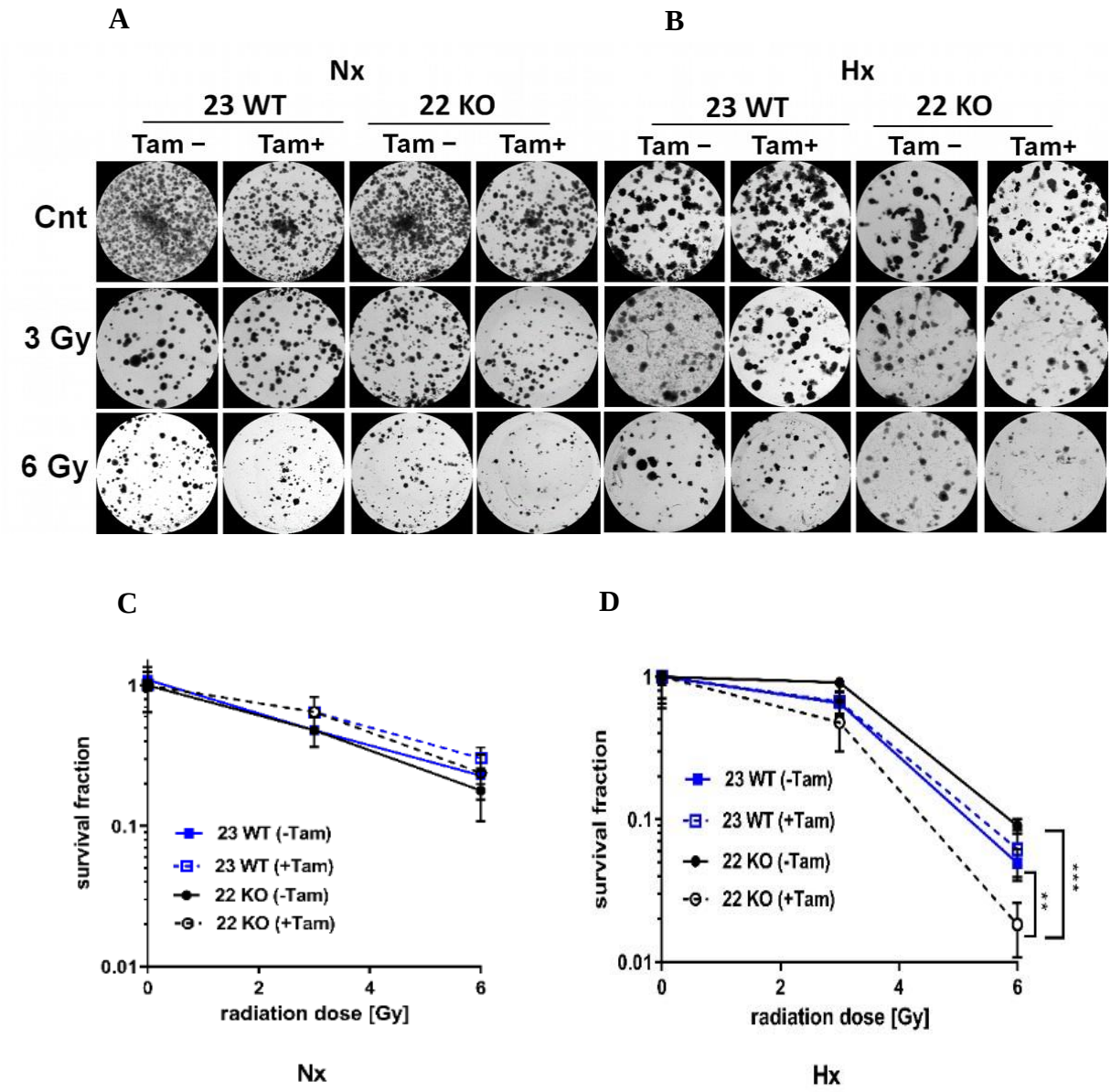

Figure 28: Evaluation of irradiation's impact on the survival of mHDC through colony formation assay (CFA) under different oxygen conditions and doses. Hypoxic cells were cultured in 1% O_2 using rat collagen-coated 6-well dishes. Following irradiation, HX cells were maintained in hypoxia for 10 days. Colonies with a minimum of 50 cells were counted after Coomassie staining. Representative images of colony formation are shown for normoxic (A) and moderately hypoxic (B) conditions with and without Tam treatment. Survival curves depict the quantification of colony formation in normoxia (C) and hypoxia (D). Each group consisted of n=6 independent cultures. Statistical analysis was conducted using two-way ANOVA, with significance set at **$p < 0.01$ and ***$p < 0.001$[158].

4.3.2 HIF-1α knockout increases radiation-induced apoptosis

Previous research has suggested that HIF-1α may play a role in promoting apoptosis in cancer cells [163]. Therefore, this study aimed to investigate the influence of HIF-1α on radiosensitivity by assessing the level of apoptosis. Specifically, the activity of the pro-apoptotic enzyme caspase-3 was measured.

To determine the effect of HIF-1α on apoptosis, cells were incubated under hypoxic conditions for 48 hours before being collected after the 24-hour period following irradiation with 5 Gy. The results revealed a significant increase in apoptosis in HIF-1α knockout cells compared to control cells following irradiation, indicating that HIF-1α may act as a protective factor in this context (Figure 29A).

These findings suggest that HIF-1α plays a role in modulating the response of mHDCs to radiation-induced DNA damage, possibly through the regulation of apoptosis. To further validate the role of HIF-1α in apoptosis, additional experiments were conducted using Western blotting analysis with a poly [ADPribose] polymerase 1 (PARP-1) antibody. PARP-1 is involved in apoptosis and serves as a substrate for caspase-3 and caspase-7. Cleaved PARP-1 fragments indicate the occurrence of apoptotic cell-death inducing proteases.

The mHDC cells were incubated for 48 hours under hypoxic conditions, irradiated, and lysed after 1, 4, 8, or 24 hours in hypoxia to investigate apoptosis levels (Figure 29B). The results demonstrated an increased PARP cleavage in HIF-1α-depleted cells within the first 8 hours after irradiation, which confirmed the caspase-3 results. These findings demonstrate that HIF-1α plays a protective role in irradiated cells by inhibiting apoptosis induction.

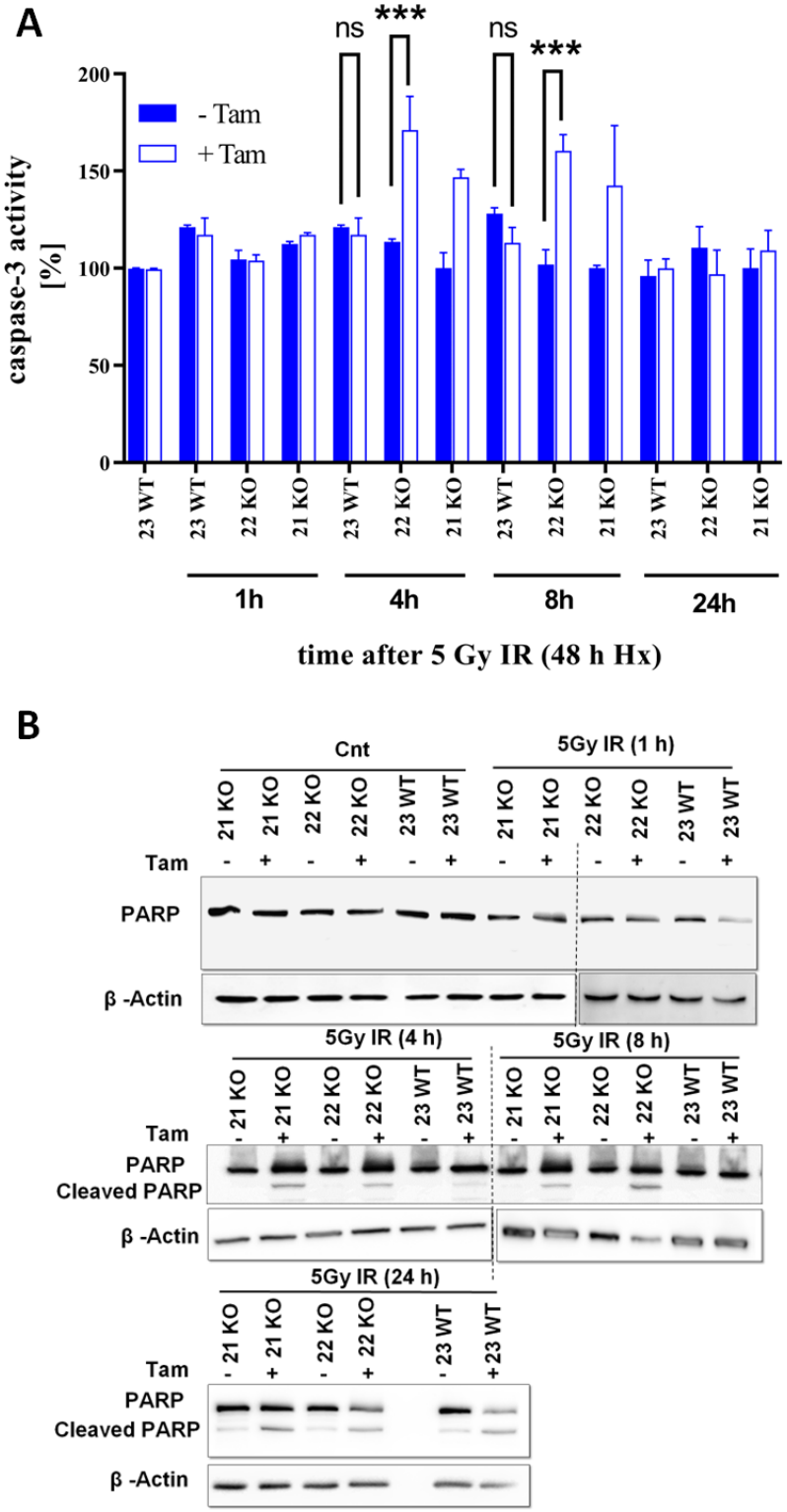

Figure 29: Assessment of apoptosis induction in mHDC cells lacking HIF-1α under hypoxic conditions. A) Measurement of caspase-3 activity in mHDC lysates during the initial 24 hours following a 48-hour incubation under hypoxia (Hx) and exposure to 5 Gy of ionizing radiation (IR). The data represents a representative experiment with n=6, repeated three times. The graphs display the mean ± standard deviation (SD), and group comparisons were conducted using two-way ANOVA. *** indicates

highly significant differences between group means ($p<0.001$). B) Western blot analysis using a PARP-1 antibody, detecting both full-length PARP and a cleaved form with a lower molecular weight, indicating PARP cleavage as an apoptosis marker. Cells were subjected to 48 hours of hypoxia, followed by 5 Gy irradiation[158].

4.3.3 HIF-1α deficiency impinges on DNA damage repair

One of the primary mechanisms by which ionizing radiation (IR) induces DNA damage is through the generation of double-strand breaks (DSBs). The cells' ability to respond to and repair this damage is known to be affected by hypoxia, resulting in genomic instability and radiation resistance[74]. Previous studies have identified HIF-1α as a regulator of DNA damage response (DDR) and checkpoint control[164]. Therefore, in this study, the effect of HIF-1α depletion on IR-induced DNA damage was investigated by analysing the generation of γH2AX foci, which serve as markers for DSBs. H2AX is a histone variant present throughout mammalian chromatin, and upon DSB induction, H2AX at the break site is phosphorylated at serine 139 by ATM/ATR kinases, generating γH2AX foci that can be visualized by immunofluorescent staining.

Following irradiation with 5 Gy, the number of γH2AX foci was significantly higher ($p<0.001$) in HIF-1α-depleted cells compared to cells containing HIF-1α. Additionally, the removal of these foci was delayed for up to 24 hours in the HIF-1α-deficient cells (Figure 30 A-C).

To further investigate the role of HIF-1α in this process, we examined the effects of dimethyloxalylglycine (DMOG), a compound commonly used to induce HIF expression independently of oxygen. DMOG did not induce γH2AX foci in the absence of IR. However, when HIF-1α knockout cells were treated with DMOG in normoxia and then exposed to IR, they exhibited significantly higher levels of γH2AX foci compared to all other cells. Notably, this experiment also revealed that DMOG increased DNA damage induced by IR in normoxia in all HIF-1 wildtype cells, while reducing DNA damage in the same cells under hypoxia. These results demonstrate that HIF-1 promotes radiation resistance in mHDC by regulating DDR and DNA repair.

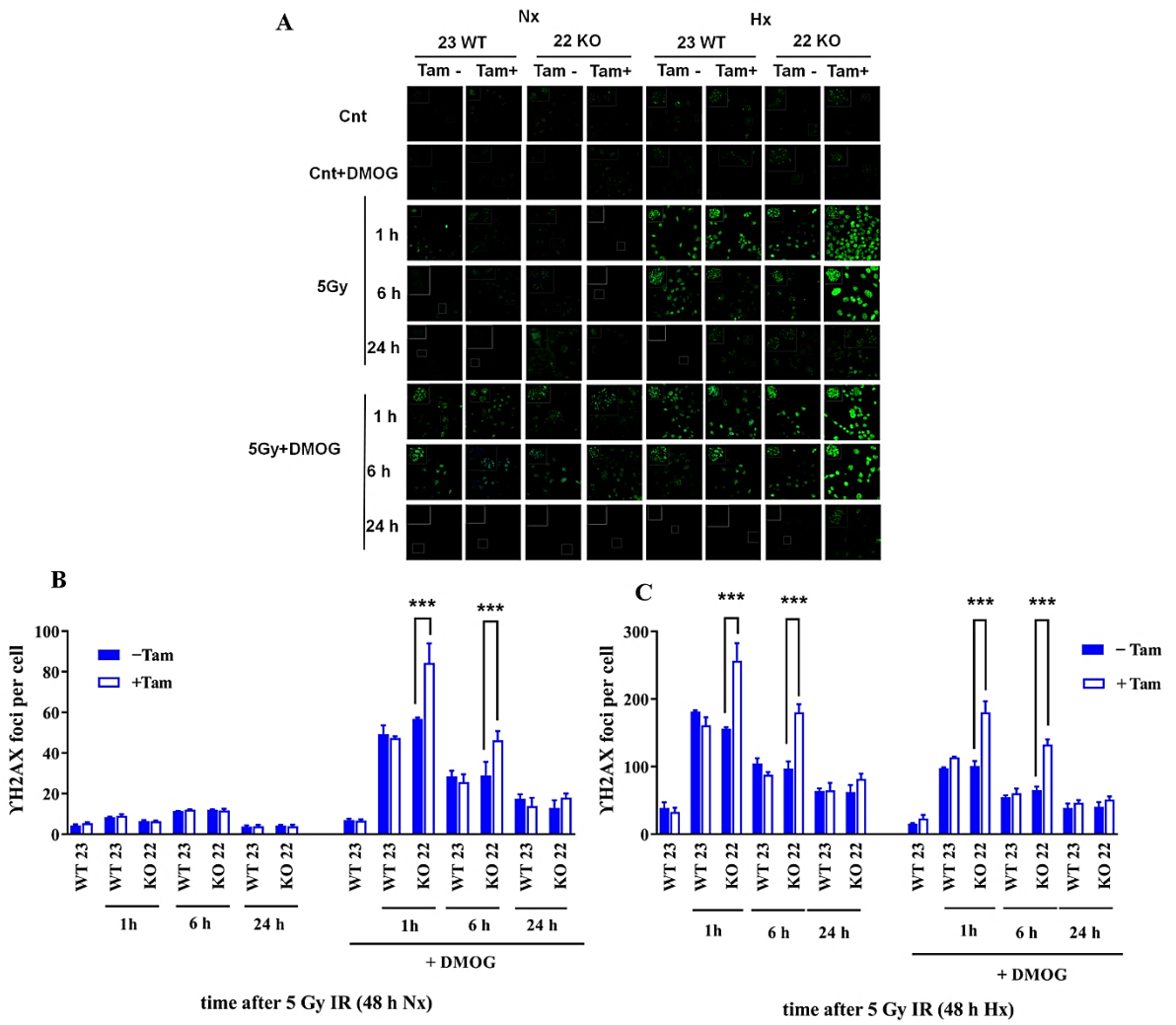

Figure 30: Effect of HIF-1α knockout and DMOG treatment on γH2AX foci formation after irradiation in mHDC under normoxic and hypoxic conditions. A) The mHDC were incubated in normoxia or moderate hypoxia for 48 hours and then irradiated with 5 Gy. The cell cultures were then transferred back to hypoxia or normoxia and stained after the indicated times. Images were taken with a Zeiss LSM510 confocal microscope. The number of γH2AX foci per nucleus in B) normoxia and C) hypoxia, with the first pair of bars (23 WT) representing non-irradiated mHDC that contain HIF-1α. Each experiment was performed three times, and the graphs show mean ± SD. Statistical significance was determined using two-way ANOVA and Bonferroni post-hoc test, ***$p<0.001$[158].

To validate the results obtained through γH2AX immunohistochemistry, we employed the Comet assay, a highly sensitive method for detecting DSB induction and rejoining in a single cell[165]. DSB induction leads to DNA fragmentation, which becomes visible as a comet head and tail when the fragmented DNA migrates through nuclear pores during electrophoresis[154]. The extent of DNA damage was determined by analyzing the tail moment, which represents the percentage of DNA in the tail[166].

Our findings showed that the percentage of DNA damage can be assessed based on the length of the tail (tail moment). Following ionizing radiation, under hypoxic conditions and upon depletion of HIF-1α, the tail moment (percentage of DNA in the tail) increased by 1.6-1.9-fold at 5 and 30 minutes after IR (Figure 31 A-C). This suggests an elevated number of DSBs following IR. In contrast, under normoxic conditions, most DSBs were repaired within 30 to 60 minutes after IR.

We determined the impact of HIF-1α deficiency on ROS generation and the potential role of ROS in the observed effects. To assess ROS levels, we utilized a fluorescent dye named CellRox Green and performed measurements in both normoxia and hypoxia before and after ionizing radiation in mHDC. There were no significant variations in ROS levels, except for a decrease in ROS under hypoxic conditions across all treatment groups. Consequently, it is highly improbable that ROS plays a role in the effects attributed to HIF-1α deficiency (Figure 32).

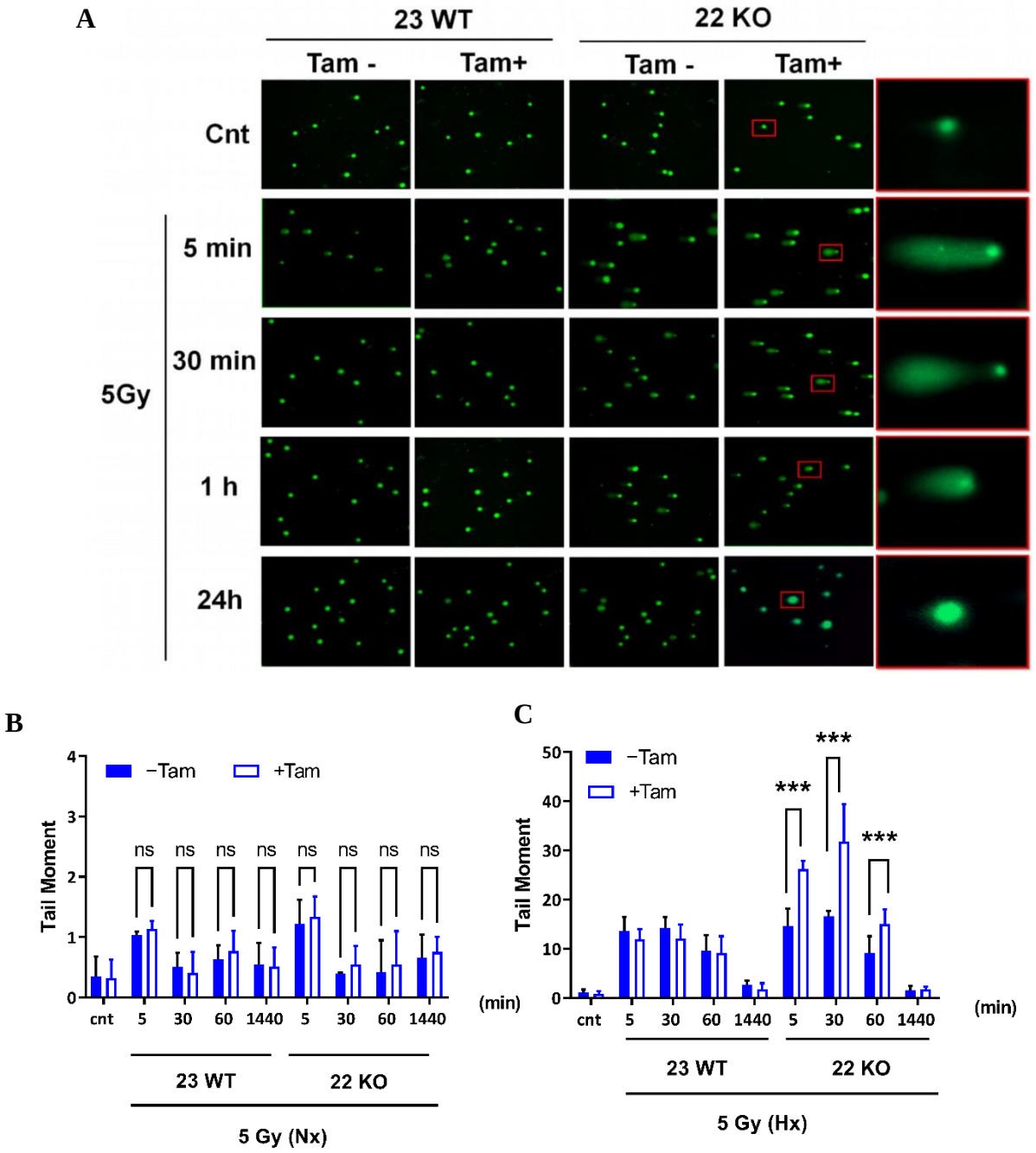

Figure 31: The impact of HIF-1α knockout on the rejoining of double-strand breaks (DSBs) induced by ionizing radiation (IR), as assessed by the neutral comet assay. After being exposed to IR, the cells were immersed in 1% agarose gels, then lysed and underwent electrophoresis at 25 V and 300 mA for 25 minutes. Representative fluorescence microscopy images are displayed A) The extent of DNA damage was quantified by measuring the tail moment, which reflects the percentage of DNA in the tail of the comet, in 50 cells per slide using OpenComet v1.3.1 analysis software. The results are presented for cells under B) normoxic and C) hypoxic conditions. The bars represent the mean ± SD, and statistical analysis was performed using two-way ANOVA, with *** $p<0.001$ indicating significances[158].

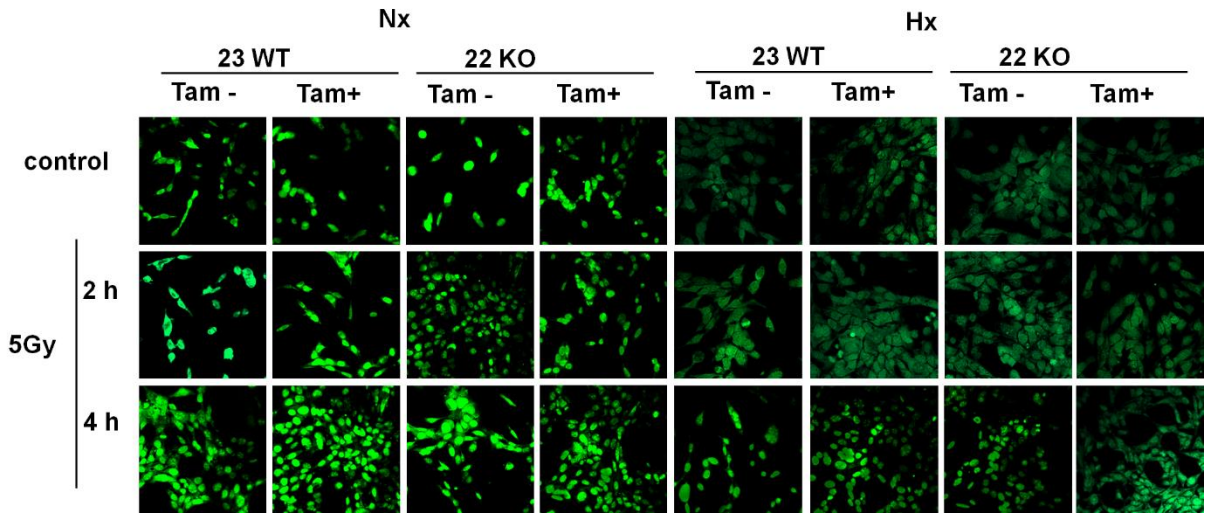

Figure 32: The detection of ROS generation using CellROX Green Reagent. CellROX (green) confocal fluorescence images displaying production of ROS in mHDC incubated under normoxic and hypoxic conditions before and after ionizing radiation with 5 Gy.

5 Discussion

5.1 Importance of hepatocyte *in vitro* model

The use of hepatocyte *in vitro* models is crucial for various liver-based tests, as they provide a representation of the cell types found in the liver of the human body. Primary human cells are considered the gold standard for these tests, as they closely mimic *in vivo* conditions[167]. However, the availability of primary cells is limited, and their quality varies due to the source of biopsy material and isolation techniques[168]. Additionally, donor-to-donor variation adds complexity to the interpretation of assay results. Cell cultures of differentiated primary hepatocytes, whether from humans or rodents, hold immense significance in biomedical research. However, the establishment of these cells *in vitro* has faced challenges due to rapid de-differentiation that occurs in a cell culture environment. To address this issue, various alternative models have been developed as substitutes for freshly isolated primary hepatocytes.

One widely used approach involves utilizing hepatic cell lines such as HepG2 (which are genetically unstable), Hep3B, and HepaRG[169]. These cell lines have been commercially available for nearly four decades, but they do have limitations. HepG2, for instance, exhibits low expression of CAR (coxsackievirus and adenovirus receptor) and PXR (pregnane x receptor), raising doubts about their resemblance to differentiated hepatocytes. Moreover, HepG2 express α-fetoprotein[170], which is a marker associated with fetal liver cells or hepatocellular carcinoma (HCC). Newer cell lines, including Hep-aRG and induced pluripotent stem cells (iPSCs) differentiated into hepatocytes, have also been developed. However, similar concerns arise regarding their authenticity as differentiated hepatocytes, as reviewed recently[171]. Compared to primary hepatocytes, hepatic cell lines generally exhibit lower expression of phase I and phase II enzymes[172].

Fortunately, another promising option has emerged: the use of "upcyte® cells"[10,147]. Human upcyte® hepatocytes are proliferating hepatocytes that closely resemble primary human hepatocytes[10]. These cells offer the advantage of providing large quantities of metabolically competent cells from multiple donors, making them suitable for higher throughput assays like metabolism and drug-drug interaction (DDI) studies. The use of primary endothelial cells, such as mvECs and LSECs, in *in vitro* models has certain limitations that need to be addressed. Firstly, these cells tend to de-differentiate rapidly when cultured *in vitro*, leading to the loss of endothelial cell markers[173–175]. Secondly, establishing standardized *in vitro* test systems using primary endothelial cells is challenging due to donor-to-donor variation[173]. Additionally,

primary LSECs have a limited proliferative capacity, with a short life span of only 2-3 population doublings *in vitro*[176,177]. Moreover, obtaining high purity and yields of primary LSECs is difficult compared to other cell types, such as hepatocytes or mvECs. Furthermore, the existing research on LSECs is limited, and a comprehensive characterization of these cells is still lacking.

To overcome these limitations, upcyte® mvECs and upcyte® LSECs were generated using upcyte® technology. These cells exhibit enhanced proliferative capacity and retain their endothelial cell-specific markers when cultured *in vitro*[11,12]. The upcyte® technology enables the production of a large number of cells, allowing the establishment of *in vitro* test systems. Additionally, obtaining cells from multiple donors facilitates the study of donor-to-donor variations in cell responses and characteristics.

In the context of this cell culture protocol, differentiated human hepatocytes from adult donors are isolated from liver biopsies. These hepatocytes are then transduced with proliferation-inducing genes, resulting in cells that are not fully immortalized but can grow up to 45 population doublings, depending on donor and species. Importantly, proliferation can be halted at any time by withdrawing growth factors. Therefore, this system combines the generation of large quantities of cells with the utilization of differentiated, quiescent hepatocytes in actual experiments. In a gene expression analysis, upcyte® cells exhibited a closer resemblance to primary human hepatocytes than HepG2 cells[169]. In our study, we successfully generated upcyte® cells from the murine liver for the first time. This procedure enabled the creation of differentiated hepatocyte cultures from both wild type and genetically modified mice. The cells reached confluence in a monolayer, which was crucial as our study necessitated uniform oxygen delivery to all cells. Our cultures remained stable for approximately two months regarding the expression of hepatocyte differentiation markers, such as cytokeratin 8/18, albumin, and acetylcholine esterase.

5.2 Aiming for the right target

This thesis focuses on hypoxia and HIF-1α signaling and their roles as crucial factors in mediating the response to ionizing radiation (IR). Cellular adaptation to low oxygen levels, known as the hypoxia response, primarily relies on the activity of HIFα, which becomes rapidly activated under hypoxic conditions.

HIF-1 has several adaptive effects on cell metabolism, especially in the absence of adequate oxygen supply, i.e. hypoxia[178]. The regulation of HIF primarily occurs at the posttranslational

level: under high oxygen levels, the α-subunit is hydroxylated and degraded through the ubiquitin-proteasome pathway[179]. Additional regulatory pathways, including transcriptional activation of the Hif1a gene and phosphorylation events, have also been reported[180]. In hypoxia, degradation is blocked because hydroxylation requires molecular oxygen, causing HIF-1α to translocate to the nucleus and induce the transcription of target genes through dimerization with its β-subunit[181].

The role of HIF-1 in hepatocytic stress responses has been a subject of debate in recent years. Therefore, our study aimed to investigate the involvement of HIF-1 in the induction of proliferation and apoptosis in response to IR. We chose IR as it provides a reproducible and quantitatively defined method for inducing cellular stress, applicable in both normoxia and hypoxia. Moreover, studying IR in liver cells holds translational significance because it is increasingly considered a therapeutic option for advanced hepatocellular carcinoma. Technological advancements, such as stereotactic extracorporal radiation, have improved outcomes when combined with local interventions[182]. Therefore, it is crucial to examine the radiation responses of hepatocellular carcinoma cells at various differentiation levels, as well as untransformed hepatocytes near the tumor. In many types of cancer, activation of the HIF pathway in hypoxic cells leads to radiation resistance. High levels of HIF-1α correlate with tumor progression and poor patient outcomes[183].

To directly investigate the unique functions of HIF-1α, we established permanently HIF-1α-deficient mHDC cultures. These cultures serve as a perfect tool for studying the effects of HIF on proliferation, metabolism, and sensitivity to ionizing radiation.

5.3 HIF-1α conditional knockout

To investigate the effect of HIF-1α signaling in mHDC, mice with a conditional knockout (KO) of HIF-1α were essential. Global knockout of HIF-1 has been shown to cause embryonic lethality[184], so mice with tamoxifen-inducible conditional HIF-1 KO were created. In this model, exon 2 of the HIF-1 gene is flanked by LoxP sequences recognized by Cre recombinase. The addition of the estrogen antagonist tamoxifen activates Cre recombinase expression under the control of a promoter with a mutated estrogen receptor, resulting in the deletion of exon 2 from the Hif1a gene in this model.

The deletion of exon 2 raised the question of whether a shortened version of the HIF-1 protein, lacking exon 2, would be expressed or if the protein would be produced at all. Analysis of the mRNA sequence and samples from HIF $1^{fl/fl}$Cre $ER^{ki/wt}$ mice revealed that exon 2 deletion

resulted in a frameshift of the sequence. According to the mRNA sequence, the theoretical amino acid sequence expected in HIF $1^{fl/fl}$Cre $ER^{ki/wt}$ mice consists of only 16 amino acids followed by a stop codon. Thus, the data show that induction of Cre expression by tamoxifen treatment led to the irreversible destruction of the Hif1a gene in the cell cultures. The most likely explanation for the shortened version of HIF-1α in our Western blots is that translation can start from an ATG codon internal to exon 3, so that a protein is produced which contains the ODDD and is recognized by HIF-1α antibodies but fails to induce target gene expression in hypoxia and is thus functionally inactive.

It is important to note that the upcyte protocol was used to generate all relevant control cultures. Cells isolated from Cre-negative mice were used to control for Cre-independent tamoxifen effects. Additionally, cultures from Cre-positive animals that were not treated with tamoxifen allowed for a comparison between uninduced and induced states in syngeneic cells. Since even cells within the same culture are not clonal, functional inactivation of HIF-1α was demonstrated by a complete lack of target gene induction in hypoxia using qPCR. Conversely, the cell culture of HIF-1α negative mHDCs, which exhibited months without apparent growth delay compared to control cells, confirmed that HIF-1 is not vital as long as the cells are sufficiently oxygenated.

5.4 HIF-1α deficiency and metabolic profiling

The aim of this study was to investigate the relationship between hypoxia and metabolic flux and to determine the impact of HIF-1α deletion on cellular respiratory metabolism. Hypoxia is a critical factor in various physiological and pathological conditions, and understanding how cells adapt their metabolism under hypoxic conditions is of great importance. HIF-1α is a key transcription factor involved in the cellular response to hypoxia and has been shown to play a crucial role in metabolic reprogramming. In this section, the implications of our results obtained from the Mito Stress Test Kit, focusing on the changes observed in the oxygen consumption rate (OCR) and extracellular acidification rate (ECAR) under hypoxic conditions are discussed.

Our findings indicate that hypoxia caused a significant decrease in OCR in control cells, suggesting a shift towards glycolysis as the primary ATP source. This metabolic switch is a well-known adaptive response to low oxygen levels and allows cells to maintain energy production under hypoxic conditions. However, HIF-deficient cells did not exhibit this metabolic switch and maintained high levels of OCR even under hypoxic conditions. These results suggest that HIF-1α is crucial for the metabolic adaptation to hypoxia by promoting the switch to glycolysis. Furthermore, we observed that the absence of HIF-1α did not lead to

changes in ECAR regulation under normoxic conditions. However, knockout cells demonstrated a significant reduction in basal ECAR compared to wild-type cells. This decrease in glycolytic activity, as reflected by the reduction in ECAR, may affect pH levels or lactic acid production when compared to wild-type cells. These alterations may help explain the increased radiation sensitivity observed in HIF-1α knockout cells. Our findings align with previous studies that have demonstrated the role of HIF-1α in promoting the switch to glycolysis under hypoxic conditions. The metabolic reprogramming towards glycolysis is a well-established phenomenon in response to hypoxia, and HIF-1α has been identified as a key regulator of this process[185,186]. Our results further support the notion that HIF-1α deficiency disrupts this metabolic switch and prevents the cells from adapting to hypoxic conditions. However, it is important to note that some studies have reported conflicting results regarding the role of HIF-1α in metabolic reprogramming. Some studies have suggested that HIF-1α is dispensable for the glycolytic switch under hypoxia, while others have highlighted the importance of HIF-1α in this process, demonstrating impaired glycolytic gene expression and reduced glucose metabolism in HIF-1α-deficient cells[187,188]. These discrepancies could be attributed to differences in experimental conditions, cell types, or model systems. The use of different cell lines or animal models, variations in the duration and severity of hypoxia exposure, and differences in the techniques used to measure metabolic parameters may contribute to the observed differences in results. Nevertheless, our findings contribute to the growing body of evidence supporting the role of HIF-1α in metabolic adaptation to hypoxia.

The metabolic switch towards glycolysis in control cells under hypoxic conditions is likely mediated by HIF-1α-induced transcriptional activation of key enzymes involved in glycolysis. HIF-1α regulates the expression of several glycolytic enzymes, such as glucose transporters and glycolytic enzymes, which promote the increased uptake and metabolism of glucose. In the absence of HIF-1α, these transcriptional changes are not induced, leading to a lack of metabolic adaptation to hypoxia. Future research should focus on elucidating the specific mechanisms by which HIF-1α regulates metabolic reprogramming under hypoxic conditions. Understanding the downstream targets of HIF-1α and their roles in glycolysis and oxidative phosphorylation will provide further insights into the metabolic adaptations that occur under hypoxia. Additionally, investigating the potential crosstalk between HIF-1α and other metabolic regulators, such as AMP-activated protein kinase (AMPK) and mammalian target of rapamycin (mTOR), could uncover novel regulatory mechanisms in cellular metabolism.

Furthermore, the observed reduction in basal ECAR in HIF-deficient cells raises intriguing questions about the impact of altered glycolytic activity on pH levels and lactic acid production. Future studies could explore the effects of these metabolic changes on cellular homeostasis, cell signaling, and overall cellular function. Additionally, investigating whether restoring glycolytic activity in HIF-1α knockout cells can rescue their radiation sensitivity could provide valuable insights into the link between metabolic reprogramming and the cellular response to radiation. This research has implications in various fields, including cancer biology, ischemic diseases, and metabolic disorders. By uncovering the molecular mechanisms underlying the metabolic changes associated with HIF-1α deficiency, our study opens avenues for future research aimed at developing targeted therapeutic strategies to modulate cellular metabolism in hypoxic conditions.

Erythropoietin (EPO) is a hormone that plays a crucial role in regulating the production of red blood cells in response to changes in oxygen levels. Understanding the mechanisms involved in the regulation of EPO expression is of great importance for developing therapies for anemia and other blood disorders. In this study, we aimed to unveil the role of HIF-1α in the regulation of EPO expression in mHDCs. By investigating the effects of HIF-1α knockout (KO) on EPO expression under both hypoxic and normoxic conditions, we have gained valuable insights into the complex interplay between HIF-1α and EPO regulation, providing a foundation for future research and potential therapeutic interventions. The regulation of EPO expression is a tightly controlled process, as its dysregulation can lead to severe consequences such as anemia. Previous studies have identified HIF-1α as a critical transcription factor involved in the upregulation of EPO expression under hypoxic conditions. Our findings further support and expand these by demonstrating that HIF-1α is necessary for the upregulation of EPO expression in response to hypoxia, as evidenced by the reduced EPO expression in HIF-1α KO cells under hypoxic conditions. This confirms the necessity of HIF-1α for EPO upregulation in response to hypoxia. Interestingly, EPO expression was increased in wild-type cells treated with DMOG, a HIF-1α stabilizer, under both hypoxic and normoxic conditions. In hypoxia and after DMOG treatment the HIF-1α knockout substantially reduced induction. In particular in mice, EPO expression has been attributed to activation of HIF-2α, which, however, does not appear to play a major role on our mHDC. This suggests that HIF-1α activation can lead to enhanced EPO expression even in the presence of normal oxygen levels in our cells. These findings highlight the intricate interactions between HIF-1α and other transcription factors involved in EPO regulation under normoxic conditions, which require further investigation.

Our results shed light on the impact of silencing hypoxia- HIF-1α on hepcidin expression in mHDCs and its implications for the regulation of iron homeostasis. This research is of paramount importance as hepcidin plays a crucial role in maintaining iron balance in the body, and understanding its regulation is essential for developing novel therapeutic approaches to iron-related disorders. Our results demonstrate that under hypoxic conditions, hepcidin expression is completely suppressed, highlighting the crucial role of hypoxia in regulating its expression. This observation aligns with previous studies that have implicated hypoxia as a key regulator of hepcidin[189]. However, an intriguing finding in our study is that hepcidin levels increased in HIF-1α knockout cells under hypoxic conditions, suggesting that HIF-1α is involved in the suppression of hepcidin expression. This novel finding expands our understanding of the complex interplay between hypoxia, HIF-1α, and hepcidin regulation. Furthermore, our results indicate a complex regulatory network under normoxic conditions. Remarkably, hepcidin levels were higher in normoxic mHDCs as compared to DMOG-treated normoxic cells. Deficiency in HIF-1α only partially reversed this effect. This result indicates that HIF-1 contributes to suppression of hepcidin but also that another factor which is modified by hydroxylation is involved. It seems possible that the additional factor is HIF-2α. These findings highlight the need for further investigations to unravel the exact mechanisms involved in this intricate regulation. The implications of our research are significant in the context of iron-related disorders. Dysregulation of hepcidin expression is associated with various pathological conditions, including anemia and hemochromatosis. By identifying HIF-1α as a key regulator of hepcidin expression under hypoxic conditions, our study opens up new avenues for therapeutic interventions. Targeting HIF-1α or the signaling pathways it regulates could offer potential strategies to modulate hepcidin expression and restore iron homeostasis in patients with iron-related disorders, such as anemia of chronic disease. In addition, this finding potentially has implications for other conditions where iron dysregulation plays a role, such as neurodegenerative diseases and cancer.

Comparing our results with previous research studies, we observe both similarities and differences. The role of hypoxia in hepcidin regulation has been well-established in the literature, and our findings align with this existing knowledge[190–192]. However, the involvement of HIF-1α in the suppression of hepcidin expression under hypoxic conditions is a novel contribution of our research. In general, hepcidin expression is regarded as being mostly regulated by extrahepatic factors[191]. However, our research adds a new dimension by highlighting the direct regulation of hepcidin expression by HIF-1α i.e. an intrahepatic signaling pathway. This expands our understanding of the intricate regulatory network involved in

hepcidin expression and provides a more comprehensive picture of its regulation[193]. Despite the significant contributions of our study, there are some limitations that should be acknowledged. Firstly, our research focused on mHDCs, which are a cellular model system. Further investigations using *in vivo* models and clinical samples would be beneficial to validate our findings and ensure their relevance in the human context. Additionally, our study primarily explored the impact of HIF-1α on hepcidin expression under hypoxic conditions. Further studies investigating the role of other factors, such as HIF-2α or other signaling pathways, in the regulation of hepcidin expression under different physiological and pathological conditions would provide a more comprehensive understanding.

5.5 HIF-1α deficiency and exposure to hypoxia increase radiation-induced apoptosis

The effect of HIF-1α on apoptosis has been discussed controversially in the literature, as the pro- and anti-apoptotic properties of HIF-1α in carcinogenesis have been described. When we assessed the proliferative activity by counting the cells in normoxia and in hypoxia, we observed an insignificant reduction in growth in hypoxic knockout cells. Reassuringly, we did not observe substantial knockout effects of HIF-1α in normoxia.

In this study, the results showed that hypoxia plus HIF-1α KO did not stimulate apoptosis induction as compared to hypoxia alone in the absence of IR. Interestingly, we also observed a reduction in viability as assessed by MTT assays in response to tamoxifen treatment. In essence, we interpret the reduction in viability in hypoxic HIF-1α knockout cells as a combination of two mildly inhibitory effects on proliferative activity: tamoxifen and the HIF-1α KO. A reduction in growth may be caused by a disturbance in energy metabolism, which has been reported for other cell lines previously[194]. However, in response to IR, our results showed that HIF-1α depletion led to elevated levels of apoptosis in mHDC. Caspase-3 activity was increased in HIF-1 KO mHDC, which is activated in apoptotic cells. HIF-1 positive cells, on the other hand, did not show an increase in apoptosis after irradiation. In line with this finding, HIF-1 depleted cells showed an increase in PARP-1 cleavage, which is caused by cell-death inducing protease activity and showed by Western blot. Thus, these findings highlight the significance of HIF-1 in cell survival under hypoxic conditions, as previously described in the literature[195]. Hypoxia has also been described to act as an anti-apoptotic factor by regulating expression of anti- and pro-apoptotic proteins independently of HIF-1 in certain cell lines[196,197]. In hepatoblastoma HepG2 cells, for example, HIF-1 is not involved in the hypoxia-induced anti-

apoptotic pathway[197]. In addition, CFA was used to investigate the effects of HIF-1α depletion on the long-term survival of cells up to 10 days. The hypoxic cells were returned to a normoxic environment for 10 days after hypoxic incubation and IR to provide ideal growth conditions and to imitate the physiological process of reoxygenation after IR. Based on colony formation assays, long-term survival of hypoxic mHDC cells with HIF-1α KO was impaired after IR with 6 Gy. Therefore, our data suggest that the deletion of HIF-1α leads to an increase in apoptosis and a reduction in clonogenic potential, which demonstrates an increase in radiosensitivity. However, the mechanism of this effect needs to be studied further. Previously it has been reported that HIF-1α knockdown leads to an impaired expression of survivin, but to elevated expression of caspase-3 and B-cell lymphoma 2 (Bcl-2)-associated X protein (Bax) proteins[198], which may contribute to elevated apoptosis levels and increased radiation sensitivity, as demonstrated in our mHDC. Several studies have focused on the mechanism of HIF-1α - mediated gene expression for cell survival and apoptosis. Takasaki et al. found that HIF-1α expression was significantly induced by anti-apoptotic proteins such as survivin in their study on resected lung cancers[199]. Furthermore, a gastric cancer study found that the HIF-1 KD reduced survivin expression, increased the expression of pro-apoptotic proteins like Bax and caspase-3, and increased radiotherapy-induced apoptosis of tumor cells[200].

5.6 mHDC and radiosensitivity: what have we learned?

Previous studies have found apparently conflicting results with respect to the interaction between HIF-1α and DNA damage repair. In this study, we have performed the first investigation on the role of HIF-1 KO in DDR in response to IR in mHDC. Detailed characterisation of hepatocyte radiobiology has thus far been impaired due to the widespread use of heterogeneous bulk hepatocyte cultures. Therefore, the use of mHDC in this study has enabled us to perform the first in depth analysis of the molecular pathways governing mHDC radiosensitivity. We have shown, for the first time, that hypoxia and HIF-1 KO alters the DDR of mHDC to IR-induced DSBs, thus enhancing mHDC radiosensitivity.

Firstly, we analyzed the induction of γH2AX foci by immuno-histochemistry. The protein γH2AX is a phosphorylated form of the histone H2AX that is generated at sites of DSBs during the initiation of DDR. Detection of γH2AX foci indicates cellular recognition of DNA damage rather than commitment to a specific DNA repair pathway. Our experiments showed an increase in γH2AX foci in HIF-1α KO cells compared to wild-type cells after IR in hypoxia. Consistent with this result, an increase in the γH2AX protein level was observed by Western blotting in HIF-1α depleted cells. Importantly, we were able to reproduce the damage-promoting effect of

HIF-1 loss in HIF-1α knockout cells in normoxia by adding DMOG, an inhibitor of prolyl hydroxylases that initiate oxygen-dependent degradation of HIF-α. In this experiment, cells that were unable to induce HIF-1 because of the knockout developed more γH2AX foci than wildtype cells which reinforces our interpretation that HIF-1 protects the cells from IR-induced DNA damage. Surprisingly, DMOG treatment of wildtype cells led to increased DNA damage in normoxia but reduction of damage in the same cells in hypoxia. While the hypoxic DMOG effect in wildtype cells is compatible with protection by HIF-1 activation, the normoxic effect clearly is not. It should be considered that DMOG is a pan-hydroxylase inhibitor, which is probably active on more than 30 2-oxoglutarate-dependent dioxygenases with an even larger number of substrates[198].

Overall, our results indicate that HIF-1α depletion in mHDC leads to an increase in DNA damage after IR. This increase in damage and the previously discussed increase in apoptosis in the first hours after IR pointed to a possible alteration in DNA repair after HIF-1α depletion. Of note, the amount of DNA damage decreased after the first 6 hours, indicating that surviving cells were, in principle, able to complete DNA repair. The DNA repair in the first hours after IR was mainly affected by a fast repair mechanism termed NHEJ. Although several recent studies have shown that DNA repair proteins are compromised in hypoxia, the findings remain controversial. As a result, the expression of NHEJ proteins in hypoxic cells is being debated in the literature. A study with murine fibroblasts reported that HIF-1α KO leads to an increase in γH2AX[124], which is in line with our results. In addition, a number of studies report an increase in NHEJ under hypoxia as a result of HIF-1 activation in glioblastoma[201] and squamous cell carcinoma[202], potentially due to HIF-1α-mediated upregulation of Ku70 and DNA-PK. In light of these studies, it is plausible that the elimination of functional HIF-1 led to an increased amount of DNA damage, which was caused by the downregulation of NHEJ in our mHDC. As a note of caution, it has been published that γH2AX foci may also be detectable in a HIF-1-dependent but DNA damage-independent manner[203]. Another study showed under hypoxia, NHEJ proteins such as DNA-PK remain unaffected in several tumor cell lines[204,205]. Gene expression studies revealed a decrease in mRNA encoding NHEJ proteins, but no significant change in protein content[206]. Other studies suggested that NHEJ was increased under Hx: an increase in Ku70 and DNA-PK expression was observed under acute hypoxia as a result of direct interaction with HIF-1[207–209]. Furthermore, HIF-1 accumulation was reduced in DNA-PK deficient cells under Hx[210]. To exclude misinterpretation of our γH2AX data, we performed neutral comet assays, which detect DSBs more directly as a result of the enhanced mobility of the smaller DNA fragments. These assays confirmed that more DNA damage was detectable in

the first hour after irradiation and that repair was completed but with slower kinetics, which corroborated the γH2AX results. A second important repair mechanism, homologous recombination repair (HRR), is more active in S and G2 phases of the cell cycle[211]. Alterations of HRR were also reported in response to hypoxia[212], but as our mHDC had been transferred to a quiescent state by the withdrawal of growth factors, we anticipate that hypoxia or HIF-dependent effects on HRR contributed to a lesser extent to our results, if at all.

Multiple lines of evidence suggest that certain metabolites, such as lactate, contribute to malignant behavior and a pro-metastatic phenotype in cancer patients, making it a potential prognostic biomarker[213]. Tarnawski et al. demonstrated that lactate levels detected in glioma tumors can be a prognostic parameter for predicting recurrence and overall survival after postoperative radiotherapy[214]. Lactate plays a regulatory role in various biological activities within the cell, including increased angiogenesic capacity, antioxidative and immunosuppressive effects, which contribute to tumor evasion and therapy resistance[77,215]. Moreover, reducing lactate levels in tumors has been shown to improve the response to high-dose single-fraction radiotherapy[216].

In this study, we demonstrate that HIF-1α deficiency leads to a significant decrease in baseline ECAR levels, also known as non-glycolytic acidification. This reduction potentially contributes to the observed increased radiation sensitivity in mHDC cells. Previous research has investigated the impact of lactic acidosis on cellular glucose metabolism, revealing that higher lactic acidosis and proton density impair several glycolytic enzymes, leading to reduced glycolysis[217]. Based on a forementioned results, HIF-1α-deficient cells exhibit a defect in the glycolytic pathway, likely due to decreased lactate levels, resulting in a radiosensitive phenotype. However, further investigation is needed to determine the precise mechanism by which HIF-1 regulates lactate levels.

In summary, we have successfully established murine hepatocyte-derived cells as a culture model for differentiated adult mouse hepatocytes using the "upcyte" technology. Our findings indicate a strong correlation between the permanent and complete knockout of functional HIF-1α, decreased cell survival, and increased DNA damage in response to ionizing radiation, particularly under hypoxic conditions. Our mHDC model will serve as a valuable tool for in-depth analysis of HIF-1 effects on DNA repair pathways. Additionally, it will enable a broader investigation of HIF-1 effects on hepatocyte cell cycle, metabolism, and stress responses.

5.7 Future directions

Primary human hepatocytes are in short supply for biomedical research, despite the fact that protocols for short-term culture of human hepatocytes or long-term culture of hepatocyte-like cells differentiated from non-parenchymal epithelial cells have been developed. Given the large number of genetically modified mice that are now commercially available, it would be highly desirable to have established a reproducible, long-term culture method of differentiated hepatocytes. Furthermore, hepatocyte culture technology would be extremely useful in reducing and refining animal experimentation. The upcyte® mouse hepatocytes established in this work represent an alternative to animal model. The upcyte® technology can be used with other cell types and hepatocyte cultures can be generated from patients. A lot of work will certainly be put into the further development of the Upcyte® hepatocytes in the future. The main focus will be on the improved differentiation of the modified hepatocytes.

It is crucial to select and target tumor biomarkers when treating cancer patients to overcome resistance to conventional therapy. Over the last few decades, plenty of new studies on biomarker discovery and validation have been tested in preclinical and clinical trials, demonstrating that selective biomarker targeting is a thriving field of study. In order to improve outcomes, we must target resistant cancer cells. The remarkable ability of cancer cells to adapt to new environmental conditions is one of the most frustrating characteristics of therapy resistance. On the other hand, the introduction of new targeting strategies such as Crispr/Cas9 technology allows for the development of new treatment options.

Approximately half a million people worldwide are diagnosed with hepatocellular carcinoma, which is the fifth most common cancer among men and the seventh most common cancer among women. In addition, it is the third most common cause of cancer-related deaths worldwide. In HCC, as in many other solid tumors, hypoxia is a hallmark of malignancy. HIF stabilization has been associated with tumor progression, metastasis, and reduced sensitivity to chemotherapy and radiation treatment and is thus regarded as a marker predictive for poor patient outcome. In this thesis, the scientific relevance of modulating the HIF-1α protein and hypoxia in murine hepatocyte derived cell model in the context of radiation treatment has been demonstrated. Knowledge of cancer allows us not only to better understand the basic molecular mechanisms behind a tumorigenic phenotype, but also to develop new technologies and treatment strategies that benefit society as a whole. A population of cells that is resistant to radiation has been targeted in this thesis by inhibiting the proteins expressed by these cells and thereby improving the effectiveness of radiation. There are already many biomarkers that aid

in the management of patients in terms of treatment. Since many cancer patients receive radiation treatment, approaches that influence this treatment can have a substantial impact on patients' lives. HIF-α proteins are transcription factors whose stability and activity are often tumor-specific especially under hypoxic conditions and are generally associated with poor outcome for cancer patients. Thus, HIF-1α may be considered a valuable biomarker for stratifying cancer patients, although the specific treatment based on this type of stratification needs to be investigated further. Since the early 1990s, HIF has been identified as a potential target for the development of novel cancer therapeutics. Through direct and indirect mechanisms, these inhibitors target the expression and/or function of HIF-1, HIF-2, or both. Several HIF inhibitors have been developed, and while some are still being studied, monotherapy treatments with HIF inhibitors have not been successful in clinical trials, and many have been discontinued. However, these inhibitors may be useful in sensitizing resistant cells to traditional treatment modalities such as radiotherapy. This could potentially be applied to other treatment modalities such as chemotherapy or immunotherapy, resulting in better patient care.

We discovered that a complete and permanent knockout of functional HIF-1 caused a strong correlation between decreased cell survival and increased DNA damage in response to ionizing radiation, particularly under hypoxic conditions. Our mHDC will be a valuable tool for further investigating the effects of HIF-1 on DNA repair pathways. Furthermore, it will enable a more comprehensive analysis of HIF-1's effects on hepatocyte cell cycle, metabolism, and stress responses. Other potential future studies may include the following:

i. How deletion of HIF-1α would affect cellular ROS response following irradiation in mHDC.
ii. How deletion of HIF-1α would change mitochondrial homeostasis following irradiation.
iii. How the mitochondrial content correlated to mitochondrial function after irradiation in WT and KO mHDC.
iv. How HIF-1α regulates transcriptional targets after hypoxia and radiation in mHDC.

6 Summary

Hepatocellular Carcinoma (HCC) is a prevalent cancer affecting a significant number of individuals worldwide. Enhancing the efficacy of radiotherapy, a treatment modality for HCC which is under development, holds great potential for improving patient outcomes. In this study, we established cultured murine hepatocyte derived cells (mHDC) as an *in vitro* model and aimed to elucidate the impact of Hypoxia-inducible Factor 1 alpha (HIF-1α) on DNA damage repair, radiation sensitivity, and cellular metabolism in murine hepatocyte-derived cells (mHDC).

To better understand the role of HIF-1α, we developed an *in vitro* model using murine hepatocyte-derived cells (mHDC) that bear a complete knockout for HIF-1α. We assessed the impact of HIF-1α deficiency on DNA damage repair following ionizing radiation (IR) exposure under hypoxic conditions.

Our findings revealed that HIF-1α deficiency increased IR-induced apoptosis and significantly reduced the surviving fraction of mHDC as compared to HIF-1α expressing cells in colony formation assays. Moreover, HIF-1α-depleted cells exhibited increased accumulation of IR-induced DNA damage, as evidenced by upregulated γH2AX foci. Furthermore, HIF-1α-deficient cells displayed delayed DNA repair after IR treatment in hypoxia, suggesting a potential effect on non-homologous end joining (NHEJ) repair capacity, as observed in neutral comet assays. Notably, there were no significant differences in reactive oxygen species (ROS) levels among the treatment groups, suggesting that the effects caused by HIF-1α deficiency are unlikely to be mediated by ROS.

To further investigate the relationship between HIF-1α and cellular metabolism, we analyzed the respiratory metabolism and mitochondrial morphological changes in HIF-1α knockout cells. Interestingly, HIF-1α-deficient cells exhibited a significant increase in the oxygen consumption rate (OCR) and a reduction in the extracellular acidification rate (ECAR) compared to wildtype cells. Additionally, we observed alterations in mitochondrial morphology, with a decrease in the number of mitochondria following hypoxia, but an increase in knockout cells compared to wildtype cells.

Collectively, our results suggest that HIF-1α inactivation enhances radiation sensitivity in mHDC cells, accompanied by an elevation in OCR and reduced glycolysis. These findings contribute to a better understanding of the molecular mechanisms underlying radioresistance and metabolic changes in mHDC.

7 Zusammenfassung

Das hepatozelluläre Karzinom (HCC) ist ein weit verbreiteter maligner Tumor, der weltweit eine große Anzahl von Menschen betrifft. Die Verbesserung der Wirksamkeit der Strahlentherapie, einer Behandlungsmethode für HCC, die sich in der Entwicklung befindet, birgt ein großes Potenzial zur Verbesserung der Patientenergebnisse. In dieser Studie haben wir kultivierte aus Leberzellen generierte Hepatozyten Zellen (mHDC) aus Mäusen als in-vitro-Modell etabliert und die Auswirkungen des Hypoxie-induzierbaren Faktors 1 alpha (HIF-1α) auf die DNA-Schadenreparatur, die Strahlenempfindlichkeit und den Zellstoffwechsel in den mHDC untersucht.

Um die Rolle von HIF-1α besser zu verstehen, haben wir ein in-vitro-Modell mit mHDC entwickelt, bei denen HIF-1α komplett ausgeschaltet ist. Wir haben die Auswirkungen des HIF-1α-Mangels auf die DNA-Schadensreparatur nach Behandlung mit ionisierender Strahlung (IR) unter hypoxischen Bedingungen untersucht.

Unsere Ergebnisse zeigen, dass der HIF-1α-Mangel die durch IR ausgelöste Apoptose erhöhte und die überlebende Fraktion der mHDC im Vergleich zu HIF-1α exprimierenden Zellen in Koloniebildungsassays signifikant reduzierte. Darüber hinaus wiesen HIF-1α-depletierte Zellen eine erhöhte Anhäufung von durch IR verursachten DNA-Schäden auf, wie durch hochregulierte γH2AX-Foci belegt. Darüber hinaus zeigten HIF-1α-defiziente Zellen eine verzögerte DNA-Reparatur nach IR-Behandlung in Hypoxie, was auf eine potenzielle Auswirkung auf die Reparaturkapazität der nicht-homologen Endverknüpfung (NHEJ) hindeutet, wie in neutralen Kometenassays beobachtet wurde. Bemerkenswerterweise gab es keine signifikanten Unterschiede in den reaktiven Sauerstoffspezies (ROS) zwischen den Behandlungsgruppen, was darauf hindeutet, dass die durch HIF-1α-Mangel verursachten Effekte wahrscheinlich nicht durch ROS vermittelt werden.

Um die Beziehung zwischen HIF-1α und dem Zellstoffwechsel weiter zu untersuchen, haben wir den respiratorischen Stoffwechsel und die morphologischen Veränderungen der Mitochondrien in HIF-1α-Knockout-Zellen analysiert. Interessanterweise zeigten HIF-1α-defiziente Zellen eine signifikante Zunahme der Sauerstoffverbrauchsrate (OCR) und eine Verringerung der extrazellulären Azidifizierungsrate (ECAR) im Vergleich zu Wildtyp-Zellen. Darüber hinaus beobachteten wir Veränderungen in der mitochondrialen Morphologie, mit einer Abnahme der Anzahl von Mitochondrien nach Hypoxie, aber einer Zunahme in den Knockout-Zellen im Vergleich zu Wildtyp-Zellen.

Zusammenfassend deuten unsere Ergebnisse darauf hin, dass die Inaktivierung von HIF-1α die Strahlenempfindlichkeit in mHDC-Zellen erhöht, was einhergeht mit einer Erhöhung der OCR und einer verminderten Glykolyse. Diese Erkenntnisse tragen zu einem besseren Verständnis der molekularen Mechanismen bei, die der Strahlenresistenz und den Stoffwechselveränderungen in mHDC zugrunde liegen.

8 References

1. Gebhardt, R. & Matz-soja, M. Liver zonation : Novel aspects of its regulation and its impact on homeostasis. **20**, 8491–8504 (2014).
2. Treyer, A. & Müsch, A. Hepatocyte polarity. *Compr. Physiol.* **3**, 243–287 (2013).
3. Wisse, E., Braet, F., Luo, D., Zanger, R. D. E. & Jans, D. Structure and Function of Sinusoidal Cells in the Liver * Lining. 100–111 (2015).
4. Hay, M., Thomas, D. W., Craighead, J. L., Economides, C. & Rosenthal, J. Clinical development success rates for investigational drugs. **32**, (2014).
5. Stevan A. Gonzalez, E. B. K. Chronic viral hepatitis: epidemiology, molecular biology, and antiviral therapy. 225–250 (2011).
6. Forbes, S. J., Gupta, S. & Dhawan, A. Review Cell therapy for liver disease : From liver transplantation to cell factory. *J. Hepatol.* **62**, S157–S169 (2015).
7. Bañares, R., Catalina, M. & Vaquero, J. Liver Support Systems : Will They Ever Reach Prime Time ? (2013) doi:10.1007/s11894-013-0312-x.
8. Takano, H. *et al.* Downregulation of CYP1A2, CYP2B6, and CYP3A4 in human hepatocytes by prolyl hydroxylase domain 2 inhibitors via hypoxia-inducible factor-α stabilization. *Drug Metab. Dispos.* **49**, 20–30 (2021).
9. Duret, C. *et al.* Isolation, Characterization, and Differentiation to Hepatocyte-Like Cells of Nonparenchymal Epithelial Cells from Adult Human Liver. *Stem Cells* **25**, 1779–1790 (2007).
10. Burkard, A. *et al.* Generation of proliferating human hepatocytes using upcyte® technology: Characterisation and applications in induction and cytotoxicity assays. *Xenobiotica* **42**, 939–956 (2012).
11. Scheller, K. *et al.* Upcyte® microvascular endothelial cells repopulate decellularized scaffold. *Tissue Eng. - Part C Methods* **19**, 57–67 (2013).
12. Nörenberg, A. *et al.* Optimization of upcyte® human hepatocytes for the in vitro micronucleus assay. *Mutat. Res. - Genet. Toxicol. Environ. Mutagen.* **758**, 69–79 (2013).
13. Nikolett Nagy, T. & Evenburg, Sandra Rohrmoser, Astrid Noerenberg, T. J. *Generation of proliferating mouse hepatocytes*. https://www.upcyte.com/upload/27poster-uptec-201901-mousehepas-9e9gf8.pdf (2019).
14. Makino, Y., Kanopka, A., Wilson, W. J., Tanaka, H. & Poellinger, L. Inhibitory PAS domain protein (IPAS) is a hypoxia-inducible splicing variant of the hypoxia-inducible factor-3α locus. *J. Biol. Chem.* **277**, 32405–32408 (2002).
15. Bunn, H. F. & Poyton, R. O. Oxygen sensing and molecular adaptation to hypoxia. *Physiol. Rev.* **76**, 839–885 (1996).
16. Blanchard, K. L., Fandrey, J., Goldberg, M. A. & Bunn, H. F. Regulation of the erythropoietin gene. *Stem Cells* **11**, 1–7 (1993).
17. Shweiki, D., Itin, A., Soffer, D. & Keshet, E. Vascular endothelial growth factor induced by hypoxia may mediate hypoxia-initiated angiogenesis. *Nature* **359**, 843–845 (1992).
18. Heiden, M. G. V., Cantley, L. C. & Thompson, C. B. Understanding the warburg effect: The metabolic requirements of cell proliferation. *Science (80-.).* **324**, 1029–1033 (2009).
19. Warburg, O. On the origin of cancer cells. *Science (80-.).* **123**, 309–314 (1956).
20. Firth, J. D., Ebert, B. L. & Ratcliffe, P. J. Hypoxic regulation of lactate dehydrogenase A: Interaction between hypoxia-inducible factor 1 and cAMP response elements. *J. Biol. Chem.* **270**, 21021–21027 (1995).
21. Gatenby, R. A. & Gillies, R. J. Why do cancers have high aerobic glycolysis? *Nat. Rev. Cancer* **4**, 891–899 (2004).
22. Ebert, B. L., Firth, J. D. & Ratcliffe, P. J. Hypoxia and mitochondrial inhibitors regulate expression of glucose transporter-1 via distinct cis-acting sequences. *J. Biol. Chem.* **270**, 29083–29089 (1995).

23. Johnson, A. B., Denko, N. & Barton, M. C. Hypoxia induces a novel signature of chromatin modifications and global repression of transcription. *Mutat. Res. - Fundam. Mol. Mech. Mutagen.* **640**, 174–179 (2008).
24. Hurst, J. H. William Kaelin, Peter Ratcliffe, and Gregg Semenza receive the 2016 Albert Lasker Basic Medical Research Award. *J. Clin. Invest.* **126**, 3628–3638 (2016).
25. Ziello, J. E., Jovin, I. S. & Huang, Y. Hypoxia-Inducible Factor (HIF)-1 regulatory pathway and its potential for therapeutic intervention in malignancy and ischemia. *Yale J. Biol. Med.* **80**, 51–60 (2007).
26. Smith, T. G., Robbins, P. A. & Ratcliffe, P. J. The human side of hypoxia-inducible factor. *Br. J. Haematol.* **141**, 325–334 (2008).
27. Semenza, G. L. Hypoxia-inducible factors in physiology and medicine. *Cell* **148**, 399–408 (2012).
28. Nambu, J. R., Lewis, J. O., Wharton, K. A. & Crews, S. T. The Drosophila single-minded gene encodes a helix-loop-helix protein that acts as a master regulator of CNS midline development. *Cell* **67**, 1157–1167 (1991).
29. Reddy, P., Jacquier, A. C., Abovich, N., Petersen, G. & Rosbash, M. The period clock locus of D. melanogaster codes for a proteoglycan. *Cell* **46**, 53–61 (1986).
30. Wiesener, M. S. *et al.* Widespread hypoxia-inducible expression of HIF-2alpha in distinct cell populations of different organs. *FASEB J.* **17**, 271–273 (2003).
31. Hu, C.-J., Wang, L.-Y., Chodosh, L. A., Keith, B. & Simon, M. C. Differential Roles of Hypoxia-Inducible Factor 1α (HIF-1α) and HIF-2α in Hypoxic Gene Regulation. *Mol. Cell. Biol.* **23**, 9361–9374 (2003).
32. Tian, H., McKnight, S. L. & Russell, D. W. Endothelial PAS domain protein 1 (EPAS1), a transcription factor selectively expressed in endothelial cells. *Genes Dev.* **11**, 72–82 (1997).
33. Ema, M. *et al.* A novel bHLH-PAS factor with close sequence similarity to hypoxia-inducible factor 1α regulates the VEGF expression and is potentially involved in lung and vascular development. *Proc. Natl. Acad. Sci. U. S. A.* **94**, 4273–4278 (1997).
34. Gu, Y. Z., Moran, S. M., Hogenesch, J. B., Wartman, L. & Bradfield, C. A. Molecular characterization and chromosomal localization of a third α- class hypoxia inducible factor subunit, HIF3α. *Gene Expr.* **7**, 205–213 (1998).
35. Wang, G. L., Jiang, B. H., Rue, E. A. & Semenza, G. L. Hypoxia-inducible factor 1 is a basic-helix-loop-helix-PAS heterodimer regulated by cellular O2 tension. *Proc. Natl. Acad. Sci. U. S. A.* **92**, 5510–5514 (1995).
36. Jiang, B. H., Rue, E., Wang, G. L., Roe, R. & Semenza, G. L. Dimerization, DNA binding, and transactivation properties of hypoxia- inducible factor 1. *J. Biol. Chem.* **271**, 17771–17778 (1996).
37. Bruick, R. K. & McKnight, S. L. A conserved family of prolyl-4-hydroxylases that modify HIF. *Science (80-.).* **294**, 1337–1340 (2001).
38. Kallio, P. J., Pongratz, I., Gradin, K., McGuire, J. & Poellinger, L. Activation of hypoxia-inducible factor 1α: Posttranscriptional regulation and conformational change by recruitment of the Arnt transcription factor. *Proc. Natl. Acad. Sci. U. S. A.* **94**, 5667–5672 (1997).
39. Berra, E., Roux, D., Richard, D. E. & Pouysségur, J. Hypoxia-inducible factor-1α (HIF-1 escapes O2-driven proteasomal degradation irrespective of its subcellular localization: Nucleus or cytoplasm. *EMBO Rep.* **2**, 615–620 (2001).
40. Maxwell, P. H. *et al.* The tumour suppressor protein VHL targets hypoxia-inducible factors for oxygen-dependent proteolysis. *Nature* **399**, 271–275 (1999).
41. Wenger, R. H., Stiehl, D. P. & Camenisch, G. Integration of oxygen signaling at the consensus HRE. *Sci. STKE* **2005**, 1–14 (2005).
42. Liu, W., Shen, S. M., Zhao, X. Y. & Chen Dr., G. Q. Targeted genes and interacting

proteins of hypoxia inducible factor-1. *Int. J. Biochem. Mol. Biol.* **3**, 165–178 (2012).
43. Hayashi, M. *et al.* Induction of glucose transporter 1 expression through hypoxia-inducible factor 1α under hypoxic conditions in trophoblast-derived cells. *J. Endocrinol.* **183**, 145–154 (2004).
44. Ramakrishnan, S., Anand, V. & Roy, S. Vascular endothelial growth factor signaling in hypoxia and inflammation. *J. Neuroimmune Pharmacol.* **9**, 142–160 (2014).
45. Jamali, S. *et al.* Hypoxia-induced carbonic anhydrase IX facilitates lactate flux in human breast cancer cells by non-catalytic function. *Sci. Rep.* **5**, 1–16 (2015).
46. Ortmann, B., Druker, J. & Rocha, S. Cell cycle progression in response to oxygen levels. *Cell. Mol. Life Sci.* **71**, 3569–3582 (2014).
47. Rademakers, S. E. *et al.* Molecular aspects of tumour hypoxia. *Mol. Oncol.* **2**, 41–53 (2008).
48. Wang, G. L. & Semenza, G. L. Characterization of hypoxia-inducible factor 1 and regulation of DNA binding activity by hypoxia. *J. Biol. Chem.* **268**, 21513–21518 (1993).
49. Dimova, E., Michiels, C. & Kietzmann, T. Kinases as Upstream Regulators of the HIF System: Their Emerging Potential as Anti-Cancer Drug Targets. *Curr. Pharm. Des.* **15**, 3867–3877 (2009).
50. Kietzmann, T., Mennerich, D. & Dimova, E. Y. Hypoxia-Inducible Factors (HIFs) and phosphorylation: Impact on stability, localization, and transactivity. *Front. Cell Dev. Biol.* **4**, 1–14 (2016).
51. Semenza, G. L. *et al.* Hypoxia response elements in the aldolase A, enolase 1, and lactate dehydrogenase a gene promoters contain essential binding sites for hypoxia-inducible factor 1. *J. Biol. Chem.* **271**, 32529–32537 (1996).
52. Mathupala, S. P., Rempel, A. & Pedersen, P. L. Glucose catabolism in cancer cells: Identification and characterization of a marked activation response of the type II hexokinase gene to hypoxic conditions. *J. Biol. Chem.* **276**, 43407–43412 (2001).
53. Gwak, G. Y. *et al.* Hypoxia stimulates proliferation of human hepatoma cells through the induction of hexokinase II expression. *J. Hepatol.* **42**, 358–364 (2005).
54. Hamaguchi, T., Iizuka, N., Tsunedomi, R., Hamamoto, Y., Miyamoto, T., Iida, M., Tokuhisa, Y., Sakamoto, K., Takashima, M., Tamesa, T., et al. Glycolysis module activated by hypoxia-inducible factor 1α is related to the aggressive phenotype of hepatocellular carcinoma. *Int. J. Oncol.* **35**, 725–731 (2008).
55. Xia, O. *et al.* Integrative analysis of HIF binding and transactivation reveals its role in maintaining histone methylation homeostasis. *Proc. Natl. Acad. Sci. U. S. A.* **106**, 4260–4265 (2009).
56. Pajuelo Reguera, D. *et al.* Cytochrome c Oxidase Subunit 4 Isoform Exchange Results in Modulation of Oxygen Affinity. *Cells* **9**, (2020).
57. Fukuda, R. *et al.* HIF-1 Regulates Cytochrome Oxidase Subunits to Optimize Efficiency of Respiration in Hypoxic Cells. *Cell* **129**, 111–122 (2007).
58. Schulze, A. & Harris, A. L. How cancer metabolism is tuned for proliferation and vulnerable to disruption. *Nature* **491**, 364–373 (2012).
59. Kam, W. W. Y. & Banati, R. B. Effects of ionizing radiation on mitochondria. *Free Radic. Biol. Med.* **65**, 607–619 (2013).
60. Kim, G. J., Chandrasekaran, K. & Morgan, W. F. Mitochondrial dysfunction, persistently elevated levels of reactive oxygen species and radiation-induced genomic instability: A review. *Mutagenesis* **21**, 361–367 (2006).
61. Ganz, T. Systemic iron homeostasis. *Physiol. Rev.* **93**, 1721–1741 (2013).
62. Nemeth, E. & Ganz, T. The role of hepcidin in iron metabolism. *Acta Haematol.* **122**, 78–86 (2009).
63. Schmidt, P. J. Regulation of iron metabolism by hepcidin under conditions of

inflammation. *J. Biol. Chem.* **290**, 18975–18983 (2015).
64. Bernier, J., Hall, E. J. & Giaccia, A. Radiation oncology: A century of achievements. *Nat. Rev. Cancer* **4**, 737–747 (2004).
65. Horsman, M. R. & Vaupel, P. Pathophysiological basis for the formation of the tumor microenvironment. *Front. Oncol.* **6**, (2016).
66. Thomlinson, R. H. & Gray, L. H. The histological structure of some human lung cancers and the possible implications for radiotherapy. *Br. J. Cancer* **9**, 539–549 (1955).
67. GRAY, L. H., CONGER, A. D., EBERT, M., HORNSEY, S. & SCOTT, O. C. The concentration of oxygen dissolved in tissues at the time of irradiation as a factor in radiotherapy. *Br. J. Radiol.* **26**, 638–648 (1953).
68. Aebersold, D.M., et al. Expression of hypoxia-inducible factor-1alpha: a novel predictive and prognostic parameter in the radiotherapy of oropharyngeal cancer. *Cancer Res* **61**, 2911–6 (2001).
69. Eui, J. M., Brizel, D. M., Chi, J. T. A. & Dewhirst, M. W. The potential role of intrinsic hypoxia markers as prognostic variables in cancer. *Antioxidants Redox Signal.* **9**, 1237–1294 (2007).
70. Quintiliani, M. The oxygen effect in radiation inactivation of DNA and enzymes. *Int. J. Radiat. Biol.* **50**, 573–594 (1986).
71. Robert Grimes, D. & Partridge, M. A mechanistic investigation of the oxygen fixation hypothesis and oxygen enhancement ratio. *Biomed. Phys. Eng. Express* **1**, 045209 (2015).
72. Grotius, J. *et al.* Impact of exogenous lactate on survival and radioresponse of carcinoma cells in vitro. *Int. J. Radiat. Biol.* **85**, 989–1001 (2009).
73. Huang, C. Y., Kuo, W. T., Huang, Y. C., Lee, T. C. & Yu, L. C. H. Resistance to hypoxia-induced necroptosis is conferred by glycolytic pyruvate scavenging of mitochondrial superoxide in colorectal cancer cells. *Cell Death Dis.* **4**, 1–11 (2013).
74. Bristow, R. G. & Hill, R. P. Hypoxia and metabolism: Hypoxia, DNA repair and genetic instability. *Nat. Rev. Cancer* **8**, 180–192 (2008).
75. Okunieff, P. *et al.* Antioxidants reduce consequences of radiation exposure. *Adv. Exp. Med. Biol.* **614**, 165–178 (2008).
76. Groussard, C. *et al.* Free radical scavenging and antioxidant effects of lactate ion: An in vitro study. *J. Appl. Physiol.* **89**, 169–175 (2000).
77. Hirschhaeuser, F., Sattler, U. G. A. & Mueller-Klieser, W. Lactate: A metabolic key player in cancer. *Cancer Res.* **71**, 6921–6925 (2011).
78. Meijer, T. W. H., Kaanders, J. H. A. M., Span, P. N. & Bussink, J. Targeting hypoxia, HIF-1, and tumor glucose metabolism to improve radiotherapy efficacy. *Clin. Cancer Res.* **18**, 5585–5594 (2012).
79. Li, J. L. *et al.* Delta-like 4 Notch ligand regulates tumor angiogenesis, improves tumor vascular function, and promotes tumor growth in vivo. *Cancer Res.* **67**, 11244–11253 (2007).
80. Brizel, D. M., Sibley, G. S., Prosnitz, L. R., Scher, R. L. & Dewhirst, M. W. Tumor hypoxia adversely affects the prognosis of carcinoma of the head and neck. *Int. J. Radiat. Oncol. Biol. Phys.* **38**, 285–289 (1997).
81. Moeller, B. J. & Dewhirst, M. W. HIF-1 and tumour radiosensitivity. *Br. J. Cancer* **95**, 1–5 (2006).
82. Li, F. *et al.* Regulation of HIF-1α Stability through S-Nitrosylation. *Mol. Cell* **26**, 63–74 (2007).
83. Moeller, B. J., Cao, Y., Li, C. Y. & Dewhirst, M. W. Radiation activates HIF-1 to regulate vascular radiosensitivity in tumors: Role of reoxygenation, free radicals, and stress granules. *Cancer Cell* **5**, 429–441 (2004).
84. Harada, H. *et al.* The Akt/mTOR pathway assures the synthesis of HIF-1α protein in a

glucose- and reoxygenation-dependent manner in irradiated tumors. *J. Biol. Chem.* **284**, 5332–5342 (2009).
85. Harada, H. *et al.* Cancer cells that survive radiation therapy acquire HIF-1 activity and translocate towards tumour blood vessels. *Nat. Commun.* **3**, (2012).
86. Gardner, L. B. *et al.* Hypoxia Inhibits G1/S Transition through Regulation of p27 Expression. *J. Biol. Chem.* **276**, 7919–7926 (2001).
87. Box, A. H. & Demetrick, D. J. Cell cycle kinase inhibitor expression and hypoxia-induced cell cycle arrest in human cancer cell lines. *Carcinogenesis* **25**, 2325–2335 (2004).
88. Goda, N. *et al.* Hypoxia-Inducible Factor 1α Is Essential for Cell Cycle Arrest during Hypoxia. *Mol. Cell. Biol.* **23**, 359–369 (2003).
89. Press, D. The role of HIF-1 α in chemo- / radioresistant tumors. 3003–3011 (2018).
90. Moeller, B. J. *et al.* Pleiotropic effects of HIF-1 blockade on tumor radiosensitivity. *Cancer Cell* **8**, 99–110 (2005).
91. Chan, N. *et al.* Chronic hypoxia decreases synthesis of homologous recombination proteins to offset chemoresistance and radioresistance. *Cancer Res.* **68**, 605–614 (2008).
92. Jiricny, J. The multifaceted mismatch-repair system. *Nat. Rev. Mol. Cell Biol.* **7**, 335–346 (2006).
93. David, S. S., O'Shea, V. L. & Kundu, S. Base-excision repair of oxidative DNA damage. *Nature* **447**, 941–950 (2007).
94. Kuper, J. & Kisker, C. Damage recognition in nucleotide excision DNA repair. *Curr. Opin. Struct. Biol.* **22**, 88–93 (2012).
95. Dueva, R. & Iliakis, G. Alternative pathways of non-homologous end joining (NHEJ) in genomic instability and cancer. *Transl. Cancer Res.* **2**, 163–177 (2013).
96. Iliakis, G., Murmann, T. & Soni, A. Alternative end-joining repair pathways are the ultimate backup for abrogated classical non-homologous end-joining and homologous recombination repair: Implications for the formation of chromosome translocations. *Mutat. Res. - Genet. Toxicol. Environ. Mutagen.* **793**, 166–175 (2015).
97. Frankenberg-Schwager, M. *et al.* Single-strand annealing, conservative homologous recombination, nonhomologous DNA end joining, and the cell cycle-dependent repair of DNA double-strand breaks induced by sparsely or densely ionizing radiation. *Radiat. Res.* **171**, 265–273 (2009).
98. Stiff, T. *et al.* ATR-dependent phosphorylation and activation of ATM in response to UV treatment or replication fork stalling. *EMBO J.* **25**, 5775–5782 (2006).
99. Stiff, T. *et al.* ATM and DNA-PK Function Redundantly to Phosphorylate H2AX after Exposure to Ionizing Radiation. *Cancer Res.* **64**, 2390–2396 (2004).
100. Rogakou, E. P., Pilch, D. R., Orr, A. H., Ivanova, V. S. & Bonner, W. M. DNA double-stranded breaks induce histone H2AX phosphorylation on serine 139. *J. Biol. Chem.* **273**, 5858–5868 (1998).
101. Kobayashi, J. Molecular mechanism of the recruitment of NBS1/hMRE11/hRAD50 complex to DNA double-strand breaks: NBS1 binds to γ-H2AX through FHA/BRCT domain. *J. Radiat. Res.* **45**, 473–478 (2004).
102. McKinnon, P. J. ATM and ataxia telangiectasia. Second in molecular medicine review series. *EMBO Rep.* **5**, 772–776 (2004).
103. Rothkamm, K., Krüger, I., Thompson, L. H. & Löbrich, M. Pathways of DNA Double-Strand Break Repair during the Mammalian Cell Cycle. *Mol. Cell. Biol.* **23**, 5706–5715 (2003).
104. Walker, J. R., Corpina, R. A. & Goldberg, J. Structure of the Ku heterodimer bound to dna and its implications for double-strand break repair. *Nature* **412**, 607–614 (2001).
105. Singleton, B. K., Torres-Arzayus, M. I., Rottinghaus, S. T., Taccioli, G. E. & Jeggo, P. A. The C Terminus of Ku80 Activates the DNA-Dependent Protein Kinase Catalytic

Subunit. *Mol. Cell. Biol.* **19**, 3267–3277 (1999).
106. Goodarzi, A. A. *et al.* DNA-PK autophosphorylation facilitates Artemis endonuclease activity. *EMBO J.* **25**, 3880–3889 (2006).
107. Capp, J. P. *et al.* The DNA polymerase λ is required for the repair of non-compatible DNA double strand breaks by NHEJ in mammalian cells. *Nucleic Acids Res.* **34**, 2998–3007 (2006).
108. Capp, J. P. *et al.* Involvement of DNA polymerase μ in the repair of a specific subset of DNA double-strand breaks in mammalian cells. *Nucleic Acids Res.* **35**, 3551–3560 (2007).
109. Yano, K. I. *et al.* Ku recruits XLF to DNA double-strand breaks. *EMBO Rep.* **9**, 91–96 (2008).
110. Wang, Y. G., Nnakwe, C., Lane, W. S., Modesti, M. & Frank, K. M. Phosphorylation and regulation of DNA ligase IV stability by DNA-dependent protein kinase. *J. Biol. Chem.* **279**, 37282–37290 (2004).
111. Iijima, K., Ohara, M., Seki, R. & Tauchi, H. Dancing on damaged chromatin: Functions of ATM and the RAD50/MRE11/NBS1 complex in cellular responses to DNA damage. *J. Radiat. Res.* **49**, 451–464 (2008).
112. Wold, M. S. Replication protein A: A heterotrimeric, single-stranded DNA-binding protein required for eukaryotic DNA metabolism. *Annu. Rev. Biochem.* **66**, 61–92 (1997).
113. Prakash, R., Zhang, Y., Feng, W. & Jasin, M. Homologous Recombination and Human Health. *Perspect. Biol.* 1–29 (2015).
114. Haaf, T., Golub, E. I., Reddy, G., Radding, C. M. & Ward, D. C. Nuclear foci of mammalian Rad51 recombination protein in somatic cells after DNA damage and its localization in synaptonemal complexes. *Proc. Natl. Acad. Sci. U. S. A.* **92**, 2298–2302 (1995).
115. West, S. C. Molecular views of recombination proteins and their control. *Nat. Rev. Mol. Cell Biol.* **4**, 435–445 (2003).
116. Bakr, A. *et al.* Functional crosstalk between DNA damage response proteins 53BP1 and BRCA1 regulates double strand break repair choice. *Radiother. Oncol.* **119**, 276–281 (2016).
117. Dimitrova, N., Chen, Y. C. M., Spector, D. L. & De Lange, T. 53BP1 promotes non-homologous end joining of telomeres by increasing chromatin mobility. *Nature* **456**, 524–528 (2008).
118. Boulton, S. J. Cellular functions of the BRCA tumour-suppressor proteins. *Biochem. Soc. Trans.* **34**, 633–645 (2006).
119. Durant, S. T. & Nickoloff, J. A. Good timing in the cell cycle for precise DNA repair by BRCA1. *Cell Cycle* **4**, 1216–1222 (2005).
120. Isono, M. *et al.* BRCA1 Directs the Repair Pathway to Homologous Recombination by Promoting 53BP1 Dephosphorylation. *Cell Rep.* **18**, 520–532 (2017).
121. Hammond, E. M., Dorie, M. J. & Giaccia, A. J. ATR/ATM targets are phosphorylated by ATR in response to hypoxia and ATM in response to reoxygenation. *J. Biol. Chem.* **278**, 12207–12213 (2003).
122. Freiberg, R. A., Krieg, A. J., Giaccia, A. J. & Hammond, E. M. Checking in on hypoxia/reoxygenation. *Cell Cycle* **5**, 1304–1307 (2006).
123. Cam, H., Easton, J. B., High, A. & Houghton, P. J. mTORC1 signaling under hypoxic conditions is controlled by atm-dependent phosphorylation of HIF-1α. *Mol. Cell* **40**, 509–520 (2010).
124. Wirthner, R., Wrann, S., Balamurugan, K., Wenger, R. H. & Stiehl, D. P. Impaired DNA double-strand break repair contributes to chemoresistance in HIF-1α-deficient mouse embryonic fibroblasts. *Carcinogenesis* **29**, 2306–2316 (2008).

125. Hall, E.J., and Giaccia, A. J. *Radiobiology for the Radiologist.* (2012).
126. Ryan, H. E., Lo, J. & Johnson, R. S. HIF-1α is required for solid tumor formation and embryonic vascularization. *EMBO J.* **17**, 3005–3015 (1998).
127. Burkitt, K., Chun, S. Y., Dang, D. T. & Dang, L. H. Targeting both HIF-1 and HIF-2 in human colon cancer cells improves tumor response to sunitinib treatment. *Mol. Cancer Ther.* **8**, 1148–1156 (2009).
128. Carroll, V. A. & Ashcroft, M. Role of hypoxia-inducible factor (HIF)-1α versus HIF-2α in the regulation of HIF target genes in response to hypoxia, insulin-like growth factor-I, or loss of von Hippel-Lindau function: Implications for targeting the HIF pathway. *Cancer Res.* **66**, 6264–6270 (2006).
129. Williams, K. J. *et al.* Enhanced response to radiotherapy in tumours deficient in the function of hypoxia-inducible factor-1. *Radiother. Oncol.* **75**, 89–98 (2005).
130. Luo, Z. *et al.* Silencing of HIF-1α enhances the radiation sensitivity of human glioma growth in vitro and in vivo. *Neuropharmacology* **89**, 168–174 (2015).
131. Williams, K. J. *et al.* A protective role for HIF-1 in response to redox manipulation and glucose deprivation: implications for tumorigenesis. *Oncogene* **21**, 282–290 (2002).
132. Damaghi, M., Wojtkowiak, J. W. & Gillies, R. J. pH sensing and regulation in cancer. *Front. Physiol.* **4 DEC**, 1–11 (2013).
133. Van Kuijk, S. J. A. *et al.* The sulfamate small molecule CAIX inhibitor S4 modulates doxorubicin efficacy. *PLoS One* **11**, 1–14 (2016).
134. Quennet, V. *et al.* Tumor lactate content predicts for response to fractionated irradiation of human squamous cell carcinomas in nude mice. *Radiother. Oncol.* **81**, 130–135 (2006).
135. DeBerardinis, R. J. *et al.* Beyond aerobic glycolysis: Transformed cells can engage in glutamine metabolism that exceeds the requirement for protein and nucleotide synthesis. *Proc. Natl. Acad. Sci. U. S. A.* **104**, 19345–19350 (2007).
136. Cui, X. G. *et al.* HIF1/2α mediates hypoxia-induced LDHA expression in human pancreatic cancer cells. *Oncotarget* **8**, 24840–24852 (2017).
137. Nieva, C. *et al.* The Lipid Phenotype of Breast Cancer Cells Characterized by Raman Microspectroscopy: Towards a Stratification of Malignancy. *PLoS One* **7**, (2012).
138. Zhang, M. *et al.* HIF-1 Alpha Regulates the Response of Primary Sarcomas to Radiation Therapy through a Cell Autonomous Mechanism. *Radiat. Res.* **183**, 594–609 (2015).
139. Kondo, K., Kim, W. Y., Lechpammer, M. & Kaelin, W. G. Inhibition of HIF2α is sufficient to suppress pVHL-defective tumor growth. *PLoS Biol.* **1**, 439–444 (2003).
140. Raval, R. R. *et al.* Contrasting Properties of Hypoxia-Inducible Factor 1 (HIF-1) and HIF-2 in von Hippel-Lindau-Associated Renal Cell Carcinoma. *Mol. Cell. Biol.* **25**, 5675–5686 (2005).
141. Holmquist-Mengelbier, L. *et al.* Recruitment of HIF-1α and HIF-2α to common target genes is differentially regulated in neuroblastoma: HIF-2α promotes an aggressive phenotype. *Cancer Cell* **10**, 413–423 (2006).
142. Gu, Q. *et al.* Hypoxia-inducible factor 1α (HIF-1α) and reactive oxygen species (ROS) mediates radiation-induced invasiveness through the SDF-1α/CXCR4 pathway in non-small cell lung carcinoma cells. *Oncotarget* **6**, 10893–10907 (2015).
143. Roig, E. M. *et al.* Prognostic role of hypoxia-inducible factor-2α tumor cell expression in cancer patients: A meta-analysis. *Front. Oncol.* **8**, (2018).
144. Sun, J. C. *et al.* High expression of HIF-2α and its anti-radiotherapy effect in lung cancer stem cells. *Genet. Mol. Res.* **14**, 18110–18120 (2015).
145. Seibler, J. *et al.* Rapid generation of inducible mouse mutants. *Nucleic Acids Res.* **31**, e12 (2003).
146. Ryan, H. E. *et al.* Hypoxia-inducible factor-1α is a positive factor in solid tumor growth. *Cancer Res.* **60**, 4010–4015 (2000).

147. Levy, G. *et al.* Long-term culture and expansion of primary human hepatocytes. *Nat. Biotechnol.* **33**, 1264–1271 (2015).
148. Matsuzaki, Y., Umemoto, T., Tanaka, Y., Okano, T. & Yamato, M. β2-Microglobulin is an appropriate reference gene for RT-PCR-based gene expression analysis of hematopoietic stem cells. *Regen. Ther.* **1**, 91–97 (2015).
149. Livak, K. J. & Schmittgen, T. D. Analysis of relative gene expression data using real-time quantitative PCR and the 2-ΔΔCT method. *Methods* **25**, 402–408 (2001).
150. Wang, F. *et al.* RNAscope: A novel in situ RNA analysis platform for formalin-fixed, paraffin-embedded tissues. *J. Mol. Diagnostics* **14**, 22–29 (2012).
151. (n.d.). Agilent Technology.
152. Pompsch, M. *et al.* The presumed MTH1-inhibitor TH588 sensitizes colorectal carcinoma cells to ionizing radiation in hypoxia. *BMC Cancer* **18**, 1–9 (2018).
153. Classen, F. *et al.* Autophagy induced by ionizing radiation promotes cell death over survival in human colorectal cancer cells. *Exp. Cell Res.* **374**, 29–37 (2019).
154. Olive, P. L. & Banáth, J. P. The comet assay: A method to measure DNA damage in individual cells. *Nat. Protoc.* **1**, 23–29 (2006).
155. Møller, P. *et al.* Minimum Information for Reporting on the Comet Assay (MIRCA): recommendations for describing comet assay procedures and results. *Nat. Protoc.* **15**, 3817–3826 (2020).
156. Amelino-Camelia, G., Ellis, J., Mavromatos, N. E., Nanopoulos, D. V. & Sarkar, S. Tests of quantum gravity from observations of γ-ray bursts. *Nature* **393**, 763–765 (1998).
157. Branco-Price, C. *et al.* Endothelial cell HIF-1α and HIF-2α differentially regulate metastatic success. *Cancer Cell* **21**, 52–65 (2012).
158. Hamidi, A. *et al.* Depletion of HIF-1α by Inducible Cre/loxP Increases the Sensitivity of Cultured Murine Hepatocytes to Ionizing Radiation in Hypoxia. *Cells* **11**, 1–18 (2022).
159. Guo, X. *et al.* Quantitative analysis of alternative pre-mrna splicing in mouse brain sections using RNA in situ hybridization assay. *J. Vis. Exp.* **2018**, 1–8 (2018).
160. Nair, S. *et al.* Induction of Mitochondrial Fragmentation and Mitophagy after Neonatal Hypoxia–Ischemia. *Cells* **11**, 1–17 (2022).
161. Valente, A. J., Maddalena, L. A., Robb, E. L., Moradi, F. & Stuart, J. A. A simple ImageJ macro tool for analyzing mitochondrial network morphology in mammalian cell culture. *Acta Histochem.* **119**, 315–326 (2017).
162. Ichimura, T., Ito, M., Takahashi, K., Oyama, K. & Sakurai, K. Involvement of mitochondrial swelling in cytochrome c release from mitochondria treated with calcium and Alloxan. *J. Biophys. Chem.* **02**, 10–18 (2011).
163. Brown, M., Bristow, R. & Mcbride, W. Comment on " Tumor Response to Radiotherapy Regulated by. **302**, (2003).
164. Rohwer, N., Zasada, C., Kempa, S. & Cramer, T. The growing complexity of HIF-1α's role in tumorigenesis: DNA repair and beyond. *Oncogene* **32**, 3569–3576 (2013).
165. Singh, N. P., McCoy, M. T., Tice, R. R. & Schneider, E. L. A simple technique for quantitation of low levels of DNA damage in individual cells. *Exp. Cell Res.* **175**, 184–191 (1988).
166. Nossoni, F. Single-cell gel electrophoresis (comet assay): methodology, potential applications, and limitations in cancer research. *Basic Biotechnol. eJournal* **4**, 30–35 (2008).
167. Hewitt, N. J. *et al.* Primary hepatocytes: Current understanding of the regulation of metabolic enzymes and transporter proteins, and pharmaceutical practice for the use of hepatocytes in metabolism, enzyme induction, transporter, clearance, and hepatotoxicity studies. *Drug Metab. Rev.* **39**, 159–234 (2007).
168. Godoy, P. *et al. Recent advances in 2D and 3D in vitro systems using primary hepatocytes, alternative hepatocyte sources and non-parenchymal liver cells and their*

use in investigating mechanisms of hepatotoxicity, cell signaling and ADME. *Archives of Toxicology* vol. 87 (2013).
169. Tolosa, L. *et al.* Human upcyte hepatocytes: Characterization of the hepatic phenotype and evaluation for acute and long-term hepatotoxicity routine testing. *Toxicol. Sci.* **152**, 214–229 (2016).
170. Wen, P. & Locker, J. A novel hepatocytic transcription factor that binds the alpha-fetoprotein promoter-linked coupling element. *Mol. Cell. Biol.* **14**, 6616–6626 (1994).
171. Kammerer, S. Three-Dimensional Liver Culture Systems to Maintain Primary Hepatic Properties for Toxicological Analysis In Vitro. (2021).
172. Wilkening, S., Stahl, F. & Bader, A. Hepg2 With Regard To Their Biotransformation Properties. *Drug Metab. Dispos.* **31**, 1035–1042 (2003).
173. Unger, R. E., Krump-Konvalinkova, V., Peters, K. & James Kirkpatrick, C. In vitro expression of the endothelial phenotype: Comparative study of primary isolated cells and cell lines, including the novel cell line HPMEC-ST1.6R. *Microvasc. Res.* **64**, 384–397 (2002).
174. Richard, L., Velasco, P. & Detmar, M. A simple immunomagnetic protocol for the selective isolation and long- term culture of human dermal microvascular endothelial cells. *Exp. Cell Res.* **240**, 1–6 (1998).
175. Fodor, W. L. Tissue engineering and cell based therapies, from the bench to the clinic: The potential to replace, repair and regenerate. *Reprod. Biol. Endocrinol.* **1**, 1–6 (2003).
176. Kim, S. & Von Recum, H. Endothelial stem cells and precursors for tissue engineering: Cell source, differentiation, selection, and application. *Tissue Eng. - Part B Rev.* **14**, 133–147 (2008).
177. Karasek, M. A. Microvascular endothelial cell culture. *J. Invest. Dermatol.* **93(2 Suppl**, 33S–38S (1989).
178. Semenza, G. L. Oxygen Sensing, Homeostasis, and Disease. 537–547 (2011).
179. Kaelin, W. G. The von Hippel-Lindau tumour suppressor protein: O2 sensing and cancer. *Nat. Rev. Cancer* **8**, 865–873 (2008).
180. Semenza, G. L. HIF-1 mediates metabolic responses to intratumoral hypoxia and oncogenic mutations. *J. Clin. Invest.* **123**, 3664–3671 (2013).
181. Depping, R. *et al.* Nuclear translocation of hypoxia-inducible factors (HIFs): Involvement of the classical importin α/β pathway. *Biochim. Biophys. Acta - Mol. Cell Res.* **1783**, 394–404 (2008).
182. Zou, L. Q. *et al.* 3D conformal radiotherapy combined with transcatheter arterial chemoembolization for hepatocellular carcinoma. *World J. Gastroenterol.* **20**, 17227–17234 (2014).
183. Brown, J. M. & Giaccia, A. J. The unique physiology of solid tumors: Opportunities (and problems) for cancer therapy. *Cancer Res.* **58**, 1408–1416 (1998).
184. Iyer, N. V. *et al.* Cellular and developmental control of O2 homeostasis by hypoxia-inducible factor 1α. *Genes Dev.* **12**, 149–162 (1998).
185. Semenza, G. L., Roth, P. H., Fang, H. M. & Wang, G. L. Transcriptional regulation of genes encoding glycolytic enzymes by hypoxia-inducible factor 1. *J. Biol. Chem.* **269**, 23757–23763 (1994).
186. Kim, J. W., Tchernyshyov, I., Semenza, G. L. & Dang, C. V. HIF-1-mediated expression of pyruvate dehydrogenase kinase: A metabolic switch required for cellular adaptation to hypoxia. *Cell Metab.* **3**, 177–185 (2006).
187. Papandreou, I., Cairns, R. A., Fontana, L., Lim, A. L. & Denko, N. C. HIF-1 mediates adaptation to hypoxia by actively downregulating mitochondrial oxygen consumption. *Cell Metab.* **3**, 187–197 (2006).
188. Lu, H., Forbes, R. A. & Verma, A. Hypoxia-inducible factor 1 activation by aerobic glycolysis implicates the Warburg effect in carcinogenesis. *J. Biol. Chem.* **277**, 23111–

23115 (2002).
189. Shah, Y. M., Matsubara, T., Ito, S., Yim, S. H. & Gonzalez, F. J. Intestinal Hypoxia-Inducible Transcription Factors Are Essential for Iron Absorption following Iron Deficiency. *Cell Metab.* **9**, 152–164 (2009).
190. Peyssonnaux, C. *et al.* Regulation of iron homeostasis by the hypoxia-inducible transcription factors (HIFs). *J. Clin. Invest.* **117**, 1926–1932 (2007).
191. Ganz, T. Hepcidin and iron regulation, 10 years later. *Blood* **117**, 4425–4433 (2011).
192. Zhang, A. S. & Enns, C. A. Molecular mechanisms of normal iron homeostasis. *Hematology Am. Soc. Hematol. Educ. Program* 207–214 (2009) doi:10.1182/asheducation-2009.1.207.
193. Drakesmith, H., Nemeth, E. & Ganz, T. Ironing out Ferroportin. *Cell Metab.* **22**, 777–787 (2015).
194. Hubbi, M. E. & Semenza, G. L. Regulation of cell proliferation by hypoxia-inducible factors. *Am. J. Physiol. - Cell Physiol.* **309**, C775–C782 (2015).
195. Kumar, H. & Choi, D. K. Hypoxia Inducible Factor Pathway and Physiological Adaptation: A Cell Survival Pathway? *Mediators Inflamm.* **2015**, (2015).
196. Erler, J. T. *et al.* Hypoxia-Mediated Down-Regulation of Bid and Bax in Tumors Occurs via Hypoxia-Inducible Factor 1-Dependent and -Independent Mechanisms and Contributes to Drug Resistance. *Mol. Cell. Biol.* **24**, 2875–2889 (2004).
197. Piret, J. P., Cosse, J. P., Ninane, N., Raes, M. & Michiels, C. Hypoxia protects HepG2 cells against etoposide-induced apoptosis VIA a HIF-1-independent pathway. *Exp. Cell Res.* **312**, 2908–2920 (2006).
198. Abend, M. Reasons to reconsider the significance of apoptosis for cancer therapy. *Int. J. Radiat. Biol.* **79**, 927–941 (2003).
199. Takasaki, C., Kobayashi, M., Ishibashi, H., Akashi, T. & Okubo, K. Expression of hypoxia-inducible factor-1α affects tumor proliferation and antiapoptosis in surgically resected lung cancer. *Mol. Clin. Oncol.* **5**, 295–300 (2016).
200. Zhao, Q. *et al.* Enhancement of drug sensitivity by knockdown of HIF-1α in gastric carcinoma cells. *Oncol. Res.* **23**, 129–136 (2016).
201. Marampon, F. *et al.* Hypoxia sustains glioblastoma radioresistance through ERKs/DNA-PKcs/HIF- 1α functional interplay. *Int. J. Oncol.* **45**, 2121–2131 (2014).
202. Wozny, A. S. *et al.* Involvement of hif-1α in the detection, signaling, and repair of dna double-strand breaks after photon and carbon-ion irradiation. *Cancers (Basel).* **13**, 1–15 (2021).
203. Wrann, S., Kaufmann, M. R., Wirthner, R., Stiehl, D. P. & Wenger, R. H. HIF mediated and DNA damage independent histone H2AX phosphorylation in chronic hypoxia. *Biol. Chem.* **394**, 519–528 (2013).
204. Bindra, R. S. *et al.* Hypoxia-induced down-regulation of BRCA1 expression by E2Fs. *Cancer Res.* **65**, 11597–11604 (2005).
205. Sprong, D., Janssen, H. L., Vens, C. & Begg, A. C. Resistance of hypoxic cells to ionizing radiation is influenced by homologous recombination status. *Int. J. Radiat. Oncol. Biol. Phys.* **64**, 562–572 (2006).
206. Meng, A. X. *et al.* Hypoxia down-regulates DNA double strand break repair gene expression in prostate cancer cells. *Radiother. Oncol.* **76**, 168–176 (2005).
207. Kang, M. J. *et al.* DNA-dependent protein kinase is involved in heat shock protein-mediated accumulation of hypoxia-inducible factor-1α in hypoxic preconditioned HepG2 cells. *FEBS J.* **275**, 5969–5981 (2008).
208. Ren, Y. *et al.* Hypoxia modulates A431 cellular pathways association to tumor radioresistance and enhanced migration revealed by comprehensive proteomic and functional studies. *Mol. Cell. Proteomics* **12**, 485–498 (2013).
209. Um, J. H. *et al.* Association of DNA-dependent protein kinase with hypoxia inducible

factor-1 and its implication in resistance to anticancer drugs in hypoxic tumor cells. *Exp. Mol. Med.* **36**, 233–242 (2004).
210. Bouquet, F. *et al.* A DNA-dependent stress response involving DNA-PK occurs in hypoxic cells and contributes to cellular adaptation to hypoxia. *J. Cell Sci.* **124**, 1943–1951 (2011).
211. Mladenov, E., Magin, S., Soni, A. & Iliakis, G. DNA double-strand-break repair in higher eukaryotes and its role in genomic instability and cancer: Cell cycle and proliferation-dependent regulation. *Semin. Cancer Biol.* **37**–**38**, 51–64 (2016).
212. Bindra, R. S. *et al.* Down-Regulation of Rad51 and Decreased Homologous Recombination in Hypoxic Cancer Cells. *Mol. Cell. Biol.* **24**, 8504–8518 (2004).
213. Walenta, S. & Mueller-Klieser, W. F. Lactate: Mirror and motor of tumor malignancy. *Semin. Radiat. Oncol.* **14**, 267–274 (2004).
214. Tarnawski, R. *et al.* 1H-MRS in vivo predicts the early treatment outcome of postoperative radiotherapy for malignant gliomas. *Int. J. Radiat. Oncol. Biol. Phys.* **52**, 1271–1276 (2002).
215. Romero-Garcia, S., Moreno-Altamirano, M. M. B., Prado-Garcia, H. & Sánchez-García, F. J. Lactate contribution to the tumor microenvironment: Mechanisms, effects on immune cells and therapeutic relevance. *Front. Immunol.* **7**, (2016).
216. Leung, E. *et al.* Metabolic targeting of HIF-dependent glycolysis reduces lactate, increases oxygen consumption and enhances response to high-dose single-fraction radiotherapy inhypoxic solid tumors. *BMC Cancer* **17**, 1–12 (2017).
217. Xie, J. *et al.* Beyond Warburg effect - Dual metabolic nature of cancer cells. *Sci. Rep.* **4**, 1–12 (2014).

9 Appendix

9.1 Abbreviations

53BP1	p53 binding protein 1
Akt	protein kinase B
Alt-NHEJ	alternative-NHEJ
ANOVA	analysis of variance
APS	ammonium persulfate
ARNT	aryl hydrocarbon receptor nuclear translocator
ATM	ataxia telangiectasia mutated kinase
ATP	adenosine 5´-triphosphate
ATR	ataxia telangiectasia and Rad3-related kinase
B2M	ß2-microglobuline
BAX	B-cell lymphoma 2 (Bcl-2)-associated X protein
BCA	bicinchoninic acid
Bcl-2	B-cell lymphoma 2
BER	base excision repair
bHLH	basic-helix-loop-helix
BNIP3	Bcl2/adenovirus E1B 19-kDa interacting protein 3
BRCA1	breast cancer protein 1
BSA	bovine serum albumin
CAIX	carbon anhydrase isoform IX
CBP	cAMP response element-binding (CREB)-binding protein
CDK	cyclin-dependent kinase
cDNA	complementary DNA
CHAPS	3-[(3-Cholamidopropyl)dimethylammonio]-1-propane-sulfonate
COX4-1	cytochrome c oxidase subunit 4-1
Cre(-)	HIF-1$\alpha^{fl/fl}$Cre-ER$^{wt/wt}$
Cre(ki)	HIF-1$\alpha^{fl/fl}$Cre-ER$^{ki/wt}$
CTAD	C-terminal transactivation domain
CtIP	C-terminal binding protein-interacting protein
CYP	cytochrome P450
DDR	DNA damage repair
DEPC	diethyl pyrocarbonate
DEVD-AMC	Asp-Glu-Val-Asp-7-amino-4-methylcoumarin
DMSO	dimethylsulfoxide
DNA-PK	DNA-dependent protein kinase
DSB	double-strand break
DTT	dithiothreitol
E2	exon 2
EDTA	ethylenediaminetetraacetic acid
EMT	epithelial-mesenchymal transition
EPAS1	endothelial PAS protein 1

Epo	erythropoietin
ESR1	estrogen receptor
FBS	fetal bovine serum
FIH-1	factor inhibiting HIF-1
GI	gastrointestinal
GLUT	glucose transporter
h	hours
HEPES	4-(2-hydroxyethyl)-1-piperazineethanesulfonic acid
HIF	hypoxia-inducible factor
HIF-1α	hypoxia-inducible factor- 1α
HIF-2α	hypoxia-inducible factor- 2α
HK2	hexokinase 2
HR	homologous recombination
HRE	hypoxia-responsive element
HRP	horseradisch peroxidase
Hx	hypoxia
ID	inhibitory domain
IF	immunofluorescence staining
IgG	immunoglobulin G
IHC	immunohistochemistry
iNOS	inducible nitric oxide synthase
IPAS	inhibitory PER-ARNT-SIM domain
IR	ionizing radiation
IRIF	irradiation-induced foci
KD	kilodalton
ki	knock-in
KO	knockout
kV	kilovolt
LDH-A	lactate dehydrogenase-A
LIG4	DNA Ligase 4
LSECs	liver sinusoidal endothelial cells
MDC1	mediator of DNA damage checkpoint
MMR	mismatch repair
MRN	Mre11-Rad50-NBS1 complex
mRNA	messenger RNA
MW	molecular weight
mg	milligram
min	minutes
mL	milliliter
mM	millimolar
mm	millimeter
mvEC	microvascular endothelial cells
NADH	reduced form of nicotinamide adenine dinucleotide
nm	nanomolar
NBS1	Nijmegen breakage syndrome protein 1

NER	nucleotide excision repair
NHEJ	non-homologous end joining
NO	nitric oxide
NTAD	N-terminal transactivation domain
Nx	normoxia
O_2	oxygen
ODD	oxygen-dependent degradation domain
OCR	Oxygen consumption rate
P	proline
p300	300-kilodalton coactivator protein
PAGE	Polyacrylamide gel electrophoresis
PARP-1	poly [ADP-ribose] polymerase 1
PAS	PER-ARNT-SIM
PBS	phosphate-buffered saline
PCR	Polymerase chain reaction
PDGFB	platelet-derived growth factor B
PDK1	pyruvate dehydrogenase kinase isozyme 1
PER	*D. melanogaster* period clock protein
PFA	paraformaldehyde
PHD	prolyl hydroxylase domain protein
PI3K	phosphatidylinositol 3-kinase
pO_2	oxygen tension
PVDF	polyvinylidene fluoride
pVHL	von Hippel-Lindau protein
qPCR	quantitative polymerase chain reaction
RIPA	radioimmunoprecipitation assay buffer
ROS	reactive oxygen species
RPA	replication protein A
RTA	ready-to-assemble
SD	standard deviation
SDF1	stromal derived factor 1
SDS	sodium dodecyl sulfate
SIM	*D. melanogaster* single-minded locus
SSA	single-strand annealing
SSB	single-strand break
SSBR	single-strand break repair
ssDNA	single-stranded DNA
Tam	tamoxifen
TBS	Tris-buffered saline
TCA	tricarboxylic acid
TEMED	tetramethylethylenediamine
VEGF	vascular endothelial growth factor
WB	Western blot
wt	wild-type
γH2AX	phosphorylated histone protein H2AX

9.2 Figures

9.3 Tables

9.4 Acknowledgements

Throughout my graduate research education, numerous individuals have played pivotal roles in shaping my journey and assisting me in achieving my objectives. While it is impossible to express individual gratitude to everyone, I am deeply grateful to all those who have supported me along the way.

First and foremost, I am profoundly indebted to Prof. Dr. Eric Metzen, who graciously accepted me as his Ph.D. student and expertly guided me throughout this research. His unwavering support, guidance, encouragement, and patience have played an instrumental role in every step of this study, and I am immensely grateful for the academic freedom and research autonomy he provided.

Additionally, I would like to extend my special gratitude to Prof. Dr. Joachim Fandrey for enabling me to work at the Institute of Physiology, an opportunity I am truly thankful for. I am also grateful to the organizers of the graduate school GRK1739 for their structured program and facilitating scientific exchange. I would like to express my appreciation to the reviewers of this work for their valuable scientific analysis of the project.
Special thanks go to Prof. Verena Jendrossek for her willingness to act as my mentor and share knowledge and expertise in this research.
Furthermore, I would like to express my sincere gratitude to Prof. Dr. George Iliakis for his cooperation and support. I am also thankful to all the doctoral students in the GRK program for their helpful tips, words of encouragement, and the enjoyable time we spent together. Special thanks are due to Dr. Rositsa Dueva for her assistance in data analysis and interpretation, as well as to Dr. Johann Matschke for granting permission to use the Seahorse Analyzer and for engaging in insightful discussions. I am also grateful to my dear colleagues from the Institute of Physiology, especially to all past and present members of the Metzen group, for their daily assistance, moral support, and for fostering a warm and collaborative working environment. It has been a pleasure and privilege to be a part of your team. I would like to extend my special thanks to Melanie, Kirsten, Alexandra, Nadine and Erlen.
On a personal note, I would like to express my deepest appreciation to my parents, whose unwavering support and encouragement have been a constant throughout every stage of my education. Your belief in me has been invaluable. Finally, I would like to thank my friends for their presence and unwavering encouragement. Without you, the past few years would have been considerably more challenging, and I am grateful for your steadfast support.

9.5 Publication list

Hamidi, A., Wolf, A., Dueva, R., Kaufmann, M., Göpelt, K., Iliakis, G., & Metzen, E. (2022). Depletion of HIF-1α by Inducible Cre/loxP Increases the Sensitivity of Cultured Murine Hepatocytes to Ionizing Radiation in Hypoxia. *Cells, 11*(10), 1671.

Hamidi, A., Hassani, L., Mohammadi, F., Jahangoshayi, P., & Mohammadi, K. (2016). The biological effects of vanadyl curcumin and vanadyl diacetylcurcumin complexes: the effect on structure, function and oxidative stability of the peroxidase enzyme, antibacterial activity and cytotoxic effect. Journal of enzyme inhibition and medicinal chemistry, 31(6), 1124-1131.

Jahangoshaei, P., Hassani, L., Mohammadi, F., **Hamidi, A.**, & Mohammadi, K. (2015). Investigating the effect of gallium curcumin and gallium diacetylcurcumin complexes on the structure, function and oxidative stability of the peroxidase enzyme and their anticancer and antibacterial activities. *JBIC Journal of Biological Inorganic Chemistry*, *20*(7), 1135-1146.

9.6 Curriculum vitae

The curriculum vitae is not included in the online version for data protection reasons.

AWARD

• Award for the Best Poster by the 100th Annual Meeting of the German Physiology Society entitled "Analysis of growth and radiation sensitivity of HIF-1α deficient cultured murine hepatocytes". **2021**

PUBLICATIONS

Depletion of HIF-1α by Inducible Cre/loxP Increases the Sensitivity of Cultured Murine Hepatocytes to Ionizing Radiation in Hypoxia. **Hamidi, A**., Wolf, A., Dueva, R., Kaufmann, M., Göpelt, K., Iliakis, G., & Metzen, E. Cells , 11(10), 1671.l, 2022

The biological effects of vanadyl curcumin and vanadyl diacetylcurcumin complexes: the effect on structure, function and oxidative stability of the peroxidase enzyme, antibacterial activity and cytotoxic effect. **Hamidi, A**., Hassani, L., Mohammadi, F., Jahangoshayi, P., & Mohammadi, K. Journal of enzyme inhibition and medicinal chemistry, 31(6), 1124-1131. 2016

Investigating the effect of gallium curcumin and gallium diacetylcurcumin complexes on the structure, function and oxidative stability of the peroxidase enzyme and their anticancer and antibacterial activities. Jahangoshayi, P., Hassani, L., Mohammadi, F., **Hamidi, A**., & Mohammadi, K. JBIC Journal of Biological Inorganic Chemistry, 20(7), 1135-1146. 2015.

CONFERENCE PROCEEDINGS

•102nd Annual Meeting of the German Physiological Society	Poster	**2023**
•12th Annual Symposium of the Young Physiologists, Kiel	Talk	**2023**
• Europhysiology 2022, Copenhagen	Talk	**2022**
• 100th Meeting of the German Physiological Society, Frankfurt	Poster	**2021**
• 5th AEK Autumn School on Replication Stress in Cancer, Neuss	Talk	**2020**
• GRK 1739 symposium on DNA damage and beyond, Essen	Poster	**2019**
• 98th Meeting of the German Physiological Society, Ulm	Poster	**2019**

Essen, den _____ Akram Hamidi _____

9.7 Declarations

Erklärung:

Hiermit erkläre ich, gem. § 7 Abs. (2) d) +f) der Promotionsordnung der Fakultät für Biologie zur Erlangung des Dr. rer. nat., dass ich die vorliegende Dissertation selbstständig verfasst und mich keiner anderen als der angegebenen Hilfsmittel bedient, bei der Abfassung der Dissertation nur die angegebenen Hilfsmittel benutzt und alle wörtlich oder inhaltlich übernommenen Stellen als solche gekennzeichnet habe.

Essen, den _____ _____

Akram Hamidi

Erklärung:

Hiermit erkläre ich, gem. § 7 Abs. (2) e) +g) der Promotionsordnung der Fakultät für Biologie zur Erlangung des Dr. rer. nat., dass ich keine anderen Promotionen bzw. Promotionsversuche in der Vergangenheit durchgeführt habe und dass diese Arbeit von keiner anderen Fakultät/Fachbereich abgelehnt worden ist.

Essen, den _____ _____

Akram Hamidi

Erklärung:

Hiermit erkläre ich, gem. § 6 Abs. (2) g) der Promotionsordnung der Fakultät für Biologie zur Erlangung des Dr. rer. nat., dass ich das Arbeitsgebiet, dem das Thema *„Enhancing radiosensitivity of murine hepatocytes in hypoxia through HIF-1α depletion“* zuzuordnen ist, in Forschung und Lehre vertrete und den Antrag von Akram Hamidi befürworte und die Betreuung auch im Falle eines Weggangs, wenn nicht wichtige Gründe dem entgegenstehen, weiterführen werde.

_____

Name des Mitglieds der Universität Duisburg-Essen in Druckbuchstaben

Essen, den _____ _____

Prof. Dr. Eric Metzen